

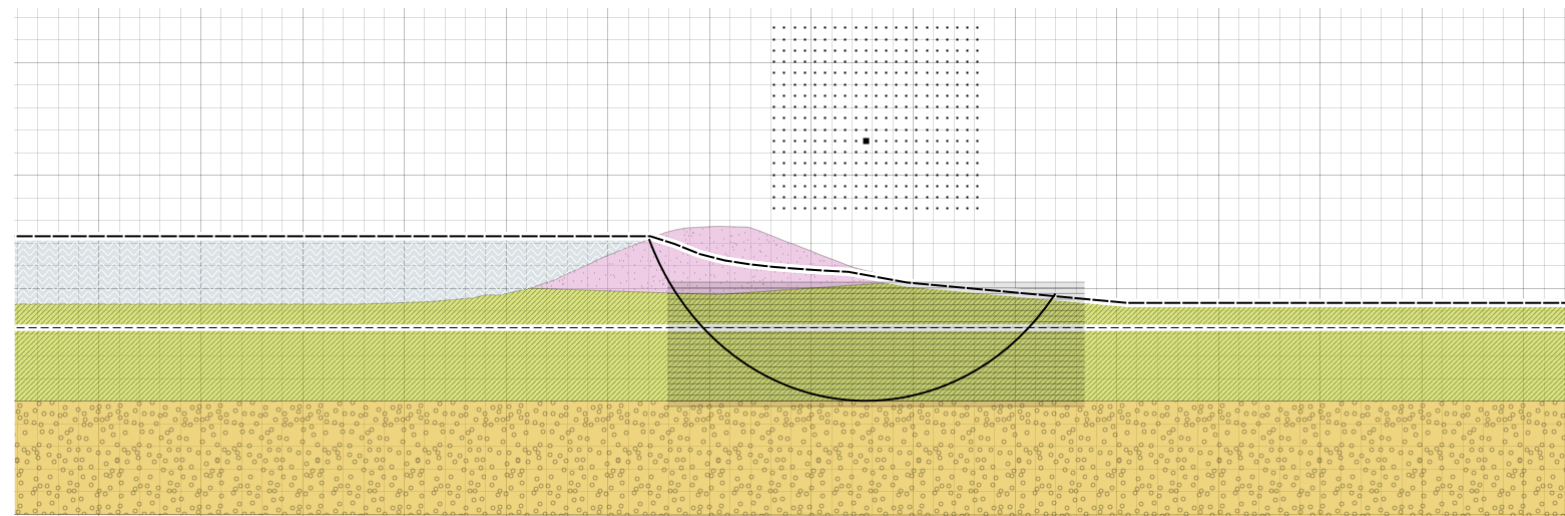


**CHARACTERIZATION OF UNDRAINED SHEAR
STRENGTH IN DUTCH SITES USING HIERARCHICAL
BAYESIAN MODELLING**

M.Sc. Thesis in Geo-Engineering

Theodoros Vinatselas

Delft, August 2023



CHARACTERIZATION OF UNDRAINED SHEAR STRENGTH IN DUTCH SITES USING HIERARCHICAL BAYESIAN MODELLING

By

Student name
Theodoros Vinatselas

Student number
5624029

in partial fulfilment of the requirements for the degree of

Master of Science

in Civil Engineering

at the Delft University of Technology,

to be defended publicly on Tuesday August 30, 2023 at 13:00 AM.

Chair supervisor Dr. Ir. Bram van den Eijnden, TU Delft

Supervisor Dr. Ir. Timo Schweckendiek, TU Delft and Deltares

Daily supervisor Ir. Antonis Mavritsakis, Deltares



SUPPORTED BY
**ONASSIS
FOUNDATION**

An electronic version of this thesis is available at <http://repository.tudelft.nl/>.

ACKNOWLEDGMENTS

I would like to express my heartfelt gratitude to the members of my thesis committee. I extend my sincere appreciation to Dr. Ir. Bram van den Eijnden, the Chair of my committee, for his valuable insights and guidance. I am deeply thankful to my supervisor, Dr. Ir. Timo Schweckendiek, whose expertise, and support significantly contributed to the success of this endeavor.

I am especially thankful to my daily supervisor, Ir. Antonis Mavritsakis, whose unwavering assistance played a pivotal role throughout my thesis. His guidance in the topics of Bayesian statistics has been invaluable.

I am grateful to my colleagues within Deltares, whose generous assistance and support was instrumental in overcoming challenges related to the Deltares software.

My deepest gratitude goes to my family, whose unwavering support has been the cornerstone of my accomplishments. Their encouragement and sacrifices have enabled me to pursue the MSc Track in Geo Engineering at TU Delft. Despite the distance, their belief in my abilities and their motivational words have uplifted me during challenging times.

To my friends and fellow students at TU Delft, I extend my appreciation for the shared learning experiences that enriched my academic journey. Also, to my friends back in Greece. Their encouragement and constant support have been a driving force behind my academic journey.

Lastly, I extend profound thanks to the Onassis Foundation for their scholarship support. Their financial assistance was accompanied by an ethical endorsement that affirmed the significance of my academic pursuits. This multifaceted support was invaluable in making my educational aspirations a reality. Their unwavering backing served as a motivating force as well, compelling me to push myself even harder in the pursuit of excellence.

ABSTRACT

This thesis discusses the characterization of the undrained shear strength, S_u from the net cone resistance, q_{net} of clay in Dutch sites using Hierarchical Bayesian Modelling (HBM). The performance of the HBM is compared with the current practice methods of the site characterization which propose either the use of only site-specific observations (unpooled models) or the whole data simultaneously (pooled models). HBM can incorporate information from multiple sources such as prior knowledge of the engineers and behaviour met in the examined and the neighbouring sites. The use of different sources of information has been proposed by Eurocode-7 without providing a formal / mathematical procedure.

Literature studies have highlighted the potential benefits of incorporating the HBM into the characterization of the geotechnical parameter values. Therefore, this thesis aims to assess whether HBM can enhance the geotechnical decision-making by precisely quantifying the uncertainty in the geotechnical parameter values and making more accurate predictions of them. The impact of using input from the HBM results in a reliability analysis of a dike slope is examined as well.

First, a considerable number of paired $q_{net}-S_u$ measurements is collected, and subsequently is divided into groups. Different statistical models are employed to describe this collected data. Two components characterize a statistical model; the functional form which is the relationship between S_u and q_{net} and the pooling family (pooled, unpooled and HBM), the method followed to train the statistical model parameters. The statistical models are applied in a comparative study to select the fittest one and to compare the behaviour of the HBM to the other pooling families. The comparative study is performed by applying the Bayesian Data Analysis (BDA) whose applicability is ensured by applying it in an artificial example using artificial data.

The first result of the BDA with real data is the comparison of the HBM with the current practice pooled and unpooled models suggesting the $\ln S_u - \ln q_{net}$ HBM as the fittest model. The HBM estimations for the statistical model parameters fall between the current practice's methods and they experience lower uncertainty by borrowing

information from the neighbouring sites to make site-specific estimations. Between the current practice and the HBM, the latter predicts the S_u with lower uncertainty.

The reliability analysis using input from the HBM yields different reliability indices than those proposed by the current practice models. This situation combined with the choice of the HBM after following the BDA workflow propose that the HBM can lead to safer and more economic design.

Overall, the use of the HBM for predicting the S_u from q_{net} with grouped data can be beneficial for the engineering practice. First, the HBM reduces the uncertainty of the statistical model parameters without inheriting extreme values and provides more certain prediction for the S_u accounting for the prior engineering knowledge and the behaviour met in neighbouring sites. Additionally, performing reliability analysis of a dike slope exhibits that the use of HBM derived values can suggest safer and more economic design over the standard approach.

CONTENTS

ACKNOWLEDGMENTS	iv
ABSTRACT	v
NOMENCLATURE	x
LIST OF FIGURES	xi
LIST OF TABLES	xiv
1. INTRODUCTION	1
1.1 BACKGROUND	2
1.2 MOTIVATION	3
1.3 RESEARCH QUESTIONS	4
1.4 RESEARCH OBJECTIVES	4
1.5 APPROACH OF THE THESIS	5
1.6 OUTLINE OF THE THESIS	5
2. LITERATURE REVIEW	7
2.1 CURRENT PRACTICE OF EUROCODE-7	7
2.2 CURRENT PRACTICE OF SITE CHARACTERIZATION	9
2.3 DATA DRIVEN SITE CHARACTERIZATION AND BAYESIAN INFERENCE	11
2.3.1 Bayesian inference	11
2.3.2 DDSC applications using Bayesian inference	12
2.4 CPT BASED DERIVATION OF S_u	17
2.5 CONCLUSIONS	17
3. BAYESIAN DATA ANALYSIS BACKGROUND AND THESIS METHODOLOGY	19
3.1 INTRODUCTION	19
3.2 HIERARCHICAL BAYESIAN MODELLING AND POOLING FAMILIES	19
3.3 BAYESIAN INFERENCE	21
3.4 FUNCTIONAL FORMS OF THE STATISTICAL MODELS	22
3.4.1 x - y functional form	22
3.4.2 x - $\ln y$ functional form	24
3.4.3 $\ln x$ - $\ln y$ functional form	25
3.5 ORDINARY LINEAR REGRESSION PER POOLING FAMILY	25
3.5.1 Pooled model	25
3.5.2 Unpooled model	26
3.5.3 Hierarchical Bayesian Model	27

3.5.4	One – parameter partially pooled model	28
3.6	PRIOR / HYPERPRIOR DISTRIBUTIONS	29
3.7	INFERENCE AND COMPUTATION	31
3.8	BAYESIAN DATA ANALYSIS WORKFLOW-COMPARING THE MODELS.....	31
3.9	MODEL CHECKING AND VALIDATION	32
3.9.1	Model checking	32
3.9.2	Model validation	33
3.10	PREDICTION	35
3.11	PROCEDURE FOR OBTAINING THE RESEARCH OBJECTIVES.....	36
4.	DATA COLLECTION	38
4.1	INTRODUCTION.....	38
4.2	DATA ACQUISITION	38
4.3	DIVISION OF DATA INTO GROUPS.....	38
5.	ARTIFICIAL EXAMPLE	41
5.1	INTRODUCTION.....	41
5.2	PURPOSE OF THE ARTIFICIAL EXAMPLE.....	41
5.3	PROCEDURE OF THE ARTIFICIAL EXAMPLE	41
5.4	BDA WORKFLOW VALIDATION CRITERIA.....	42
5.5	GENERATION OF ARTIFICIAL DATASETS.....	43
5.6	RESULTS AND DISCUSSION	44
5.6.1	Validation with model ranking.....	44
5.6.2	Validation with posterior distributions	48
5.7	CONCLUSIONS.....	53
6.	REAL CASE ANALYSIS	54
6.1	PURPOSE OF THE REAL CASE ANALYSIS.....	54
6.2	PROCEDURE OF THE REAL CASE ANALYSIS	54
6.3	RESULTS AND DISCUSSION	55
6.3.1	Models' ranking.....	55
6.3.2	Model checking	57
6.3.3	Posterior estimations of θ	59
6.3.4	Posterior predictive estimations of Su	63
6.4	CONCLUSIONS.....	66
7.	RELIABILITY ANALYSIS.....	68

7.1	INTRODUCTION.....	68
7.2	RELIABILITY ANALYSIS PROCEDURE	69
7.3	SETUP OF THE RELIABILITY ANALYSIS	71
7.4	RESULTS AND DISCUSSION	73
7.4.1	Reliability analysis for deterministic <i>qnet</i>	73
7.4.2	Reliability analysis with stochastic <i>qnet</i> per site	76
7.4.3	Reliability analysis with stochastic <i>qnet</i> and dike material φ	78
7.5	CONCLUSIONS.....	79
8.	CONCLUSIONS	80
9.	LIMITATIONS AND FURTHER RESEARCH RECOMMENDATIONS	82
	BIBLIOGRAPHY.....	83
	APPENDIX	86
	SUMMARY STATISTICS	86
	STATISTICAL MODELS.....	87
	DATASET	88

NOMENCLATURE

BDA	Bayesian Data Analysis	MCMC	Markov Chain Monte Carlo
DDSC	Data Driven Site Characterization	CI	Credible Interval
θ	Statistical model parameters	PPI	Posterior Predictive Interval
q_{net}	Net cone resistance	pdf	Probability density function
X	Covariate	L	Likelihood
y	Dependent parameter	$p()$	Probability
HBM	Hierarchical Bayesian Model	f_N	Normal pdf
σ_y	Standard deviation	f_N	LogNormal pdf
EC-7	Eurocode-7	CV	Cross Validation
φ	Friction angle	LOO	Leave one out
CI	Credible Interval	LOGO	Leave one group out
PPI	Posterior Predictive Interval	S_u	Undrained shear strength
β	Reliability Index		

LIST OF FIGURES

FIGURE 2.1: PROCEDURE FOR SITE CHARACTERIZATION IN STANDARD PRACTICE, TAKEN FROM BAECHER & CHRISTIAN (2003) ..	10
FIGURE 2.2: PROCEDURE OF THE DDSC OBTAINED BY BAECHER & CHRISTIAN (2003)	11
FIGURE 3.1: GRAPHICAL REPRESENTATION OF THE STATISTICAL MODEL FAMILIES INSPIRED BY BOZORGZADEH ET AL. (2019).....	21
FIGURE 3.2: STRUCTURE OF THE HIERARCHICAL MODEL INSPIRED BY GELMAN ET AL. (2013).....	21
FIGURE 3.3: GRAPHICAL REPRESENTATION OF THE ORDINARY LINEAR REGRESSION BETWEEN $qnet$ AND Su INSPIRED BY DAVIDSON (2003).....	23
FIGURE 3.4: POOLED MODEL'S PROBABILISTIC GRAPHICAL MODEL.....	26
FIGURE 3.5: UNPOOLED MODEL'S PROBABILISTIC GRAPHICAL MODEL	27
FIGURE 3.6: HBM'S PROBABILISTIC GRAPHICAL MODEL	28
FIGURE 3.7: HBM OF EITHER SLOPE OR INTERCEPT PROBABILISTIC GRAPHICAL MODEL	29
FIGURE 3.8: DESCRIPTION OF THE BDA WORKFLOW AS DESCRIBED IN GELMAN ET AL. (2020).....	32
FIGURE 3.9: PROCEDURE FOLLOWED IN THE THESIS TO ANSWER THE RESEARCH QUESTIONS AND TO OBTAIN THE RESEARCH OBJECTIVES	37
FIGURE 4.1: GEOGRAPHICAL POSITIONS OF THE TOTAL DATASETS OF PAIRED MEASUREMENTS $Q_{NET} - S_{ij}$ WITHOUT SUBDIVISION. THE NUMBER OF THE TOTAL MEASUREMENTS IS PROJECTED AS WELL.....	39
FIGURE 4.2: GEOGRAPHICAL POSITIONS OF THE TOTAL DATASET SUBDIVIDED INTO GROUPS / SITES. THE NUMBER OF THE MEASUREMENTS PER SITE IS PRESENTED AS WELL.....	39
FIGURE 4.3: SCATTERPLOT OF $Su - qnet$ PER GROUP / SITE	40
FIGURE 5.1: PROCEDURE OF THE ARTIFICIAL EXAMPLE	42
FIGURE 5.2: ARTIFICIALLY GENERATED DATA WITH POOLED, HBM AND UNPOOLED MODEL. THE MEAN VALUES AND THE 95% PERCENTILE OF THE GENERATED DATA	44
FIGURE 5.3: MODEL RANKINGS BASED ON THE LOO-CV FOR THE POOLED DATASET.....	45
FIGURE 5.4: MODEL RANKINGS BASED ON THE LOGO-CV FOR THE POOLED DATASET.....	45
FIGURE 5.5: MODEL RANKINGS BASED ON THE LOO-CV FOR THE PARTIALLY POOLED DATASET.....	46
FIGURE 5.6: MODEL RANKINGS BASED ON THE LOGO-CV FOR THE PARTIALLY POOLED DATASET	46
FIGURE 5.7: MODEL RANKINGS BASED ON THE LOO-CV FOR THE UNPOOLED DATASET.....	47
FIGURE 5.8: MODEL RANKINGS BASED ON THE LOGO-CV FOR THE UNPOOLED DATASET.....	47
FIGURE 5.9: COMBINED PLOT OF POSTERIOR DISTRIBUTION, OLS ESTIMATOR, OLS UNCERTAINTY AND PARAMETER USED FOR DATA GENERATION FOR BOTH SLOPE AND INTERCEPT. RESULTS PRESENTED FOR ALL GROUPS AND FOR THE CASE OF POOLED DATASET.....	49
FIGURE 5.10: POSTERIOR DISTRIBUTION OF THE σ_y AND THE VALUE USED FOR DATA GENERATION. CASE OF POOLED MODEL....	49
FIGURE 5.11: COMBINED PLOT OF POSTERIOR DISTRIBUTION, OLS ESTIMATOR, OLS UNCERTAINTY AND PARAMETER USED FOR DATA GENERATION FOR BOTH SLOPE AND INTERCEPT. RESULTS PRESENTED FOR ALL GROUPS AND FOR THE CASE OF PARTIALLY POOLED DATASET.....	51

FIGURE 5.12: POSTERIOR DISTRIBUTION OF THE σ_y AND THE VALUE USED FOR DATA GENERATION. CASE OF PARTIALLY POOLED MODEL.....	51
FIGURE 5.13: COMBINED PLOT OF POSTERIOR DISTRIBUTION, OLS ESTIMATOR, OLS UNCERTAINTY AND PARAMETER USED FOR DATA GENERATION FOR BOTH SLOPE AND INTERCEPT. RESULTS PRESENTED FOR ALL GROUPS AND FOR THE CASE OF UNPOOLED DATASET. THE POSTERIOR DISTRIBUTION IS OBTAINED FROM THE HBM (1 ST RANKED MODEL).....	52
FIGURE 5.14: POSTERIOR DISTRIBUTION OF σ_y OBTAINED BY THE HBM (1 ST RANKED MODEL) AND THE σ_y VALUE USED FOR DATA GENERATION. CASE OF UNPOOLED DATASET	53
FIGURE 6.1: WORKFLOW OF THE ANALYSIS WITH REAL DATA.....	55
FIGURE 6.2: MODELS RANKING BASED ON THE LOO – CV FOR ANALYSIS WITH REAL DATA	56
FIGURE 6.3: MODEL RANKING BASED ON THE LOGO – CV FOR ANALYSIS WITH REAL DATA.	56
FIGURE 6.4: POSTERIOR PREDICTIVE CHECK FOR THE LNX – LNY HBM AND REAL DATA.....	58
FIGURE 6.5: PLOT OF THE LNX – LNY HBM ALONG WITH OBSERVED DATA INCLUDING THE 90% POSTERIOR PREDICTIVE INTERVAL AND CREDIBLE INTERVAL	59
FIGURE 6.6: PLOT OF THE LNX – LNY UNPOOLED ALONG WITH OBSERVED DATA INCLUDING THE 90% POSTERIOR PREDICTIVE INTERVAL AND CREDIBLE INTERVAL.....	59
FIGURE 6.7: COMBINED FOREST PLOTS OF 90 % CI FOR POSTERIOR DISTRIBUTIONS OF SLOPE AND INTERCEPT PER SITE AND FOR THE WHOLE DATASET. RESULTS OBTAINED BY ALL THE STATISTICAL MODELS OF THE LNX – LNY FUNCTIONAL FORM.	61
FIGURE 6.8: SCATTER PLOT OF THE POSTERIOR MEAN VALUES FOR THE SLOPE AND THE INTERCEPT. THE DASHED LINE REPRESENTS THE CHANGE OF THE POINT ESTIMATES BETWEEN THE UNPOOLED MODEL AND THE HBM	62
FIGURE 6.9: FOREST PLOT OF σ_y 90% CREDIBLE INTERVAL OF POSTERIOR DISTRIBUTION. RESULTS OBTAINED BY ALL THE STATISTICAL MODELS OF THE LNX – LNY FUNCTIONAL FORM.....	63
FIGURE 6.10: POSTERIOR PREDICTIVE ESTIMATION OF S_{ij} FOR FIVE RANDOM POINTS OF SITE 1.	64
FIGURE 6.11: POSTERIOR PREDICTIVE ESTIMATION OF S_{ij} FOR FIVE RANDOM POINTS OF SITE 2.	65
FIGURE 6.12: POSTERIOR PREDICTIVE ESTIMATION OF S_{ij} FOR FIVE RANDOM POINTS OF SITE 3.	65
FIGURE 6.13: POSTERIOR PREDICTIVE ESTIMATION OF S_{ij} FOR FIVE RANDOM POINTS OF SITE 4.	66
FIGURE 6.14: POSTERIOR PREDICTIVE ESTIMATION OF S_{ij} FOR FIVE RANDOM POINTS OF SITE 5.	66
FIGURE 7.1: GEOMETRY AND MATERIALS OF THE DIKE	69
FIGURE 7.2: WATER LEVEL NEXT TO THE DIKE AND HYDRAULIC CONDITIONS IN THE DIKE	69
FIGURE 7.3: EACH SITE'S AND WHOLE DATASET'S q_{net} VALUES WITH FITTED DISTRIBUTIONS	70
FIGURE 7.4: CI AND PPI FOR A RANDOM DETERMINISTIC VALUE OF q_{net}	70
FIGURE 7.5: FLOW CHART FOR THE RELIABILITY ANALYSIS PROCEDURE FOR EACH CASE OF q_{net}	71
FIGURE 7.6: SEARCH GRID FOR THE CENTRE OF THE SLIP PLANE AND THE TANGENT ARE OF THE POSSIBLE POSITIONS OF THE HORIZONTAL TANGENT OF THE SLIP PLANE	72
FIGURE 7.7: RELIABILITY INDEX, β PER SITE AND FOR A NEW SITE WITHOUT AVERAGING OUT THE SOIL PROPERTIES OVER THE SUBSURFACE	74
FIGURE 7.8: RELIABILITY INDEX, β PER SITE AND FOR A NEW SITE WITH AVERAGING OUT THE SOIL PROPERTIES OVER THE SUBSURFACE	75

FIGURE 7.9: COMPARISON OF THE MEAN VALUES OBTAINED BY THE HBM, POOLED AND UNPOOLED MODEL IN THE REGION OF <i>qnet</i> = 380 kPa.....	76
FIGURE 7.10: RELIABILITY INDICES PER SITE FOR THE CASE OF NO AVERAGING OF <i>Su</i> OVER THE SUBSURFACE WITH STOCHASTIC <i>qnet</i> ASSUMED.	77
FIGURE 7.11: RELIABILITY INDICES PER SITE FOR THE CASE OF FULL AVERAGING OF <i>Su</i> OVER THE SUBSURFACE WITH STOCHASTIC <i>qnet</i> ASSUMED.	78
FIGURE 7.12: PLOT OF THE LN <i>x</i> – LN <i>y</i> POOLED, PARTIALLY POOLED AND UNPOOLED MODELS OF GROUP FIVE.....	78
FIGURE 7.13: DISTRIBUTION OF CALCULATED SHEAR STRESSES ALONG THE SLIP PLANE	79

LIST OF TABLES

TABLE 3.1: PRIOR AND HYPERPRIOR DISTRIBUTIONS FOR SLOPE AND INTERCEPT	30
TABLE 3.2: PRIOR DISTRIBUTION FOR THE STANDARD DEVIATION, Σ_{γ}	30
TABLE 7.1: MECHANICAL PROPERTIES OF THE SOIL MATERIALS OF THE SLOPE STABILITY MODEL.....	72
TABLE 1: SUMMARY STATISTICS PER SITE FOR THE q_{NET}	86
TABLE 2: SUMMARY STATISTICS PER SITE FOR THE SU	86
TABLE 3: SUMMARY STATISTICS PER SITE FOR THE Nkt	86
TABLE 4: COMBINATIONS OF FUNCTIONAL FORMS AND POOLING FAMILIES TO FORM THE STATISTICAL MODELS	87

1. INTRODUCTION

The design of structures demands geotechnical calculations to be made, which are based on the soil model or a representative soil stratigraphy and geotechnical parameters values. However, these parameters usually vary spatially. In addition, site investigation (SI) data is often limited and the knowledge of the subsurface is not extended at each point of the site. In other words, geotechnical parameters are observed in point measurements. Moreover, many SI tests provide measurements that need to be transformed into useable geotechnical parameters. Such transformations may induce uncertainty in parameter determination. Consequently, geotechnical parameter estimation contains uncertainty which propagates into the design. Managing this uncertainty is central to geotechnical design. Typically, standards such as Eurocode-7 (EC-7) offer guidance on dealing with uncertainty in a practical and conservative fashion.

Site characterization practice defines the geotechnical parameter values and their associated uncertainty. Typically, engineers rely not only on site-specific measurements but also on knowledge from other relevant sites and their well-established experience. Yet, this practice does not always yield optimal results and is prone to subjectivity. To counter this, data-driven site characterization (DDSC) offers a methodology that consistently quantifies information from multiple sources during the characterization of geotechnical parameters. Additionally, Bayesian statistics offer a valuable perspective to the DDSC problem. Adopting Bayesian statistics holds several advantages which allow to explicitly quantify uncertainty.

Among the numerous advantages, one investigation could be towards the DDSC capability of using data from relevant sites and prior knowledge to make conclusions for a specific site. The value of using broader data in making site-specific predictions can be explored. It is expected also that the engineering decision making will be supported as this DDSC skill is able to provide ranges–distributions of the site-specific parameter values, determining the uncertainty quantification and propagation. Moreover, a similar capability of the DDSC that could be explored is the ability to identify the three-dimensional soil variability patterns. These two branches of the application of the Bayesian methods in the context of DDSC can provide better representation of the geotechnical uncertainty.

The impact of adopting advanced statistics for the derivation of the geotechnical parameter values can be highlighted by applying their results in a reliability analysis of geotechnical structure. The results of this analysis must be compared with the results of the analysis using input data obtained by applying methods of the current practice.

It is proven from the literature that the adoption of Bayesian statistics to complement the SI holds many benefits for the geotechnical engineers. However, Bayesian statistics have not been applied extensively in the field of geotechnical engineering. Moreover, it is not thoroughly investigated the impact of applying Bayesian statistics into the uncertainty propagation from the uncertainty of the geotechnical parameter values to the design of the geotechnical structure. The current practice guidelines do not include a robust mathematical procedure to incorporate engineering experience and knowledge on relevant sites to make site specific conclusions.

1.1 BACKGROUND

The current practice of the geotechnical parameter values derivation demands a strong intuitive process from the engineers. EC-7 explicitly states that apart from the results of the direct measurements of the geotechnical parameters, engineers must account for non-quantifiable knowledge such as experience, history of the site and behaviour met in neighbouring sites to derive the site-specific geotechnical parameter values. However, a mathematical framework is missing. Furthermore, EC-7 suggests making conservative estimations to achieve safe design overcoming the geotechnical uncertainty, leading to expensive design and without accurately evaluating the probability of failure.

The geotechnical data is usually divided into different groups or sites which can be regarded as different geographical regions. In the current practice, there are two major methods of defining geotechnical parameter values having as input observations divided into different groups. The first one is the pooled model which uses the observations of all groups equally to derive the geotechnical parameter values of a specific group. The statistical model that predicts the geotechnical parameter values in this case is the same for all groups. The second model is the unpooled where the prediction of the geotechnical parameter values of

a specific site arises from a statistical model which uses only this site's available data to be trained.

The Hierarchical Bayesian Model (HBM) constitutes a statistical model which is flexible to perform between pooled and unpooled models. This model is trained based both on site-specific and global observations and it can account for the engineering experience. The pooled, unpooled and HBM can be compared by applying the Bayesian Data Analysis (BDA) workflow.

Consequently, advanced statistical methods are proposed that quantitatively combine data with engineering judgement (DDSC) as well as they can quantify the uncertainty of the geotechnical parameter values. The application of Bayesian statistics can combine data from the examined site, relevant sites, and engineering judgement to make conclusions relatively the geotechnical parameters values for the examined site, relevant sites and for a new site without available measurements.

1.2 MOTIVATION

The comprehensive study of the proposals given by the EC-7 regarding geotechnical parameter derivation and the current practice of the site characterization has made apparent the shortages of these procedures. At the same time, the introduction of advanced statistical methods in the context of DDSC gives the opportunity for supporting the engineers upon site characterization and the derivation of the geotechnical parameter values. As it will be presented in the section of literature review below several papers suggest that DDSC using Bayesian statistics presents satisfactory results. The outcome of these papers boosts further research on using the Bayesian methods for predicting geotechnical parameter values and the evaluation of their performance under some benchmark examples.

This thesis aims to assess the possible benefits of applying HBM through BDA for quantifying the uncertainty of the geotechnical parameters over the standard practice. The impact of this method will be further highlighted in the context of a reliability analysis of a slope stability project.

1.3 RESEARCH QUESTIONS

The geotechnical parameter values derivation with methods of current practice has uncertainty which can be further reduced. Geotechnical engineering community adopts conservative estimations to achieve safe design, leading to large expenditure. Recent literature studies introduce DDSC using Bayesian statistics to gain insight into the geotechnical parameter uncertainty. The aim of this thesis is to answer the following main research question.

Q: Can HBM enhance geotechnical decision-making and achieve safe, and economic designs over the standard approach?

The answer to this question is complex and it must be subdivided into simpler questions.

- Q1: What datasets that can support DDSC are available?
- Q2: How does the performance of HBM and the standard practice models compare in an artificial example?
- Q3: What is the uncertainty quantification of the geotechnical parameter values achieved by HBM versus standard approach in the datasets gathered in Q1?
- Q4: How the results of a dike slope reliability analysis when using as input the results of the HBM and the current practice models are compared?
- Q5: What steps are suggested for future research?

1.4 RESEARCH OBJECTIVES

It is desired to answer if the DDSC using Bayesian statistics can support the geotechnical decision making upon the estimation of the geotechnical parameter values reducing the conservatism. Attention is drawn to HBM because it is expected to bring added value to the engineering community. Can this advanced approach perform better than the current practice models in terms of more accurate and less uncertain predictions of the geotechnical parameter values?

Additionally, it will be beneficial for the experts to detect the impact on areliability analysis of a dike slope when implementing values from the DDSC results using Bayesian statistics. Can this procedure propose safe and simultaneously economic design over the standard approach?

1.5 APPROACH OF THE THESIS

In the context of this thesis, the uncertainty in the estimation of the undrained shear strength, S_u from measurements of the net cone resistance, q_{net} of clay in Dutch sites will be investigated using HBM. The efficiency of adopting HBM will be further reviewed by comparing its results with the standard approach. The predictions derived from different statistical models will be compared.

Two components constitute a statistical model. The relationship or functional form between S_u and q_{net} and the pooling family which describes how the grouped data is used to calibrate the models. The available pooling families are the pooled, unpooled and the HBM. The BDA workflow will render the comparison of the statistical models feasible. The focus will be on the results of HBM, and it will be judged whether it is more beneficial for the engineering practice compared to the other two pooling families. Additionally, the fittest functional form will be identified. Eventually, the impact of using HBM predictions for reliability analysis of a dike slope is evaluated by comparing the performance of the results obtained per statistical methodology in fully probabilistic analyses. The reasons lying behind choosing this project are the numerous applications that are available in the Netherlands, the big domain of influence which is sparsely covered by SI, the extensive literature, and research available.

1.6 OUTLINE OF THE THESIS

Chapter 2 presents an extensive literature review on the current practice and modern methods of site investigation. Some research projects where the HBM has been successfully applied are introduced, highlighting the potential of this method.

In chapter 3, the background of the Bayesian statistics and the thesis' methodology are presented. Chapter 4 describes the data collection and its clustering into different groups while the chapter 5 outlines the artificial example where the BDA workflow is validated to be further used with real data.

The main part of the thesis is the comparison of the HBM with the current practice models by applying the BDA workflow using real data as input in chapter 6. The comparison is based on model rankings, the posterior distributions of the statistical model parameters and the predictions of S_u achieved by each model. Subsequently, chapter 7 demonstrates the reliability analysis of a dike slope using input from the current practice models and HBM and their results are compared. The last two chapters 8 and 9 present the conclusions of the thesis by answering the research questions and the limitations along with proposals for future research respectively.

2. LITERATURE REVIEW

In this chapter, the current practice for the derivation of the geotechnical parameter values and the procedure for the SI will be presented as well as modern developments of these fields. Initially, the proposals of the EC-7 are demonstrated as well as the current practice of the SI. Following, applications of the DDSC and Bayesian statistics in the context of SI and geotechnical parameter values calculation are presented. Eventually, some conclusions are drawn from the literature review regarding the content of this thesis.

2.1 CURRENT PRACTICE OF EUROCODE-7

CEN - European Committee for standardization (2004) provides a set of harmonized technical rules for the design of geotechnical construction works. The purpose of these rules is the elimination of technical obstacles to trade and the harmonization of technical specifications. Among its guidelines, it suggests that an engineer should use his / her experience and prior knowledge to derive the geotechnical parameter values.

The procedure for the derivation of the geotechnical parameters values is not transparent. The lab and the in-situ tests can yield results for the specific point of the site or the area of influence of the test. However, EC-7 proposes that these results should not be inherited without any judgement and the engineer should use experience and critical thinking on the selection of the parameters' values for the whole site. To this extent, it proposes conservative estimations for safe derivation of geotechnical parameters. Hence, interpretation of EC – 7 leaves room for the application of statistical tools which can result to more accurate parameter estimation and to reduction of the conservatism in design.

The interpretation of some specific parts obtained by the CEN - European Committee for standardization (2004) will be presented. The proposals of these parts can be enhanced by using Bayesian statistics. These are proposing conservative estimations to the engineer and to make use of non-quantifiable knowledge, such as experience, history of the site and the behavior met in neighboring sites.

First, the EC-7 introduces some general definitions that will be continuously used as reference in the guidelines it proposes. To be more specific, it introduces “comparable experience” (1.5.2.2) (CEN - European Committee for standardization, 2004) which says that an engineer should consider relevant structures and relevant soil/rock conditions, designing the structure and the information gained locally is considered to be particularly relevant. However, it doesn’t provide any way on how to use local information from local and similar sites / soil conditions. Such a relationship can only be established through critical thinking based on the EC-7.

Another definition introduced by EC-7 is the “derived value” (1.5.2.5) (CEN - European Committee for standardization, 2004). It suggests that the parameter value that will be used in the analysis should be obtained by theory, correlation, or empiricism from test results. In other words, the engineer should not rely exclusively on the results of laboratory / in situ test but should also consider additional factors upon determining the parameter values to be used in an engineering analysis. When there is absence or insufficient tests, the parameter derivation can be supported by an advanced predictive model.

In addition, EC-7 admits that the SI is limited and not always reliable. The more limited it is and the lower quality it has, the less knowledge is gained upon the ground conditions (2.4.1 (2)) (CEN - European Committee for standardization, 2004); Thus, methods for enhancing the predictions of the soil properties at points where SI is not available must be developed which will probably use the data from sites relevant to the examined one.

EC-7 proposes that the establishment of geotechnical parameters values should consider relevant published data, local and general experience. The results of any large-scale field tests trials and measurements from neighboring structures should be accounted for (2.4.3 (5)) (CEN - European Committee for standardization, 2004). However, it is not clear how it is possible to quantify the association of the local data with the relevant published data and with experience in the surrounding region.

Following, EC-7 suggests on deriving the characteristic values of soil properties. First, in the section (2.4.5.2 (1)) indicates the same procedure as this of the “derived value”, which has been discussed above. Additionally, it states that the selection must be based on geological and other background information, such as data from previous projects (2.4.5.2

(4), 3.2.1 (1), 3.2.2 (1), 3.2.3 (5)); Nevertheless, a procedure for using this data is missing. The selection must also account for variability of the measured parameter values and other relevant information (2.4.5.2 (4)); yet the type, either local or regional of the variability is not specified. It suggests also making a conservative assumption by taking the most unfavorable combination of upper and lower values of independent parameters (2.4.5.2 (6)). In other words, it proposes to not account for the correlation between the properties and to use the extreme unfavorable values in conservatism.

EC-7 implicitly states to use statistical methods which allow to incorporate data from prior knowledge. To be more specific, using statistical methods for the characteristic values for ground properties must differentiate between local and regional sampling and make use of prior knowledge of comparable ground properties (2.4.5.2 (10), 3.1 (1)) (CEN - European Committee for standardization, 2004). However, it doesn't expand on which statistical methods exist on this case and how can the a priori knowledge be incorporated in the selection of the characteristic values. The method of exploiting samples and data from regional sites is missing. Lastly, optimization of the design can be achieved as new information is retrieved during the construction operation by updating the statistical models (3.1 (2)).

2.2 CURRENT PRACTICE OF SITE CHARACTERIZATION

Baecher & Christian (2003) define site characterization as an accumulation of actions that are executed prior to any engineering calculations and analyses. It is intended to provide the engineers with knowledge on the geology and the relevant material properties that prevail on the construction site.

So far, site characterization is largely based on engineering judgement as it constitutes a strongly intuitive process, and it is usually comprised of three stages. The first one is the reconnaissance where qualitative estimations are made upon the local and regional geology. The means for doing these estimations are the geological and topographic maps, air photos, and records of nearby constructions. At this stage, qualitative hypotheses are made which will be further investigated by sampling and testing. Secondly, the preliminary investigation is performed where the first quantitative estimations are made by executing limited borings, tests, and surveys. At this stage, the reconnaissance stage is expanded by confirming the

qualitative hypotheses and introducing the first quantitative hypotheses. The third stage is the detailed investigation, where it is sought to confirm the quantitative hypotheses made previously. More detailed measurements are executed to obtain information on the geometry and the material properties. The final measurements are available only at some specific points. The engineer should decide upon the continuity of the measurements between the points relying on the qualitative hypotheses he/she has made during exploration / investigation stage. Schematically, the procedure of site characterization is presented at Figure 2.1.

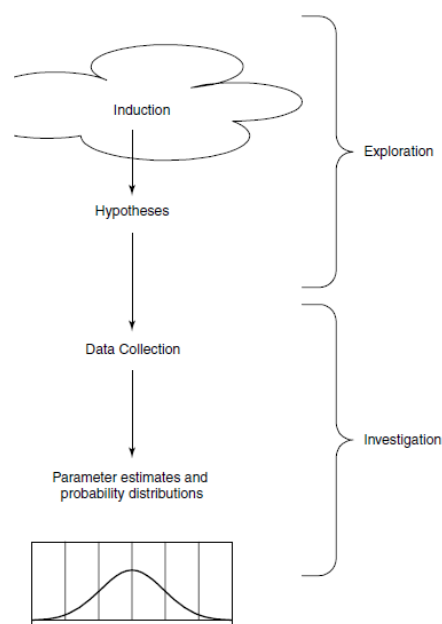


Figure 2.1: Procedure for site characterization in standard practice, taken from Baecher & Christian (2003)

The site characterization practice hints that an engineer should use prior knowledge from relevant projects and geological regimes for the expression mainly of the qualitative hypotheses. Apart from that, the records from similar and nearby constructions sites are valuable for the conceptualization of the soil subsurface where the construction works are going to operate. However, up until now this procedure is executed through the engineering judgement, without the support that it could be provided with quantifying the prior knowledge and the information that is available from neighbouring sites.

2.3 DATA DRIVEN SITE CHARACTERIZATION AND BAYESIAN INFERENCE

DDSC acts as a means to tackle the drawbacks of the standard SI procedure. DDSC has been introduced to support site characterization by quantitatively combining data with engineering judgement. The nature of useable information is very broad as it can contain site specific data and data from relevant sites either from present or the past. A schematization of the procedure employed by the DDSC can be seen in Figure 2.2.

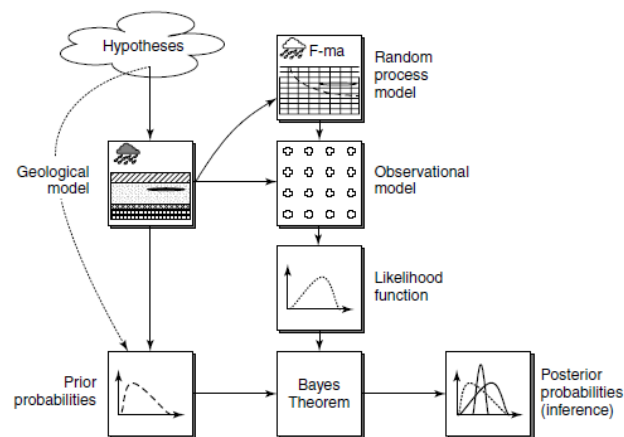


Figure 2.2: Procedure of the DDSC obtained by Baecher & Christian (2003)

DDSC has to cope with some challenges. First, it must be able to represent as accurate as possible the characteristics of the data that deviate significantly from the ideal situation. In addition, it must be able to identify the “site uniqueness”, the characteristics of the site that make it different from others. Thus, the available data that exists from other sites can be combined effectively to make inferences for the new site. Last, the procedure must be able to map the soil layers boundaries in the three – dimensional space based on the site–specific data.

2.3.1 Bayesian inference

DDSC can be performed via Bayesian statistics. The main attribute of the Bayesian statistics is the Bayesian inference, a particular type of statistical inference. According to it, a probability model (probability distribution) is used to describe the data. The parameters of the statistical model, θ are calibrated based on the prior knowledge through the prior distributions, $p(\theta)$ and the likelihood function, $p(y|\theta)$ which represents the probability of

observing the observed data given that it arises from the assumed probability model. The multiplication of these two factors results to the posterior probability, $p(\theta|y)$ of the model parameters. This represents the probability distribution of the model parameters given the observed data.

Bayesian inference yields some significant advantages, making it preferable than the frequentist inference in civil engineering problems. The first benefit presented by Gelman et al. (2013) is the clarity in its definitions which align with the engineering mindset. For instance, the Bayesian credible interval for an unknown quantity of interest, can be interpreted as a degree of belief in the interval containing the unknown quantity, whereas the frequentist confidence interval can be regarded as a sequence of similar inferences that might be made in repeated practice. Secondly, Bayesian inference can incorporate multiple levels of randomness; thus, it can combine data from multiple sources and then make estimations.

2.3.2 DDSC applications using Bayesian inference

In this section the main reported advantages of applying Bayesian methods will be presented through some acknowledged publications. The main functions of the Bayesian statistics are the identification of the three-dimensional soil properties (subsurface mapping) and the HBM which uses large databases to augment the predictions of the examined geotechnical property.

Bayesian inference is advantageous in the field of the geotechnical engineering because it can prevent the adverse effects of the limited site-specific data and can acknowledge the differences between the different sites. Bayesian inference enhances the available data by using prior knowledge in the form of prior distributions and by using already existing data with the HBM. Consequently, more accurate statistical models are obtained to describe the geotechnical parameter values by quantifying the uncertainty of the model parameters through the posterior distributions(Bozorgzadeh et al., 2019).

First, Ching & Phoon (2020) describe the methodology for addressing the special characteristics of the soil over the depth profiles. At each site, geotechnical data are typically Multivariate, Uncertain, unique (to some degree), Sparse and InComplete which is

abbreviated as MUSIC. These properties pose as significant challenges for statistical characterization of a site. Although, generic assumptions are made to describe statistically the soil parameters such as disconnecting the soil parameters from the spatial variability, Ching & Phoon (2020) have removed the depth independence assumption. The resulting method can estimate the soil parameters beyond one depth; –it can simulate the site–specific random field profiles of the soil parameters. The generated database by Ching & Phoon (2020) MUSIC, is enriched with spatial correlations resulting to MUSIC-X which makes estimations based on both soil parameter and spatial information. This method can also simulate site-specific samples for the whole design parameter depth profiles and in fact, the entire family of depth profiles for all test parameters. Moreover, MUSIC-X can also learn spatial variability patterns over depth. Ultimately, this method allows for predictions of soil parameters over the subsurface which can be used in simulating the spatial variability of soil.

Phoon et al. (2022) apply the DDSC in practical cases. Among other applications, DDSC techniques intend to produce a 3D stratigraphic map of the subsurface domain below a site and to estimate relevant engineering properties at each spatial point based on SI. Uncertainty quantification is necessary, as data is insufficient, incomplete, and/or not directly relevant to derive a deterministic map. The research in DDSC can be enhanced by benchmark examples to compare the performance of different methodologies. The purpose of Phoon et al. (2022) is to propose standard benchmark examples for DDSC subsurface mapping and a benchmarking procedure to measure the performance of any method in a balanced and unbiased way. The benchmark examples are based on synthetic cone penetration test data (cone tip resistance and sleeve friction) that are plausible outcomes from some idealized stratigraphy. The GLasso method is employed for the DDSC, and the accuracy of the predictions is quantified by two performance metrics: (1) root-mean-square error (RMSE) of the cone tip resistance and (2) identification rate (IR) of the soil behavior type (SBT). Similarly, in this thesis the research on the HBM will be enhanced by applying its results in a reliability analysis of a slope stability case.

Bozorgzadeh et al. (2019) explore the use of the Bayesian statistics by employing already existing data from other sites in the form of prior distributions, to augment the project specific data. The authors develop a Hierarchical Bayesian non-linear model for fitting the

empirical Hoek-Brown strength criterion to data sets from multiple sites of triaxial strength of a given rock type. Following, this model and an independent parameter model are applied simultaneously to 40 datasets of granite triaxial strength test results. The cross-validation results yield that the HBM predicts more accurately the strength of the above-mentioned verification dataset than does the independent parameter model. Moreover, the results of the HBM at the group-level can be further used in the future to augment the limited project specific data.

Bozorgzadeh & Bathurst (2022) demonstrate the applicability of the HBM for the statistical analysis of geotechnical engineering data. A practical application “mechanically stabilized earth wall” is elaborated and the authors propose the optimal design method for designing such structures. On the one hand, customary statistical analysis, which is broadly used, lacks the necessary perception, and assumes that all the variation is within the observed random variable without any between-group variation. On the other hand, HBM can distinguish the components of parameter variation between and within groups by utilizing data from multiple sites. Moreover, they can be applied to a significant number of different geotechnical datasets. Applying the HBM to the practical case proves that this procedure allows for the uncertainty quantification from different sources of variation which can be subsequently used for essential predictions in the context of “reliability-based design” and “load and resistance factor design”.

Bozorgzadeh et al. 2023 deal with the application of HBM for the calibration of a regression model based on CPT measurements that predicts the axial capacity of piles driven in mainly fine-grained soil. The main goals of this study are to evaluate the uncertainty of the linear regression model parameters and to assess at what extent the model parameters differ between different sites of the measurements. A database of total 39 measurements from 20 different clay sites is used and the shaft friction is only modelled by the statistical model. The calibration obtained by the HBM is compared with the corresponding calibration of the widely used complete pooling model. Initially, the Hierarchical model accounts for the site-specific data more than does the complete pooling model but with reserving large uncertainty in the model parameters avoiding the overfitting to these data. Additionally, observing the residual plots, the Hierarchical model represents more accurately the outlier measurements, and its

predictive accuracy is higher than that of the pooled model. Lastly, the HBM provides wider posterior distributions but still informative which are useful when new data is observed (updating). The paper explores the use of HBM for geotechnical model calibration, using an example of axial capacity of piles in clay. It addresses two overlooked uncertainties: statistical model parameter uncertainty and variations between sub-groups in a generic database. The HBM outperforms the complete pooling model, offering a more representative uncertainty assessment by allowing group-specific parameters and borrowing information. This paper's findings align with my thesis, where I investigate the application of HBM to characterize the S_u of clay using q_{net} in Dutch sites.

'Kahlstrom & 'Bozorgzadeh (2022) examine the adoption of an optimal statistical model for predicting the S_u from results of CPT and from the water content, w obtained by the index lab testing. The database used for the training refers to clay material primarily from Norway. Four different statistical models are trained ranging from complicated incorporating many independent parameters to the simplest accounting exclusively for the q_{net} . Bayesian regression model is used, and all the data is treated as identical without defining any sub-groups inside the dataset (pooled model). The authors point out that estimating the uncertainty in the regression model parameters allows for the accurate calculation of the mean S_u value and to the construction of prior distributions without knowing the real data. Following, the predictive accuracy of the models has been compared and it is suggested to not use the model with only independent parameter the q_{net} . Lastly, updated predictions are obtained with the models by adding a few data points. The update is not significant because the initial predictions were based on equivalently on the whole initial dataset. Authors conclude that the potential benefits of obtaining new site-specific data can be obtained by applying HBM which allows the determination of site-specific model parameters in grouped dataset. In this thesis the relationship between q_{net} and S_u will be explored because it is aimed to highlight the impact of the HBM compared to pooled and unpooled models.

Feng et al. (2023) compare the performance of the HBM with the unpooled model in the context of predicting the state of in-situ stresses of rocks using measurements obtained from the overcoring (OC) test. Bayesian regression models calibrated by the unpooled, and partially pooled technique are applied. The parameters of these statistical models are the in-

situ stresses to be determined. The database used for the calibration of these models is comprised of five boreholes with several tests per each borehole varying from three to six. HBM obtains less uncertain estimates for the in-situ stresses than the no-pooling model. The latter exhibits high epistemic uncertainty due to many uncertainty sources that affect the unpooled model since it accounts for only the test specific data. On the contrary, the partially pooled model allows the borrowing of information from neighbouring tests and provide more certain estimates for the in-situ stresses. Lastly, the predictive adequacy of the models has been compared judging the predictions of unseen new data and the partially pooled is the most competent in this field as well. Overall, the significant number of uncertainty sources that affect the calculation of the in-situ stresses of the rocks render the no-pooling models uncertain yielding not reliable point-estimates for the stresses. HBM can act as a mean to reduce the impact of these uncertainty sources and has greater predictive power than the no-pooling model. Similarly, in my thesis the HBM will be tested by characterizing the S_u from measurements of q_{net} . Its performance will be compared with the custom pooled and unpooled models.

Feng, Bozorgzadeh, et al. (2023) examine the use of Bayesian data analysis to develop statistical models for evaluating the small strain shear modulus, G_{max} based on the CPT tip resistance corrected for pore pressure, q_t . For this reason, it is crucial to incorporate data from various sources such as prior knowledge, experts' experience, and data from neighbouring sites. Moreover, this paper addresses the use of HBM to construct informative prior distributions for the future Bayesian statistical analyses based on already existing databases. The authors employ Hierarchical regression in a statistical model that characterizes the G_{max} based on q_t . The data analysed for the calibration of the model is comprised of 335 paired CPT and G_{max} measurements from 31 borehole locations and divided into 13 different soil units. The results of the analyses demonstrate that the different locations of the data have higher impact on the posterior distributions of the model parameters than that of the soil units. Additionally, the performance of the HBM in terms of making informative prior distributions is investigated. This is achieved by leaving out of the analysis one group of data and then assessing the goodness of fit of the model posterior predictive distributions at these held out points. These points are very well captured by the model indicating that the HBM can construct informative prior distributions. Overall, HBM

constitutes an appropriate method for constructing informative prior distributions. These findings motivate the use of the HBM in the context of the Bayesian data analysis to predict the S_u from CPT results and to construct informative prior distributions for this purpose.

2.4 CPT BASED DERIVATION OF S_u

Cone Penetration Test (CPT) is widely used in soft soil regimes to identify the sequence of the soil strata and the ground water conditions. Additionally, it can describe the mechanical and the physical properties of the soil layers (P. K. Robertson & K. L. Cabal, 2015). CPT is extensively used because of its significant benefits for the engineers. First, it is a fast process yielding continuous profiling and reliable data. Moreover, it has reasonable cost and there is a lot of knowledge on converting the results of the CPT into useful engineering parameters (P. K. Robertson & K. L. Cabal, 2015). The current practice employs the N_{kt} model which relates the q_{net} with the S_u . It is developed based on theoretical solutions and it accounts for the anisotropy, strain rate and the effects of the sample disturbance (P. K. Robertson & K. L. Cabal, 2015).

$$S_u = \frac{q_{net}}{N_{kt}} \quad (2.1)$$

Experts demonstrate that for clay in the Netherlands and for assessing the soil strength in a dike spanning several kilometers, such as the one assumed in this thesis, the N_{kt} can vary from values of 7 to values of 40.

2.5 CONCLUSIONS

The guidelines of the current practice propose some measures that can reduce the effects of the soil uncertainty and achieve safe design. However, these guidelines propose conservative estimations which lead to expensive design. Moreover, they propose the use of non-quantifiable knowledge such as engineering judgement, accounting for the history of the site and the behaviour met in neighbouring sites. Yet, a procedure for incorporating these factors into the design is missing.

Research on the topic of DDSC has shown that it can support the engineering judgement by providing geotechnical parameters uncertainty quantification. Especially, the application of Bayesian statistics in the context of DDSC can provide results that can be directly used by the engineers. Bayesian statistics can assist on identifying the three-dimensional patterns of the geotechnical parameter values (subsurface mapping) and to incorporate data from various sources to make site-specific estimations (HBM). In this thesis only the HBM will be investigated from the two methodologies of Bayesian statistics.

In conclusion, the research already done in these fields suggests that the application of Bayesian statistics in the context of DDSC can offer solutions for the drawbacks of the current practice. The main deficiencies are the conservative estimations and the lack of a robust methodology to incorporate the prior knowledge, engineering judgement and data from relevant sites into estimating the geotechnical parameter values. Additionally, the assumptions made by the engineers are subjective most of the times and the use of generic databases as one database does not allow to identify site-specific attributes of the data. The application of the HBM through the BDA can provide more accurate estimates of the geotechnical parameter values dealing with the current practice deficiencies. It can incorporate prior knowledge and data from relevant sites to make site specific estimations. Hence, it supports the engineers to overcome the deficiencies of the current practice site characterization.

3. BAYESIAN DATA ANALYSIS BACKGROUND AND THESIS METHODOLOGY

3.1 INTRODUCTION

In this chapter, the theoretical and mathematical background of the Bayesian statistics will be presented. In this context, the BDA workflow will be described as well as the methodology for the investigation of the thesis' project.

Davidson (2003) describes the statistical model as a probability distribution based on observations that allows inferences and decision to be created. It consists of two components: the functional form and the pooling family. The functional form describes the type of the model for example ordinary linear regression in the $x - y$ or in the $x - \ln y$ plane. The pooling family describes how the observations are used to calibrate the model.

In this thesis, the relationship of S_u as a function of q_{net} will be investigated. For this purpose, several combinations of functional forms and pooling families will be explored. For each functional form, five different pooling families can be used to calibrate the model parameters, resulting to five different statistical models. Bayesian statistics will be used to train those models.

The aim is to identify the fittest statistical model. This will be achieved by applying the BDA workflow. One step of the BDA workflow is the model validation which enables the model comparison resulting to the recognition of the fittest statistical model. The model comparison and the processing of the models' results will highlight the possible benefits of the HBM over the standard practice pooled / unpooled models. Lastly, a procedure to make predictions will be presented.

3.2 HIERARCHICAL BAYESIAN MODELLING AND POOLING FAMILIES

In the case of ordinary linear regression models used in the thesis ('Montgomery et al., 2012), the statistical models are composed of the outcome variable, y (S_u), the statistical model parameters, θ and the covariate X (q_{net}). The training of θ is based on the observed data. In the context of the geotechnical engineering the observations are usually divided into different groups or sites which represent different geographical regions.

In Figure 3.1 the ellipses with y represent a specific site with paired observations, $S_u - q_{net}$. The ellipses with θ represent the site-specific statistical model parameters. The solid lines represent statistical dependence namely the assumption that the y has been generated from the statistical model with parameters, θ . The dashed – line denotes which observed dataset is used to calibrate the θ .

In Figure 3.1 three different methodologies for developing the statistical models and calibrating their θ are presented. On the left side the unpooled model is elaborated. The statistical model of each site has different θ and it is calibrated by accounting for only the site-specific observations. The sites are different between them (high between group variability) and they do not share any similarities. Unpooled models are inefficient against the limited site-specific data (Bozorgzadeh et al., 2019) because in this case they result to θ with high uncertainty. Additionally, they are affected by various uncertainty sources that they cannot be captured by the statistical model (Feng, Gao, et al., 2023). Additionally, they cannot make predictions for a new site without available measurements. On the contrary, at the right side of the Figure 3.1 the pooled model is described. In this case, a single θ is assumed for all sites while those are perceived as one identical site. The training of θ is equivalently based on the observations of all sites.

The middle ground of these two models is the HBM as presented in the middle part of Figure 3.1. HBM is trained accounting for the site-specific data as well as it borrows information from the other similar sites (Bozorgzadeh et al., 2023) through the hyperparameters, ξ which define the θ . Fundamental concept in the HBM is the exchangeability. It means that the groups are similar and there are not significant differences that would determine the groups of the data (Thomas Wiecki, 2014). The relation between the hyperparameters and the parameters are further illustrated in Figure 3.2.

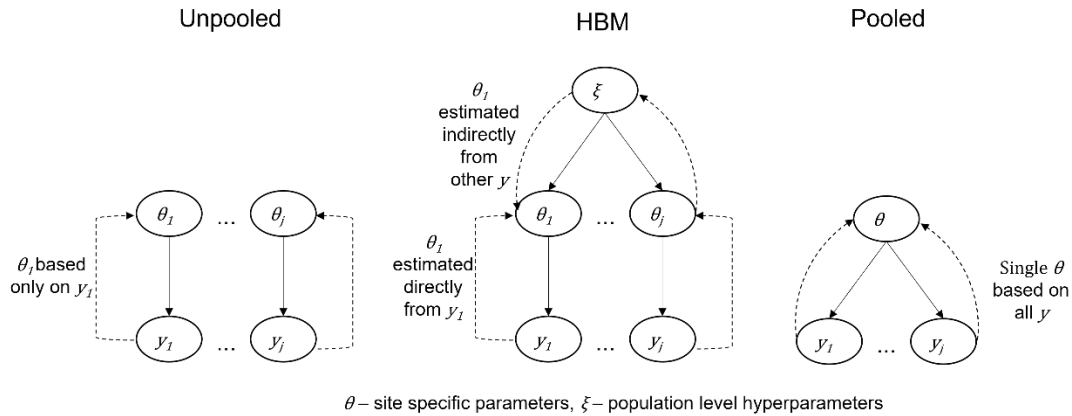


Figure 3.1: Graphical representation of the statistical model families inspired by Bozorgzadeh et al. (2019)

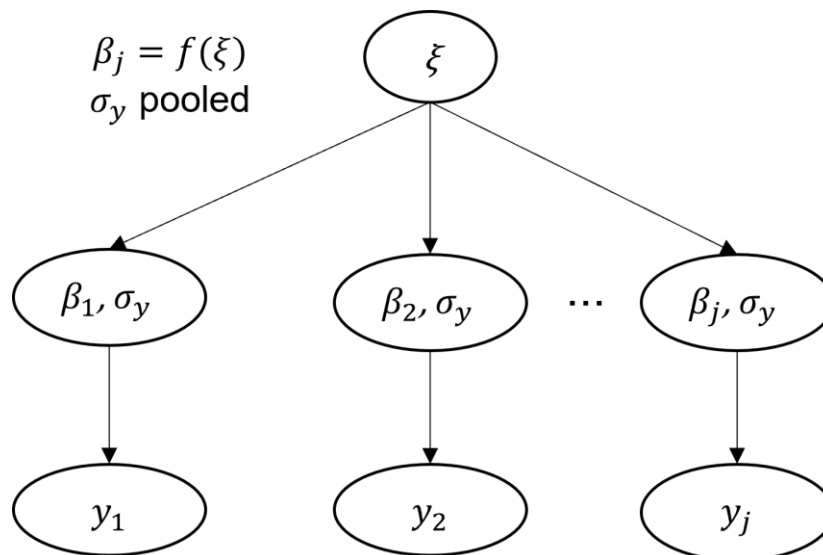


Figure 3.2: Structure of the Hierarchical model inspired by Gelman et al. (2013)

3.3 BAYESIAN INFERENCE

In section 3.2 the procedures of how the available grouped data can be used to calibrate θ are described. In this section, the mathematical process that uses the observations to calibrate θ using Bayesian inference will be elaborated. The θ are not constant numbers and they are expressed with probability distributions.

First, the core of the Bayesian inference is the Bayes' rule, Eq. (3.1) and it aims to make probability statements about θ given the observations, y .

$$p(\theta|y) = \frac{p(\theta, y)}{p(y)} = \frac{p(\theta) p(y|\theta)}{p(y)} \quad (3.1)$$

The prior distribution $p(\theta)$ represents the prior distribution of θ without observing the available data. These are made based on engineering judgement and prior knowledge.

The probability distribution $p(y|\theta)$ is the likelihood function which represents the probability for observing the observed data given θ and will be symbolized as $L(y|\theta)$. It quantifies how well the statistical model explains the observed data. Lastly, the denominator, $p(y)$ represents the evidence which is the probability of observing the data regardless the θ . It is evaluated by summing (discrete distribution) or integrating (continuous distribution) the product of the likelihood times the prior distribution over the entire space θ . Additionally, the evidence acts as normalization factor that ensures that the posterior distribution integrates or sums to one to comply with probability distribution axioms.

After performing the Eq. (3.1), the posterior probability distribution of θ given the observations y , $p(\theta|y)$ is evaluated. This process enables the updating of the knowledge one has on θ based on the observations. The uncertainty of θ is called epistemic uncertainty which represents the uncertainty of the model, and it can be reduced. On the contrary, the aleatory uncertainty refers to the uncertainty inherent in the data and it cannot be reduced.

3.4 FUNCTIONAL FORMS OF THE STATISTICAL MODELS

3.4.1 x - y functional form

In this thesis, ordinary linear regression models will be investigated which incorporate two variables. The response variable, y which represents the S_u and the independent variable or covariate X , which represents the q_{net} . Ordinary linear regression is applied where the observation errors are independent and have equal variance. Therefore, the formulation of the likelihood is $L(y|\theta, X)$ and there are n paired observations (y_i, X_i) (Gelman et al., 2013). The mathematical formulation of the ordinary linear regression is depicted in Eq. (3.2) and the graphical representation in Figure 3.3

$$y|\beta, \sigma_y, X \sim N(X \cdot \beta, \sigma_y^2) \quad (3.2)$$

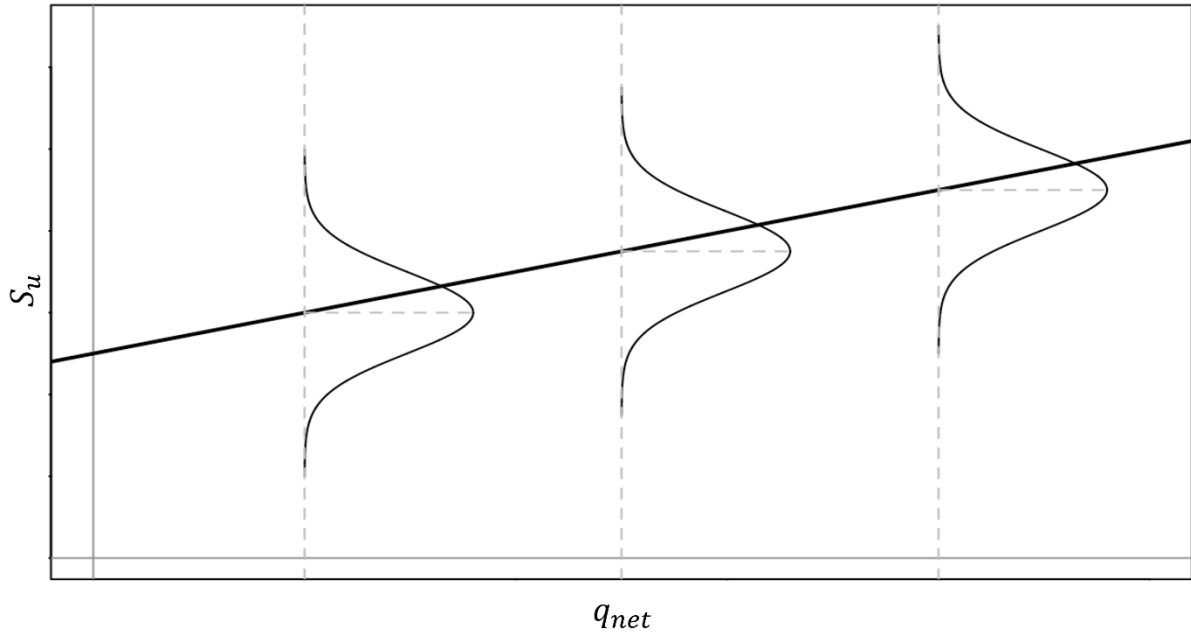


Figure 3.3: Graphical representation of the ordinary linear regression between q_{net} and S_u inspired by Davidson (2003)

The outcome variable, y is a column vector containing the depended variable, Eq. (3.3). The covariate matrix X is presented at Eq. (3.4); the first column contains ones for the intercept term while the second the measurements of the q_{net} . The β array, Eq. (3.5) contains the intercept, β_0 and slope β_1 and along with the standard deviation, σ_y of the error around the expected value constitute the θ Eq. (3.6).

$$y = \begin{bmatrix} y_1 \\ y_2 \\ \vdots \\ y_n \end{bmatrix} \quad (3.3)$$

$$X = \begin{bmatrix} 1 & X_1 \\ 1 & X_2 \\ \vdots & \vdots \\ 1 & X_n \end{bmatrix} \quad (3.4)$$

$$\beta = \begin{bmatrix} \beta_0 \\ \beta_1 \end{bmatrix} \quad (3.5)$$

$$\theta = \begin{bmatrix} \beta_0 \\ \beta_1 \\ \sigma_y \end{bmatrix} \quad (3.6)$$

The expected value, \hat{y} is evaluated by applying the Eq. (3.7) and lastly, the likelihood is evaluated by the Eq. (3.8) and it is equal to probability density function, *pdf* of the Normal distribution which is symbolized as f_N .

$$\hat{y} = X \cdot \beta \quad (3.7)$$

$$L(y|\theta, X) = f_N(y|X\beta, \sigma_y^2) \quad (3.8)$$

Ordinary linear regression will be applied in the $x - \ln y$ and the $\ln x - \ln y$ space. Hence, three different functional forms of the linear regression can be identified and will be analysed in the sections 3.4.2, and 3.4.3.

3.4.2 $x - \ln y$ functional form

At this functional form ordinary linear regression is performed at the $x - \ln y$ space where the natural logarithm of the y , is a linear function of the observed values, X Eq. (3.9)

$$\ln \hat{y} = X \cdot \beta \quad (3.9)$$

The mathematical formulation of this functional form in the $x - \ln y$ is presented in the Eq. (3.10).

$$\ln y | \hat{y}, \sigma_y \sim Normal(\ln \hat{y}, \sigma_y^2) \quad (3.10)$$

This distribution must be converted into the $x - y$ plane to be compatible with the physical meaning of the variables (q_{net}, S_u). Thus, the likelihood of this model is developed by applying the Eq. (3.11). The likelihood at this case is the *pdf* of the LogNormal distribution, f_{LN} .

$$L(y | \hat{y}, \sigma_y) = f_{LN}(\ln \hat{y}, \sigma_y^2) \quad (3.11)$$

The expected value of this model in the $x - y$ plane can be evaluated by applying the Eq. (3.12).

$$\hat{y} = e^{\ln \hat{y} + 0.5 \cdot \sigma_y^2} \quad (3.12)$$

3.4.3 $\ln x - \ln y$ functional form

This functional form represents ordinary linear regression in the $\ln x - \ln y$ space. The equations for making this functional form are the same with the $x - \ln y$ functional form except from the natural logarithm of the mean value which can be seen at the Eq. (3.13). It must be noted that the first column of the X matrix (3.4) is now equal to e and not ones.

$$\ln \hat{y} = \ln X \cdot \beta \quad (3.13)$$

Additionally, the statistical model of this functional form has the equation of the Eq.(3.10). The likelihood function of the model in the $x - y$ plane can be evaluated using the Eq. (3.11) and lastly, the mean value at the $x - y$ plane is evaluated with Eq.(3.12).

3.5 ORDINARY LINEAR REGRESSION PER POOLING FAMILY

The procedure for estimating the θ differs per pooling family. First, the evaluation procedure of the statistical model parameters, β differs between the pooling families while the standard deviation σ_y . is at all cases the same for all groups (pooled parameter). Standard deviation, σ_y is not expected to vary significantly between the sites and not enough data for training is available. Also, if it is not considered as pooled, it will render the analysis extremely costly (Bozorgzadeh et al., 2023). In this chapter the statistical model families will be presented for the case of the $x - y$ functional form.

3.5.1 Pooled model

The pooled model performs one holistic regression across all sites, without distinguishing any differences between the groups (identical sites. The expected value of the pooled model, \hat{y}_j is evaluated by applying the Eq. (3.14). The j indicates the group that the

model is referring to. The likelihood function of the model is formulated in Eq. (3.15). Figure 3.4 describes the pooled ordinary linear regression.

$$\hat{y}_j = X_j \beta \quad (3.14)$$

$$L(y_j | \hat{y}_j, \sigma_y) = f_N(\hat{y}_j, \sigma_y^2) \quad (3.15)$$

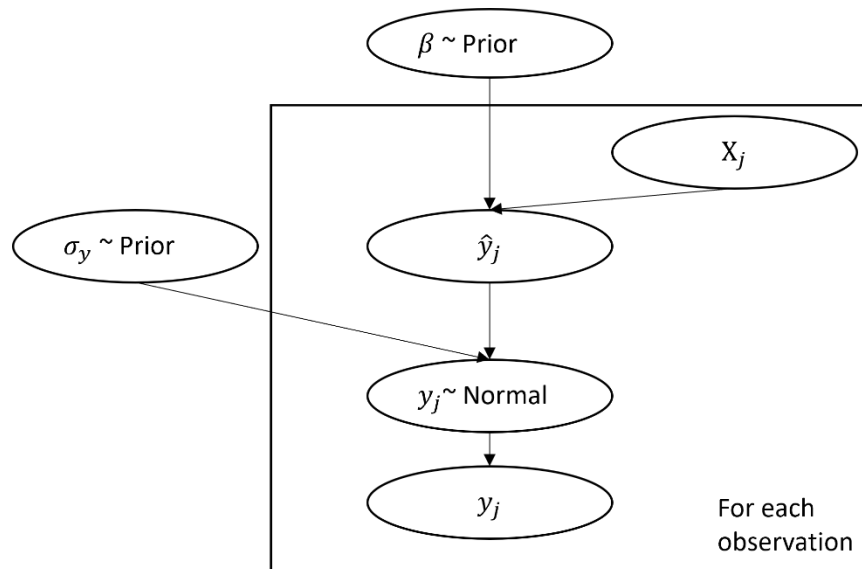


Figure 3.4: Pooled model's probabilistic graphical model

3.5.2 Unpooled model

The complete opposite model of the pooled is the unpooled (Figure 3.5). It performs separate regressions per each group, accounting for each group's data exclusively. The model parameters, β are different per each group, as it is denoted by the indicator j . The likelihood function is identical to that of the pooled model, Eq. (3.15). Figure 3.5 describes the structure of the unpooled ordinary linear regression model.

$$\hat{y}_j = X_j \beta_j \quad (3.16)$$

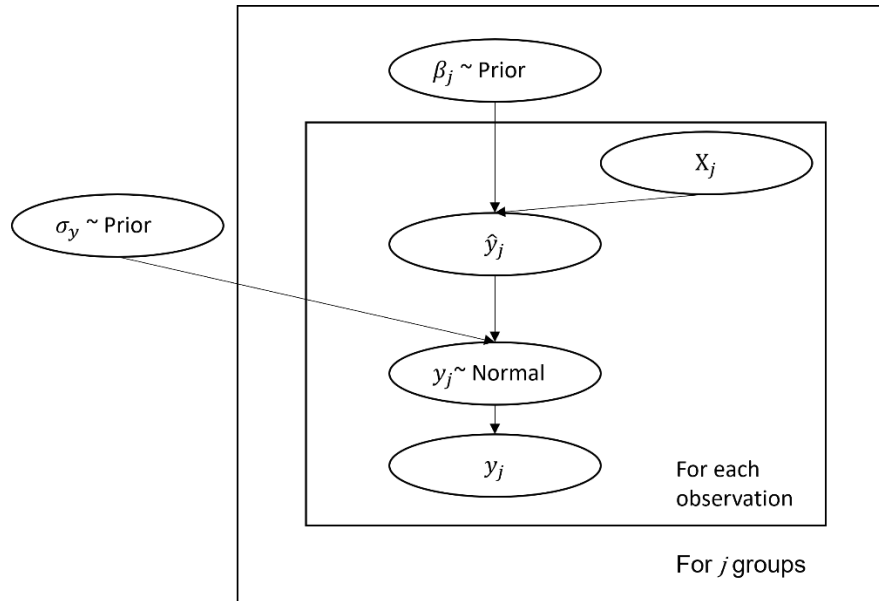


Figure 3.5: Unpooled model's probabilistic graphical model

3.5.3 Hierarchical Bayesian Model

HBM allows for the inheritance of different linear regression parameters, β at each group with considering the data of the other sites as well through the hyperprior distributions (Gelman et al., 2013).

Each parameter, β follows a prior distribution and the coefficients of the prior distributions, ξ follow a common, hyperprior distribution. The coefficients of the hyperprior distributions ξ are called hyperparameters. This structure allows the exchange of information between the sites to make site specific estimations of β . The expected value is evaluated with Eq. (3.16) and the likelihood with Eq. (3.15). Figure 3.6 describes the partially pooled ordinary linear regression.

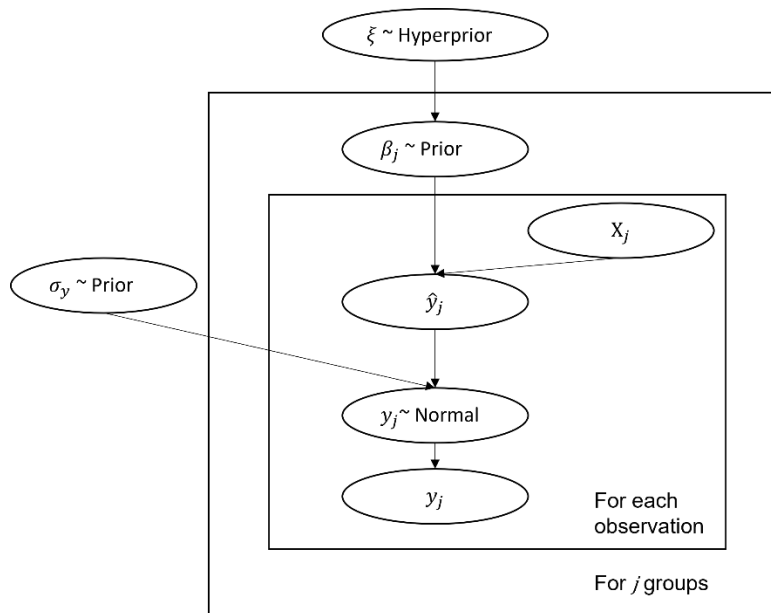


Figure 3.6: HBM's probabilistic graphical model

3.5.4 One – parameter partially pooled model

This statistical model family refers to the case when either slope or intercept is partially pooled, and the other parameter is pooled. Subsequently, two models are formulated: one with partially pooled intercept and pooled slope and another with pooled intercept and partially pooled slope.

Similarly, to the partially pooled model the expected value of the model is evaluated using the Eq. (3.16) and the likelihood is formulated using the Eq. (3.15). Figure 3.7 describes this type of model in the context of the ordinary linear regression.

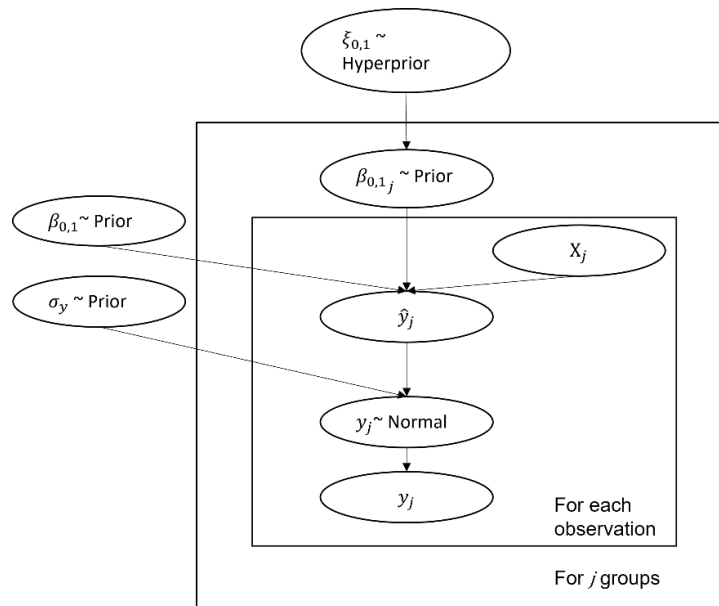


Figure 3.7: HBM of either slope or intercept probabilistic graphical model.

3.6 PRIOR / HYPERPRIOR DISTRIBUTIONS

The application of the Bayes' rule demands the determination of the prior distributions, $p(\theta)$. This reflects the prior knowledge one has on the parameters (β, σ_y) of the models without accounting for the observed data. Very weak prior distributions have been chosen (Gelman et al., 2020) because they cover the possible range of the S_u values. They must maintain reasonable values, otherwise, numerical instabilities at the sampler leading to divergencies of the Markov – Chain Monte Carlo (section 3.7) will occur. Prior predictive checks (Gelman et al., 2020) are used to define the parameters of the prior and hyperprior distributions along with the range of the N_{kt} values to maintain reasonable values of S_u .

Table 3.1 demonstrates the prior and the hyperprior distributions of the slope and the intercept while Table 3.2 informs about the prior distribution of the standard deviation σ_y .

Table 3.1: Prior and hyperprior distributions for slope and intercept

	<i>Slope, β_1</i>	<i>Intercept, β_0</i>	μ_{β_1}	σ_{β_1}	μ_{β_0}	σ_{β_0}
	<i>Truncated Normal</i>	<i>Normal</i>	<i>Truncated Normal</i>	<i>Inverse Gamma</i>	<i>Normal</i>	<i>Inverse Gamma</i>
<i>x-y</i>	$\mu_{\beta_1} = 1 / 15$ $\sigma_{\beta_1} = 1 / 70$ <i>lower = 0</i> <i>upper = ∞</i>	$\mu_{\beta_1} = 0$ $\sigma_{\beta_1} = 2$	<i>mean = 1 / 15</i> st. dev = 1 / 50 <i>lower = 0</i> <i>upper = ∞</i>	<i>mean = 1 / 50</i> st. dev = 1 / 50	<i>mean = 0</i> st. dev = 1	<i>mean = 1</i> st. dev = 1
<i>x-lny</i>	$\mu_{\beta_1} = 0.003$ $\sigma_{\beta_1} = 0.0002$ <i>lower = 0</i> <i>upper = ∞</i>	$\mu_{\beta_1} = 1.5$ $\sigma_{\beta_1} = 0.7$	<i>mean = 0.003</i> st. dev = 0.0001 <i>lower = 0</i> <i>upper = ∞</i>	<i>mean = 0.0001</i> st. dev = 0.0001	<i>mean = 1.5</i> st. dev = 0.5	<i>mean = 0.2</i> st. dev = 0.15
<i>lnx-lny</i>	$\mu_{\beta_1} = 0.6$ $\sigma_{\beta_1} = 0.04$ <i>lower = 0</i> <i>upper = ∞</i>	$\mu_{\beta_1} = -0.1$ $\sigma_{\beta_1} = 0.4$	<i>mean = 0.6</i> st. dev = 0.04 <i>lower = 0</i> <i>upper = ∞</i>	<i>mean = 0.02</i> st. dev = 0.01	<i>mean = -0.1</i> st. dev = 0.4	<i>mean = 0.2</i> st. dev = 0.1

Table 3.2: Prior distribution for the standard deviation, σ_y

	<i>Standard deviation, σ_y</i>
	<i>Truncated Normal</i>
	<i>lower = 0</i>
	<i>upper = ∞</i>
<i>x-y</i>	$\mu_{\beta_1} = 15$ $\sigma_{\beta_1} = 15$
<i>x-lny</i>	$\mu_{\beta_1} = 0.4$ $\sigma_{\beta_1} = 0.2$
<i>lnx-lny</i>	$\mu_{\beta_1} = 0.3$ $\sigma_{\beta_1} = 0.15$

3.7 INFERENCE AND COMPUTATION

The inference is done by applying the Bayes' rule of Eq. (3.1). The equation of the Bayes' rule is analytical in closed form only for the case of simple models. However, in the context of this thesis complicated models are used with many observations and multilevel randomness (HBM) rendering the solution analytically not feasible.

For this reason, numerical methods have been developed. Specifically, the Markov Chain Monte Carlo (MCMC) is employed from the Python package of PyMC5. MCMC methods utilize the concept of a Markov chain, which is a mathematical framework describing a sequence of random variables in which the probability of transitioning from one state to the next depends only on the current state. In MCMC, a Markov chain is constructed such that its equilibrium distribution matches the desired target distribution. Specifically, the Hamiltonian Monte Carlo (HMC) is employed because it is generally efficient in terms of sampling (Betancourt, 2017). The No – U turn sampler variation of HMC has been used because it enables faster evaluation of the posterior distributions. The inference is done by four parallel chains with 1000 warm – up and 1000 simulations (total 8000 simulations). All chains were examined to ensure the lack of divergencies.

3.8 BAYESIAN DATA ANALYSIS WORKFLOW-COMPARING THE MODELS

Three different functional forms and five different pooling families have been introduced. Hence, 15 different statistical models will be introduced, and it is crucial to identify the fittest one. This will be achieved by applying the Bayesian data analysis workflow (BDA).

The Bayesian inference deals exclusively with the evaluation of the posterior distribution of θ given the observed data and it comprises one step of the BDA workflow, (Gelman et al., 2020). The BDA workflow is a summation of three steps. Initially, a statistical model is generated and subsequently by applying Bayesian inference the posterior distribution of its parameters are evaluated. Lastly, the model is checked and validated. The BDA workflow can be summarized in Figure 3.8 (Gelman et al., 2020). So far, the steps of

constituting a statistical model and making inferences have been described. The subsequent steps of the BDA workflow will be described in the section 3.9.

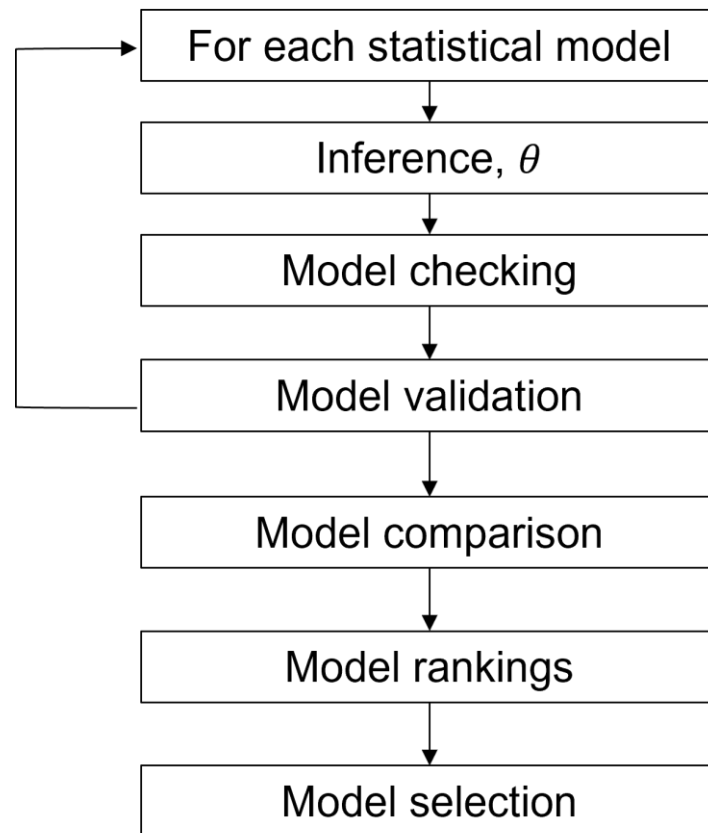


Figure 3.8: Description of the BDA workflow as described in Gelman et al. (2020)

3.9 MODEL CHECKING AND VALIDATION

3.9.1 Model checking

Model checking refers to the verification of the model fitting to the observed data and to the developers' substantive knowledge (Gelman et al., 2013). It constitutes a vital step of the Bayesian analysis as it can detect dysfunctionalities at the prior distributions, likelihood, and the hierarchy of the parameters at the case of the HBM. Model checking can be performed with a number of procedures.

In the context of this thesis posterior predictive check is performed to accomplish the model checking. The posterior predictive check draws values from the posterior predictive distribution to replicate the observed data. Following, it compares the replicated data with

the observed data, and it evaluates the fit between these two components. If there are any systematic discrepancies between the two parts, the model can possibly be invalid. The observed data and the posterior samples are compared visually by plotting the density plots of these two datasets.

3.9.2 Model validation

The process of the model validation aims to evaluate the predictive accuracy of the statistical model. Moreover, its results enable for the model comparison of many statistical models and finally propose the one that has learned most from the data to perform inferences and predictions (model selection).

Two widely used methods for applying model validation are the information criteria and the cross – validation. Cross validation is a set of techniques that assess the fitting of the data at previously unseen data. The model is trained at a subset of the observed data and performs predictions for the remaining observed data (Aki Vehtari, 2020). The accuracy of these predictions informs about the predictive power of the model. The model validation in this thesis is done by applying cross – validation and the two techniques will be analyzed in sections 3.9.2.1 and 3.9.2.2.

3.9.2.1 Leave one out cross validation

The principle of the LOO-CV is to divide the observed data into two groups; one will be the training dataset and the other constitutes the test dataset. The first one is used to fit the model while the second one is used to evaluate the precision of model's prediction. LOO-CV makes training datasets by using all the points except one, y_{-i} , repeatedly for all the points. Following, it evaluates the natural logarithm of the predictive density of the held-out data point y_i . The sum of all the natural logarithms over the whole dataset is evaluated which represents the expected log pointwise predictive density, *elpd* as described in Eq. (3.17).

$$elpd_{loo} = \sum_{i=1}^n \log p(y_i | y_{-i}) \quad (3.17)$$

The procedure that was described above is not computationally efficient; hence, a fast and stable computation for the LOO-CV have been proposed using existing simulation draws from the inference process (section 3.7). The efficient computation method used is called Pareto-smoothed importance sampling (PSIS), a procedure for regularizing importance weights (Vehtari et al., 2017). The greater the value of the *elpd*, the most accurate are the predictions and the model is considered more valid. Since the analysis does not make a full calculation of *elpd*, but rather approximates via Importance Sampling, the standard error of the *elpd* approximation is evaluated. Lastly, the *elpd* difference between these models is demonstrated along with its standard error.

3.9.2.2 Leave one group out cross validation

The second validation metric used for this purpose is the LOGO-CV. It is used evaluate the predictive accuracy for a new group without measurements. The method for calculating this metric is like the LOO-CV but instead of leaving one point out, one group is left out. Again, the higher is the value of the *elpd*, the more representative is the model and the LOGO-CV can be used for model selection (Aki Vehtari, 2022).

3.9.2.3 Akaike information criterion

Model validation is operated with the information criteria as well and they will be presented for comparison reasons. They consider the goodness-of-fit and the complexity of the model.

The predictive accuracy with this criterion is obtained by the Eq. (3.18). The evaluation of the *elpd* with this method is done by the log posterior density of the observed data y given a point estimate $\hat{\theta}_{MLE}$. Also, it incorporates correction for bias due to overfitting through the parameter k . However, AIC is not appropriate for non-linear models without flat priors where the k cannot be simply added. Hierarchical structures and informative priors tend to reduce the overfitting.

$$AIC = -2\log p(y|\hat{\theta}_{MLE}) + 2k \quad (3.18)$$

3.9.2.4 Deviance information criterion (DIC)

DIC can be regarded as the Bayesian version of the AIC. The $\hat{\theta}_{MLE}$ is replaced by the posterior mean of θ , $\hat{\theta}_{Bayes}$ and the k with a data – based bias correction (Gelman et al., 2013). It is evaluated with the Eq. (3.19). However, the WAIC validation metric that will be presented below is a more complete version of DIC.

$$DIC = -2\log p(y|\hat{\theta}_{Bayes}) + 2p_{DIC} \quad (3.19)$$

3.9.2.5 Watanabe – Akaike or widely available information criterion (WAIC)

WAIC is a more Bayesian approach to predict the expectation of the out-of-sample points. It computes the log pointwise posterior predictive density, and it adds a correction for effective number of parameters to adjust for overfitting (Gelman et al., 2013). The estimated log pointwise posterior density at the case of WAIC is evaluated by the following formula.

$$\widehat{elpd}_{waic} = \widehat{lpd} - \hat{p}_{waic} \quad (3.20)$$

Where \hat{p}_{waic} is a simulation-estimated effective number of parameters.

$$\hat{p}_{waic} = \sum_{i=1}^n V_{s=1}^S (\log p(y_i|\theta^s)) \quad (3.21)$$

Where $V_{s=1}^S$ represents the sample variance.

WAIC sums the variance for each datapoint rendering more stable than DIC. WAIC is asymptotically equal to LOO – CV but the latter when evaluated by the PSIS is more robust (Vehtari et al., 2017).

3.10 PREDICTION

After performing the BDA workflow and comparing the models the subsequent step is the prediction of S_u values (\tilde{y}) by evaluating the posterior predictive distribution, $p(\tilde{y}|y)$. It is evaluated with Eq. (3.22) for the case of pooled and unpooled models (Gelman et al., 2013) and with Eq. (3.23) for the case of the HBM.

$$p(\tilde{y}|y) = \int p(\tilde{y}|\theta) p(\theta|y) d\theta \quad (3.22)$$

$$p(\tilde{y}|y) = \int p(\tilde{y}|\theta) \cdot p(\xi, \theta) \cdot p(\theta, \xi | y) d\theta \quad (3.23)$$

The predictions, \tilde{y} refer to the predictions of observable quantities (S_u) at the X -points where measurements are available. Whatsoever, it is desired to obtain predictions at points where measurements are not available. These predictions are denoted as, $p(\tilde{y}_{pred}|y)$ and they can be evaluated by applying the Eq. (3.24) for the cases of unpooled and pooled models. The corresponding formula for predictions with the partially pooled model is Eq. (3.25).

$$p(\tilde{y}_{pred}|y) = \int p(\tilde{y}_{pred}|\theta) p(\theta|y) d\theta \quad (3.24)$$

$$p(\tilde{y}_{pred}|y) = \int p(\tilde{y}_{pred}|\theta) \cdot p(\xi, \theta) \cdot p(\theta, \xi | y) d\theta \quad (3.25)$$

Lastly, one of the goals of the process is to make predictions for a new group. This is possible only for the cases of the pooled and the partially pooled models. The formula for the case of pooled model is Eq. (3.24) while for the HBM can be seen below.

$$p(\tilde{y}_{pred, new\ group}|y) = \int p(\tilde{y}_{pred, new\ group}|\theta) \cdot p(\xi, \theta) \cdot p(\theta, \xi | y) d\theta \quad (3.26)$$

3.11 PROCEDURE FOR OBTAINING THE RESEARCH OBJECTIVES

As stated at the section 1.3 of the research questions, the first step is to find appropriate dataset that can be further used for the training of the statistical models (Q1). Following, the BDA workflow is applied at an artificial example using replicated data. The HBM is compared with the pooled and unpooled models and it is judged whether the BDA workflow is validated, and it can subsequently be applied with real data (Q2).

Upon validation of the BDA workflow, it is applied using as input the real data. The analysis is operated with all the statistical models and the models' rankings are constituted based on the validation metrics. Following, the optimal model is selected based on the

rankings and the engineering judgement. Moreover, the posterior distributions of θ obtained by the models of the top ranked functional form are compared. In addition, random predictions of S_u at the points of measurements proposed by the models of the top ranked functional form are compared as well. The focus of the comparison is between the HBM, and the current practice pooled and unpooled models. Conclusions are drawn regarding the uncertainty quantification obtained between these models (Q3).

The subsequent step is to assess the impact of using data from the HBM results at a reliability analysis of a dike slope. These reliability analysis results will be compared with the corresponding results of the current practice pooled and unpooled models. Conclusions will be drawn on whether the HBM can propose safe and economic design over the standard approach of pooled and unpooled models (Q4). The procedure followed in this thesis is depicted in the form of a flow chart in Figure 3.9.

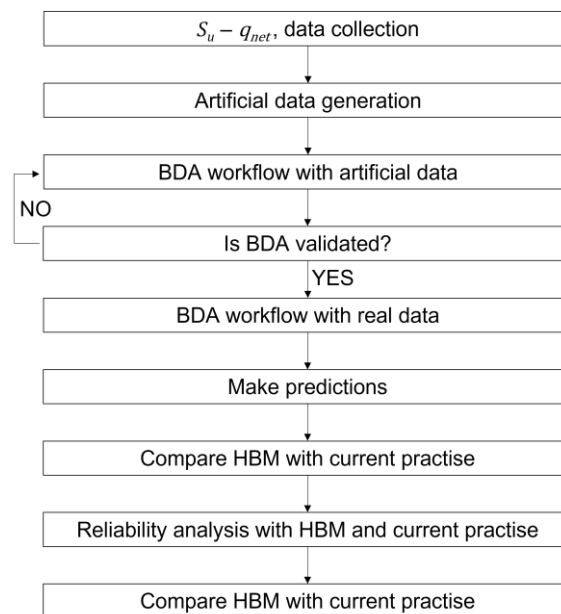


Figure 3.9: Procedure followed in the thesis to answer the research questions and to obtain the research objectives

4. DATA COLLECTION

4.1 INTRODUCTION

In this chapter, the datasets that can support the DDSC will be collected and processed. Initially, the process of data acquisition will be presented referring to the type of the data obtained, the databases used and the handling of the data. Following, the procedure of clustering the data into groups is presented. The complete dataset and its summary statistics are provided in the appendix (APPENDIX).

4.2 DATA ACQUISITION

Paired measurements from the same depth and position of q_{net} , and S_u of clay in Dutch sites have been retrieved. Both the measurements of q_{net} and S_u have been converted to units of kPa. The S_u measurements are obtained by triaxial undrained compression (TX) tests. The S_u measurement at high strain level is examined because geotechnical practice adopts it for dike slope stability problems, as the case that is examined later in section 7. Moreover, the coordinates of the measurements have been retrieved because the data will be divided into different sites. The main sources of data are the database STOWA of Rijkswaterstaat (STOWA, n.d.), the database of ('Lengkeek, 2022) and databases from Deltares' projects. In conclusion, 458 paired measurements have been obtained (Figure 4.1).

4.3 DIVISION OF DATA INTO GROUPS

Initially, the positions of the measurements have been pointed at the map (Figure 4.1) and subsequently data have been divided into groups / sites (Figure 4.2). They have been split accounting for geographical position of the measurements and the q_{net} by applying K-means clustering (Mannor et al., 2011). The K-means clustering algorithm uses the standardized coordinates and standardized q_{net} between the minimum and maximum values to create the groups of the data. The q_{net} influences the clustering as it splits the groups per similar q_{net} values which is expected to occur in the reality. The procedure for the clustering maintains the exchangeability of the data which renders the HBM applicable. The exchangeability refers

to similar slope and intercept values of the model between the groups. Lastly, Figure 4.3 shows the scatterplot of the $S_u - q_{net}$ with the data divided into groups.

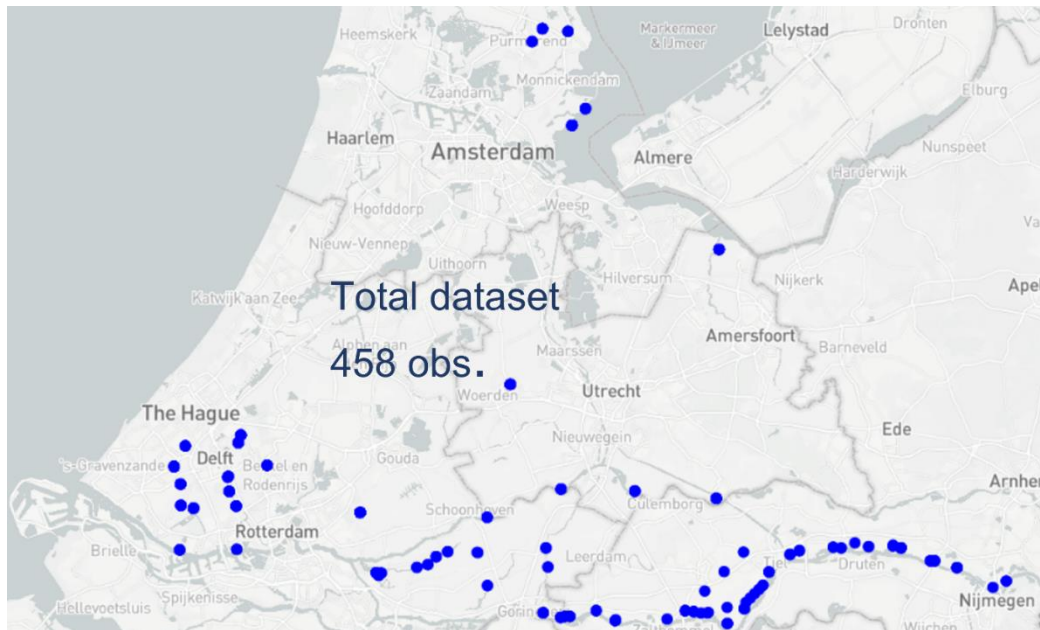


Figure 4.1: Geographical positions of the total datasets of paired measurements $q_{net} - S_u$ without subdivision. The number of the total measurements is projected as well.

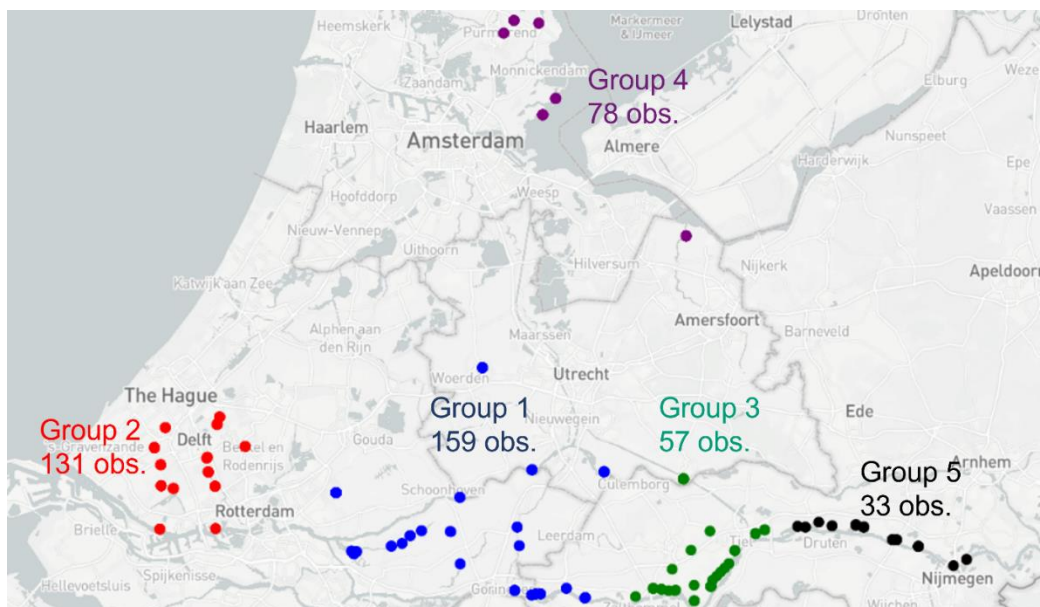


Figure 4.2: Geographical positions of the total dataset subdivided into groups / sites. The number of the measurements per site is presented as well.

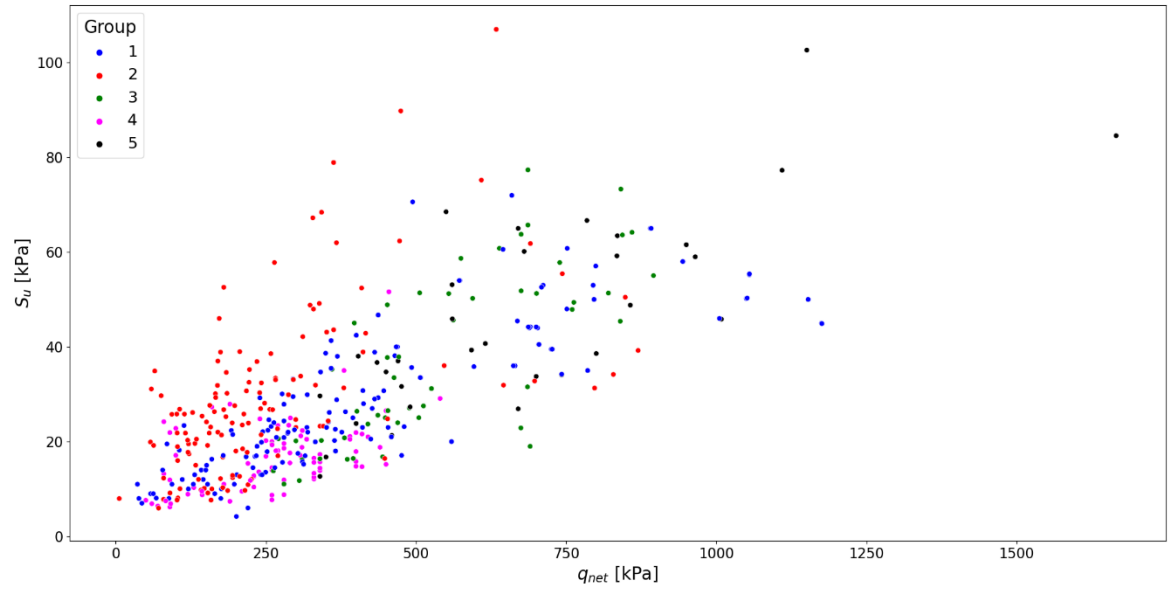


Figure 4.3: Scatterplot of S_u - q_{net} per group / site

5. ARTIFICIAL EXAMPLE

5.1 INTRODUCTION

Before using the data of chapter 4 the HBM is compared with the current practice models of pooled and unpooled in an artificial example. This comparison is performed by the application of the BDA workflow in the artificial example. The goal is to assess the effectiveness of the BDA in several cases of pooling, in order to ensure that it can be further applied in analyzing the real data.

5.2 PURPOSE OF THE ARTIFICIAL EXAMPLE

Before applying the BDA on the actual data, its applicability should be validated. For this reason, an artificial example has been determined where the BDA workflow is applied at artificial data and the performance of the HBM is compared with the current practice of pooled and unpooled models. Consequently, the purpose of the artificial example is to verify the adequacy of the BDA and approve it for further use with real data.

In the artificial example, artificial data is used to train several soil strength models in a Bayesian context and the proposed BDA is then used to select the fittest one. If the choice of the fittest model and its posterior distributions fulfill the validation criteria, the BDA can further be applied at the real data.

5.3 PROCEDURE OF THE ARTIFICIAL EXAMPLE

In this section, the procedure followed for the artificial example will be analyzed. In short, the basic processes of the artificial example are the artificial data generation, their use for training different models and finally the criticism of the BDA results based on two criteria.

Three different clustered datasets are generated using a selected functional form, each one representing a pooled, an unpooled dataset and a partially pooled (HBM) dataset. Following, each dataset is used as input in the BDA workflow (section 3.8). Monitoring the posterior distributions of the models and the model rankings, it is examined if the BDA is

validated (5.4). The procedure of the artificial example is presented concisely at the figure below.

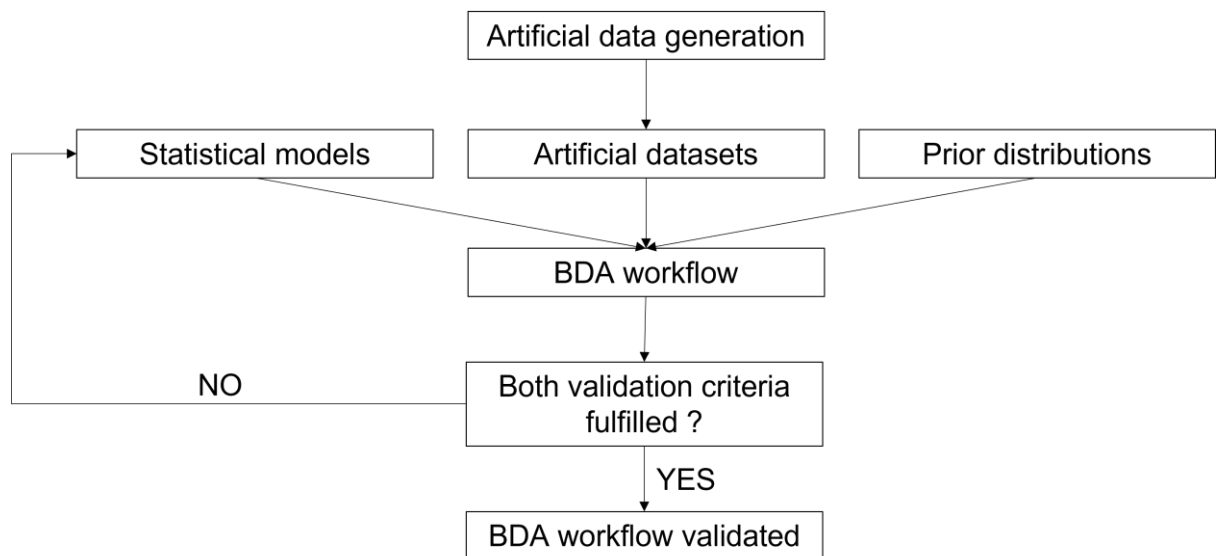


Figure 5.1: Procedure of the artificial example

5.4 BDA WORKFLOW VALIDATION CRITERIA

Two criteria have been implemented for validation purposes. The first one is relevant to model ranking. After running the BDA workflow for each of the three different datasets, two rankings are created using each of the LOO-CV and LOGO-CV. The name of this criterion is: *validation with model rankings* and its formulation is the following:

Does the first ranked model per artificial dataset using LOO-CV and LOGO-CV coincide with the model that generated the artificial data?

Satisfying this criterion, the workflow will propose the correct model to perform the statistical analysis with the real data where no knowledge on the “true” statistical model, in regard to pooling and functional form, is available.

The second validation criterion refers to the comparison of the model parameters posterior distributions with the parameters that were used to generate the artificial data. The uncertainty of the model parameters is called credible interval (CI) of the model parameter. Also, the CI of a model represents the uncertainty of the model and the distribution of the

mean value. The name of the second validation criterion is *validation with posterior distributions* and its formulation is the following:

Does the 90% posterior credible interval of a model parameter obtained by the first ranked model from the former validation criterion contain the parameter that was used for the artificial data generation?

Fulfilling this criterion verifies that the posterior distributions of the best model proposed the BDA workflow can approximate the parameter set that generated the data.

5.5 GENERATION OF ARTIFICIAL DATASETS

Three different artificial datasets are generated in the context of the artificial example; namely pooled, partially pooled and unpooled datasets. In the case of the pooled dataset, it is assumed that the separate groups are generated using the same underlying parameters. On the other hand, in the case of the unpooled dataset it is assumed that the groups are completely different among each other. Lastly, the partially pooled dataset assumes that the data between the groups come from different distributions, which are following a global trend. The presentation of each artificial dataset can be seen at Figure 5.2 along with the models for generating and the 95 % percentiles of the data. The functional form of the models that generated the artificial data is $\ln x - \ln y$ because the trend of the real data is concave, S_u is bound to non-negative values and the variance increases as the q_{net} increases.

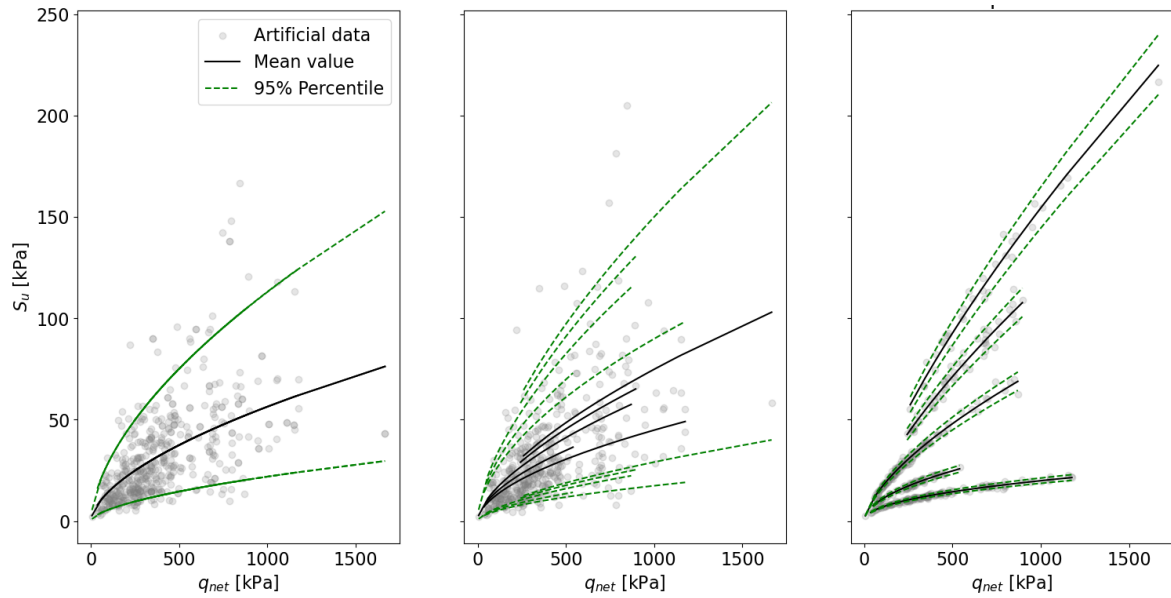


Figure 5.2: Artificially generated data with pooled, HBM and unpooled model. The mean values and the 95% percentile of the generated data

5.6 RESULTS AND DISCUSSION

5.6.1 Validation with model ranking

The model rankings for the analysis of the pooled the dataset are inspected. The BDA identifies the $\ln x - \ln y$ pooled model as the fittest which coincides with the artificial data generating model. This model achieves the greatest ranking in both LOO-CV (Figure 5.3) and LOGO-CV (Figure 5.4).

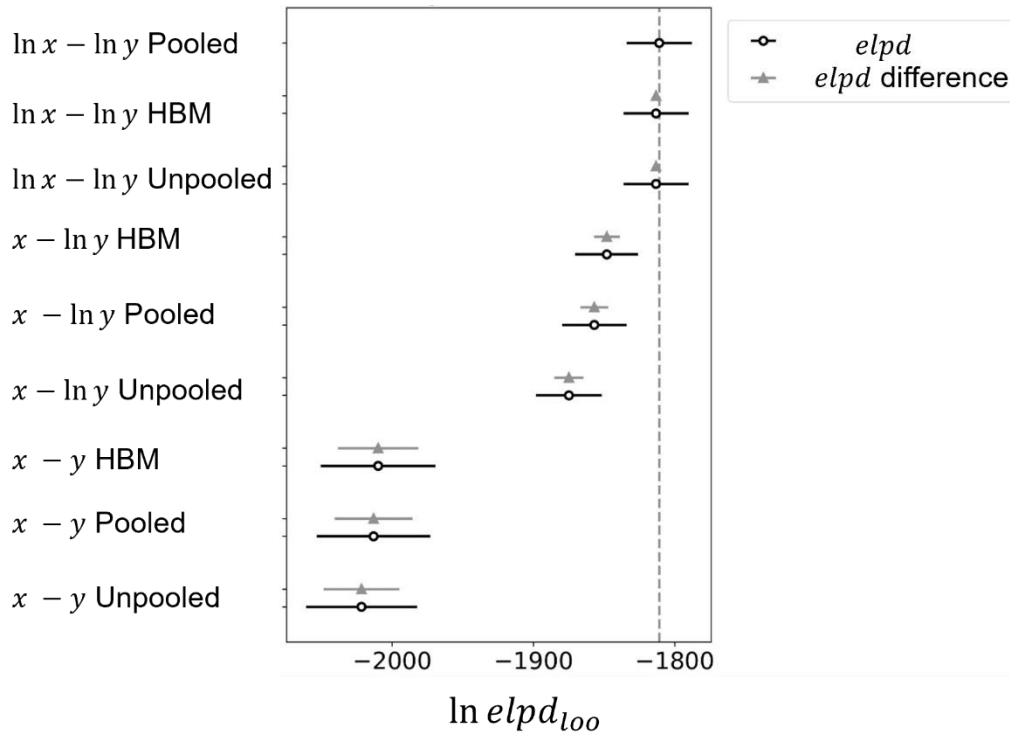


Figure 5.3: Model rankings based on the LOO-CV for the pooled dataset.

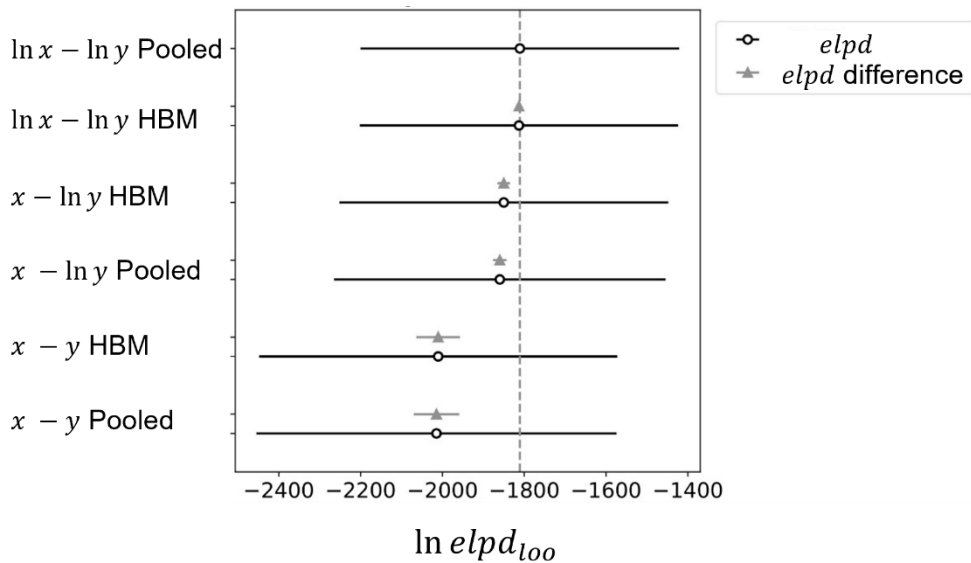


Figure 5.4: Model rankings based on the LOGO-CV for the pooled dataset.

The next rankings that will be presented are created after running the BDA workflow for the partially pooled dataset. The model rankings created by the LOO-CV show that the best model is the $\ln x - \ln y$ HBM that accords with the artificial data generation model (Figure 5.5). As far as the LOGO-CV ranking, the first model is again the model used for artificial data generation (Figure 5.6).

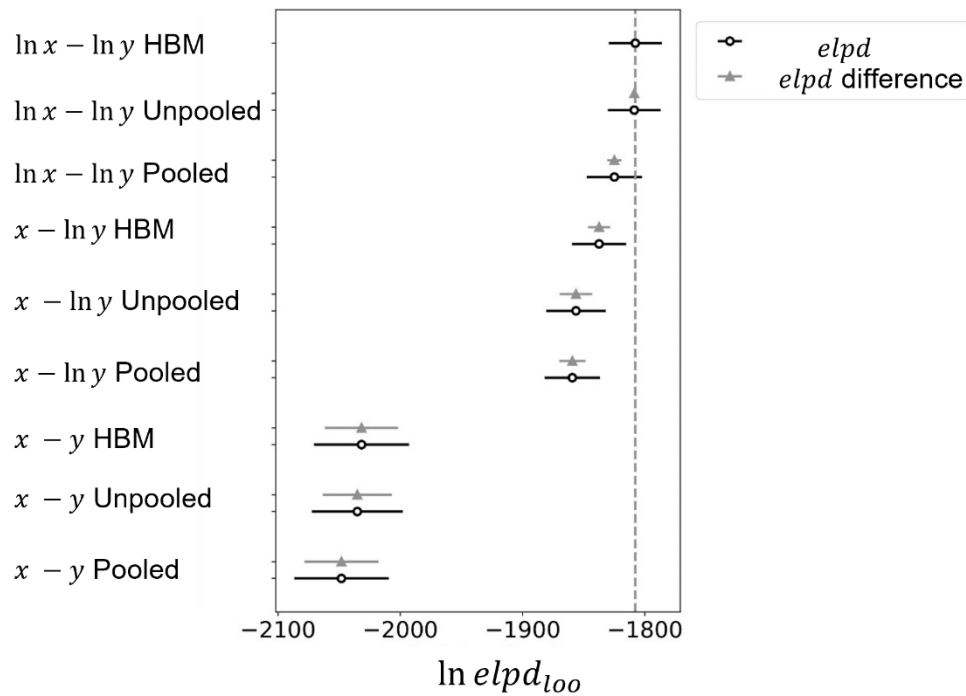


Figure 5.5: Model rankings based on the LOO-CV for the partially pooled dataset.

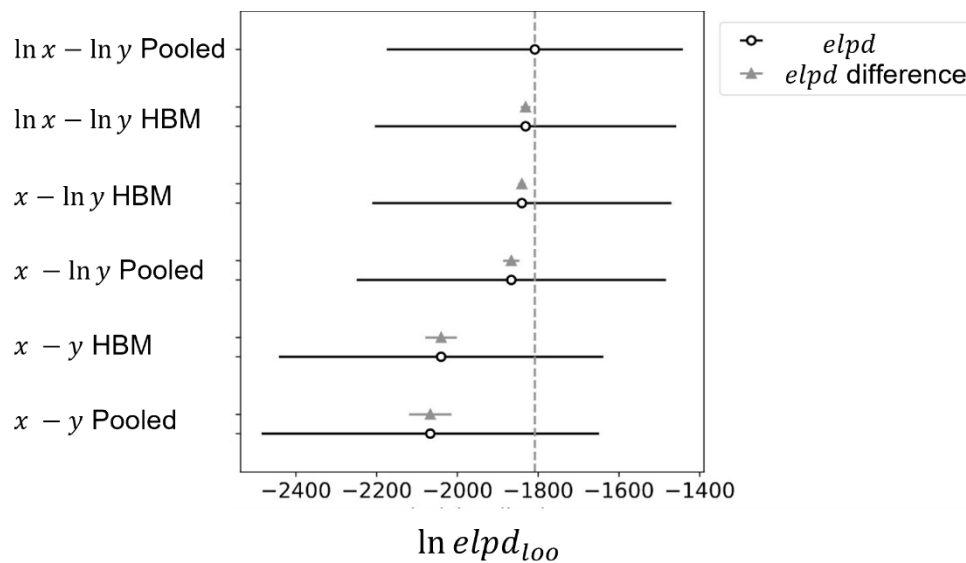


Figure 5.6: Model rankings based on the LOGO-CV for the partially pooled dataset

Lastly, the results of the model rankings after running the BDA workflow for the unpooled dataset are presented. The ranking based on the LOO-CV exhibits that the optimally performing model is the $\ln x - \ln y$ HBM while the $\ln x - \ln y$ unpooled model is ranked second. However, the difference between the first and the second model is negligible, and it is sensible to consider that the criterion is still fulfilled (Figure 5.7). The HBM has flexibility to tend to the unpooled model if needed.

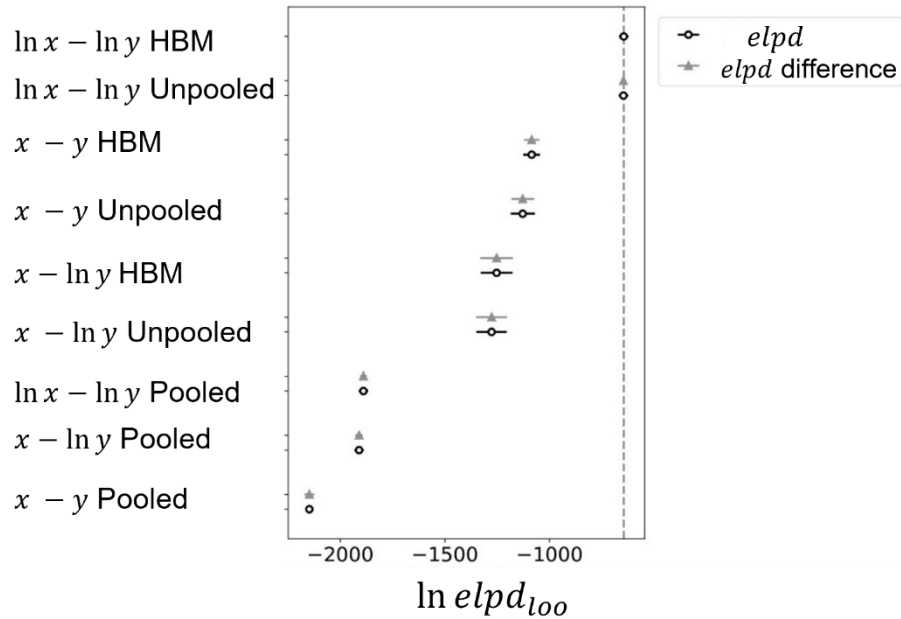


Figure 5.7: Model rankings based on the LOO-CV for the unpooled dataset.

For the case of the LOGO-CV, the unpooled models are not included as they are not able of making predictions for the geotechnical parameter values of groups without paired measurements. In this case, the $\ln x - \ln y$ HBM model is ranked first (Figure 5.8).

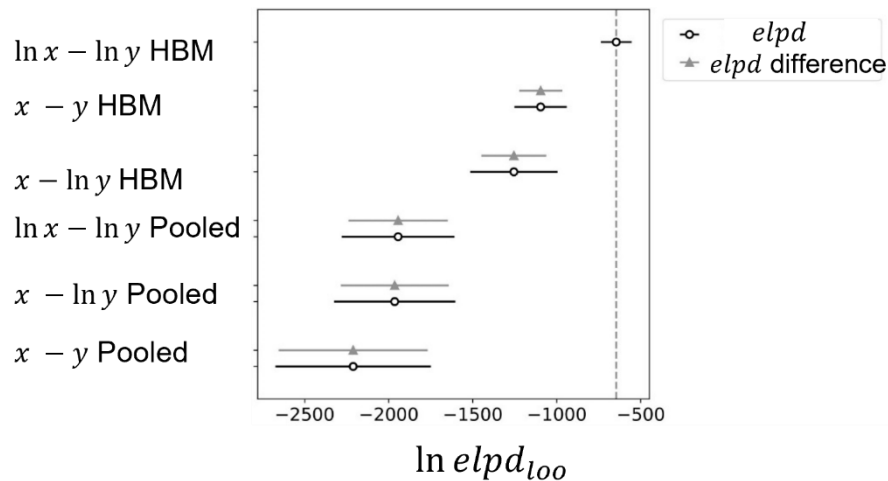


Figure 5.8: Model rankings based on the LOGO-CV for the unpooled dataset.

In conclusion, after running the BDA workflow for the three different datasets, the models ranked first using the LOO-CV and the LOGO-CV coincide with the models that were used to generate each artificial dataset. An exception is met in the case of the unpooled dataset, where the HBM is the best model based on the LOO-CV. However, the difference between the second – unpooled model is negligible and this ranking is acceptable.

5.6.2 Validation with posterior distributions

The second validation criterion refers to the comparison of the model parameters posterior distributions with the parameters that were used to generate the artificial data. The answer to this validation criterion is not straightforward because the Bayesian model does not realize the parameter used for data generation but the information that artificial data can transfer. Since linear regression models are employed, the raw information transfer is expressed by the Ordinary Least Squares (OLS) (Montgomery et al., 2012) estimators and their uncertainty. Therefore, it is essential to compare the statistical parameters of slope and intercept obtained by the OLS regression complemented by their uncertainty. For the case of σ_y only the posterior distribution and the value used for data generation are depicted. These figures are presented in the following sections for each dataset.

First, the posterior distributions of $\ln x - \ln y$ pooled model will be presented when trained at the $\ln x - \ln y$ pooled dataset. The training of this model is done directly using the entire dataset and one common posterior distribution is produced for all groups per model parameter.

The $\ln x - \ln y$ pooled artificial data has OLS estimators that tend to the “true” parameter and their uncertainty is low (Figure 5.9). The reason that in pooled modelling, training uses all observations of the data simultaneously, leading to a great decrease of epistemic uncertainty. The 90% CI’s of the OLS estimators contain the “true” parameter. Moreover, the 90 % CI of the posterior distribution contain the OLS estimator. Thus, the posterior distributions can represent the “true” parameters that were used for the data generation.

In the case of the posterior distribution of the σ_y , the 90% CI of the posterior distribution contain the value that was used for data generation (Figure 5.10).

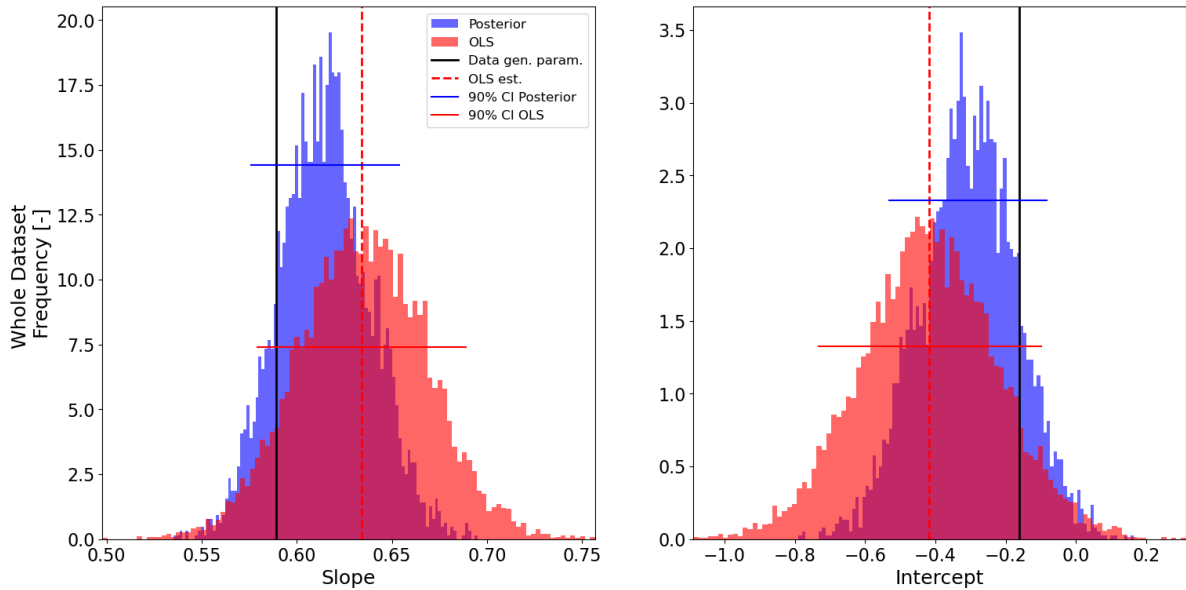


Figure 5.9: Combined plot of posterior distribution, OLS estimator, OLS uncertainty and parameter used for data generation for both slope and intercept. Results presented for all groups and for the case of pooled dataset

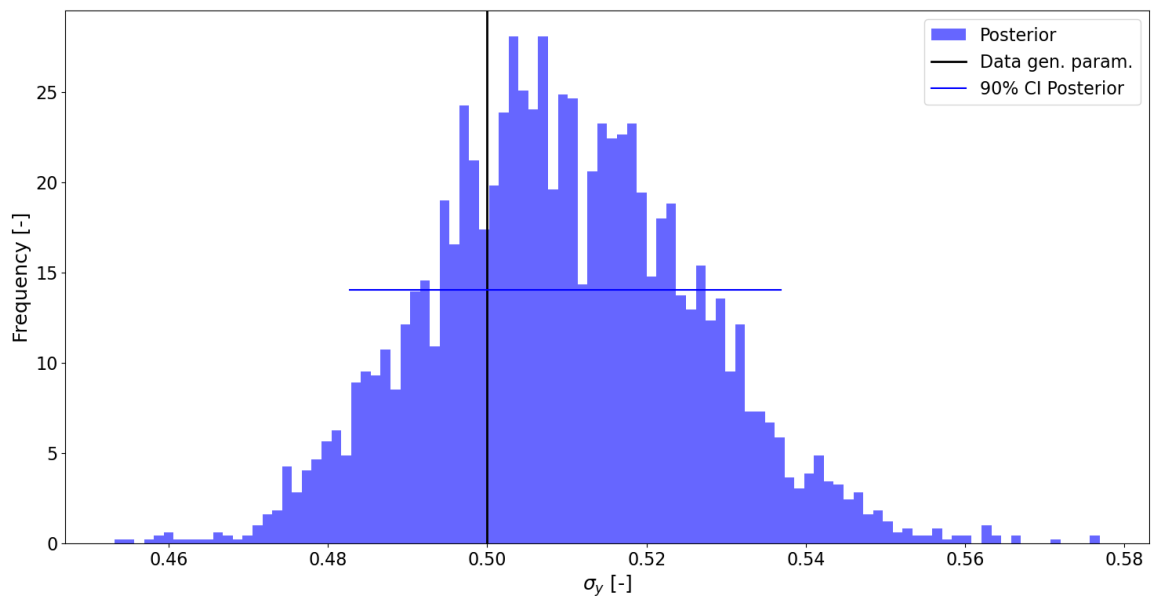


Figure 5.10: Posterior distribution of the σ_y and the value used for data generation. Case of pooled model

In the case of the partially pooled dataset, the parameters of the slope and the intercept used for data generation are similar (Figure 5.11). The posterior distributions for each group are retrieved from inference with the $\ln x - \ln y$ HBM which is the top ranked model for this dataset. The OLS statistics of the artificially generated data of each group have great

uncertainty, especially in the groups three and five where the data points are significantly fewer than the other groups. The OLS uncertainty is significantly larger compared to the OLS uncertainty of the $\ln x - \ln y$ unpooled dataset (Figure 5.13) because the σ_y used for each dataset is larger, causing for higher OLS uncertainty of the examined dataset than the unpooled.

The posterior distributions' 90 % CI of groups two, three and five contain the "true" parameter. Groups three and five have small amount of data and they are subsequently affected by the HBM "borrowing" information from other groups. In groups three and five is noticed large uncertainty of the OLS estimators because they have small amount of data. Their posterior distributions are affected significantly by the HBM. Consequently, their posterior distributions contain the "true" parameters that was used for the data generation. Additionally, the 90 % CI of the second group posterior distribution can grasp directly the "true" parameter that was used for artificial data generation.

Lastly, the most complex situations are those of group one and four. In group one the HBM can grasp the OLS estimator while in group four the 90 % CI of the posterior overlaps significantly with the OLS 90 % CI. The OLS estimator represents the learning ability of the model but due to the large OLS estimator variance the "true" parameter is far. Bayesian inference is successful because the posterior distributions can grasp the OLS. However, it happens that OLS is too uncertain, and the estimates lie far from the truth.

At many cases the 90% CI of the posterior distributions does not represent the "true" parameter of the artificial data. However, the HBM grasps the OLS which represents the learning ability of the model. The OLS sometimes has large uncertainty, and its estimates lie far from the "true" parameters. Therefore, the meeting of the OLS by the HBM 90 % CI is considered success for the second validation criterion.

The 90 % CI of the σ_y posterior distribution contains the σ_y used for data generation (Figure 5.12).

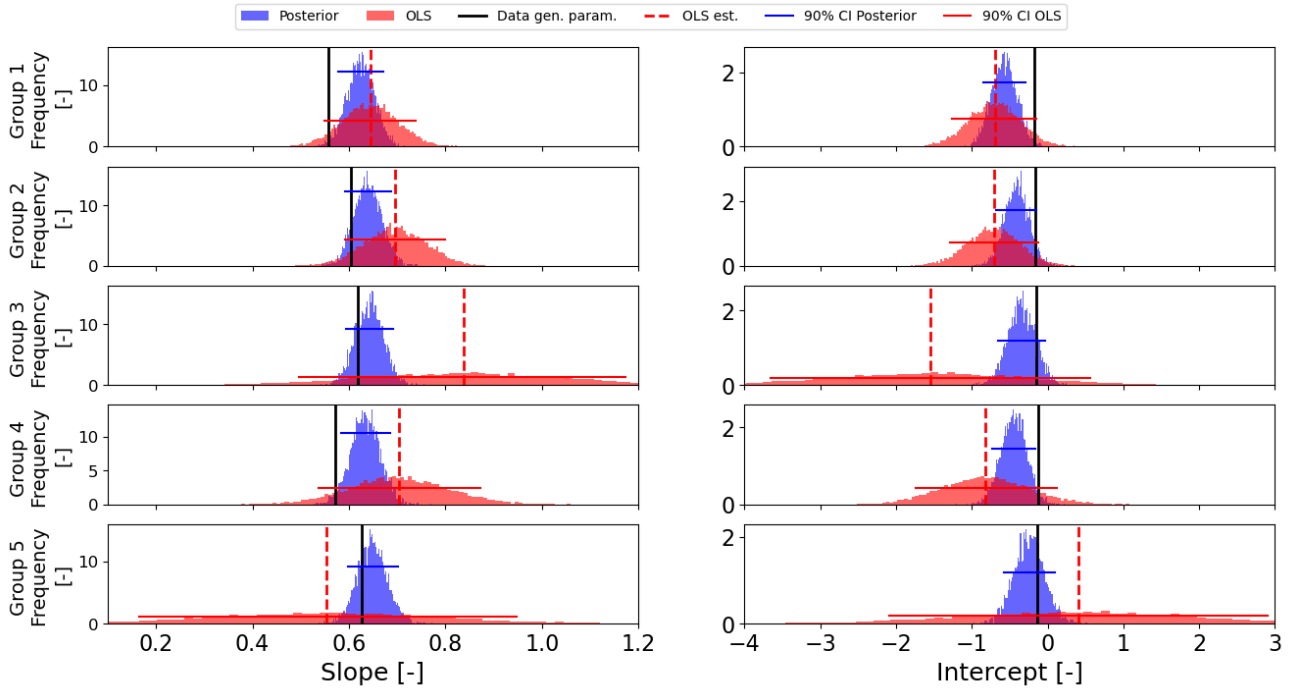


Figure 5.11: Combined plot of posterior distribution, OLS estimator, OLS uncertainty and parameter used for data generation for both slope and intercept. Results presented for all groups and for the case of partially pooled dataset.

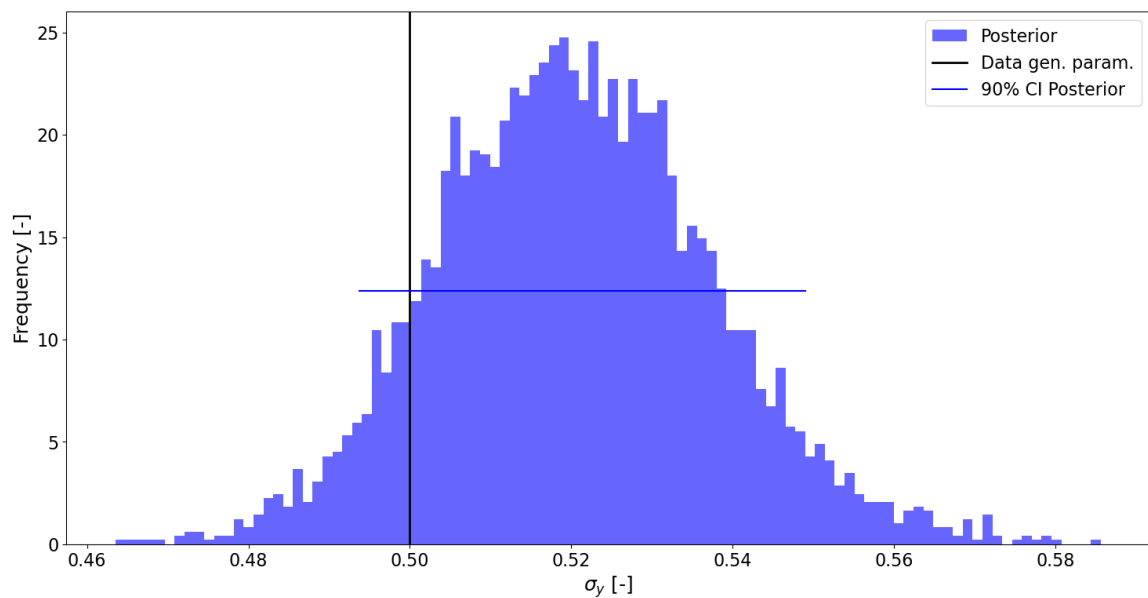


Figure 5.12: Posterior distribution of the σ_y and the value used for data generation. Case of partially pooled model

The generation of the unpooled dataset uses low σ_y value, leading to data that is concentrated around lines. At this case, the uncertainty of the OLS estimators is significantly restricted as it is visible from the following distributions (Figure 5.13).

There is low influence between the groups in the case of the unpooled dataset. Moreover, weak prior distributions have been used leading to domination of the likelihood in the inference. The OLS is purely based on the likelihood; hence, posterior distribution meets the OLS, and the second criterion is validated at the unpooled dataset. The 90% CI posterior distribution of the σ_y contains the parameter that was used for unpooled artificial data generation (Figure 5.14).

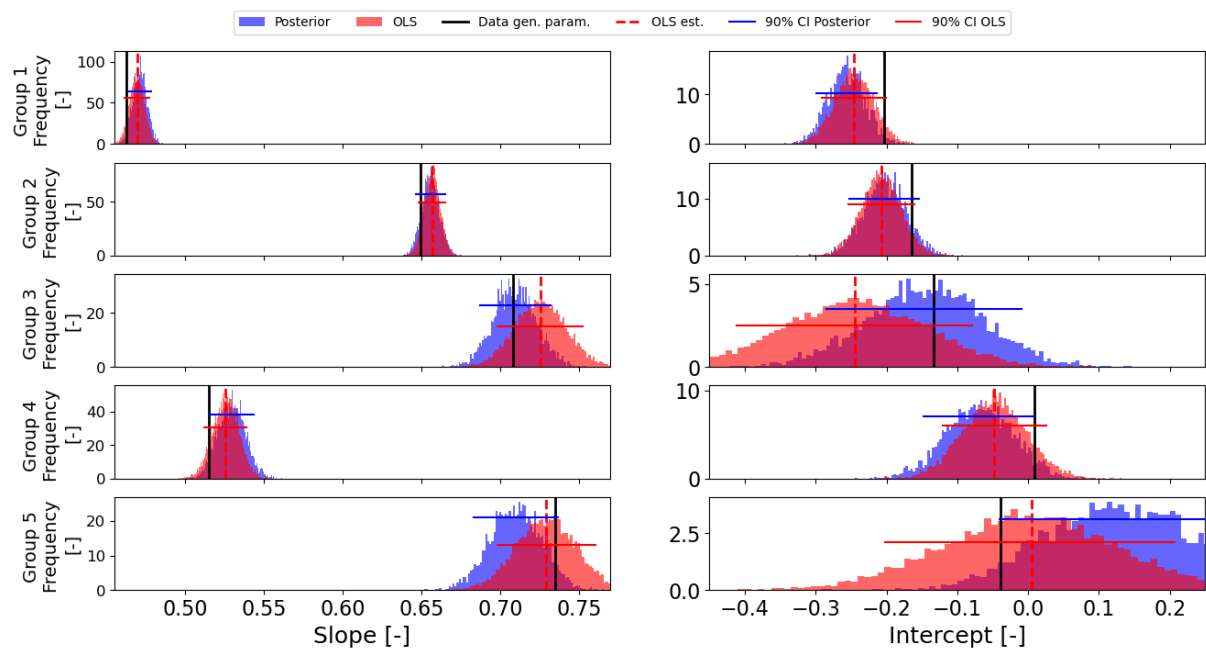


Figure 5.13: Combined plot of posterior distribution, OLS estimator, OLS uncertainty and parameter used for data generation for both slope and intercept. Results presented for all groups and for the case of unpooled dataset. The posterior distribution is obtained from the HBM (1st ranked model)

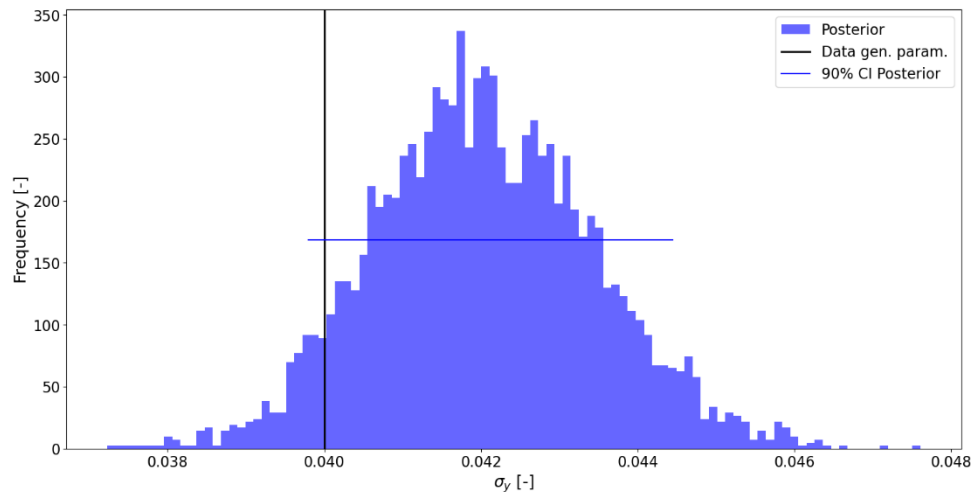


Figure 5.14: Posterior distribution of σ_y obtained by the HBM (1st ranked model) and the σ_y value used for data generation. Case of unpooled dataset

5.7 CONCLUSIONS

The validity of the BDA workflow is examined at two different criteria: the validation with model ranking and the validation with examining the posterior distributions. In the case of model rankings, the top ranked model is the same with the model used for data generation except from the case of the unpooled dataset. The *elpd* difference of the fittest model from the second contender, the unpooled model, which was used to generate the dataset, is negligible. Hence, the BDA workflow can identify the “true” model, in terms of pooling and functional form and the first criterion is satisfied.

As far the second criterion is concerned, the posterior distributions obtained by the pooled dataset contain the “true” parameter. In the case of the partially pooled datasets, in some groups the posterior distribution contains the “true” parameters and in the remaining groups they contain the OLS. The OLS can have large variance and its estimates can lie far from the true parameter. Therefore, the posterior distributions can represent the true parameter and if not, the reason lies at the large uncertainty of the OLS.

Therefore, both the first and the second criteria are satisfied, and the BDA workflow is validated.

6. REAL CASE ANALYSIS

This chapter delves into the primary objective of this thesis: investigating the relationship between q_{net} and S_u using real data. This investigation involves calibrating the relationship through Bayesian inference, utilizing the Hierarchical Bayesian Model (HBM), and comparing it against the pooled and unpooled models by following the BDA.

6.1 PURPOSE OF THE REAL CASE ANALYSIS

The main aim of this real case analysis serves a dual purpose. Firstly, it seeks to quantify the uncertainty in S_u by employing the q_{net} derived from the HBM and the pooled and unpooled models. Secondly, it strives to identify the most appropriate statistical model that accurately represents the relationship between S_u and q_{net} . The calibration of these models utilizes real-world data, and the BDA workflow facilitates a comprehensive comparative assessment. Importantly, the feasibility of applying the BDA workflow has been previously established and confirmed in chapter 5.

6.2 PROCEDURE OF THE REAL CASE ANALYSIS

The procedure of the real case analysis will be presented in this section. Initially, the data is clustered as it is described in section 4. Following, the combinations of functional forms and statistical model families are formed, resulting to 15 different statistical models (Appendix Table 4).

The BDA workflow is applied for the above-mentioned models using real data resulting to the model comparison and the fittest model. The first outcome of the analyses are the posterior distributions θ based on the paired observations (q_{net}, S_u) , $p(\theta|q_{net}, S_u)$. The second outcome of the analyses are the posterior predictive distributions of potentially observable quantities of S_u , $p(\widetilde{S}_u|q_{net}, S_u)$. After running the analyses with all models, the results of the HBM with the current practice models (pooled, unpooled) of the fittest functional form will be compared. This comparison will answer the first research objective relatively the performance of the HBM compared with the current practice pooled and

unpooled models. Lastly, the results of those models will be further used as input for reliability analysis of a dike slope (chapter 7) to answer the second research objective. The procedure followed in the real case analysis can be seen in Figure 6.1.

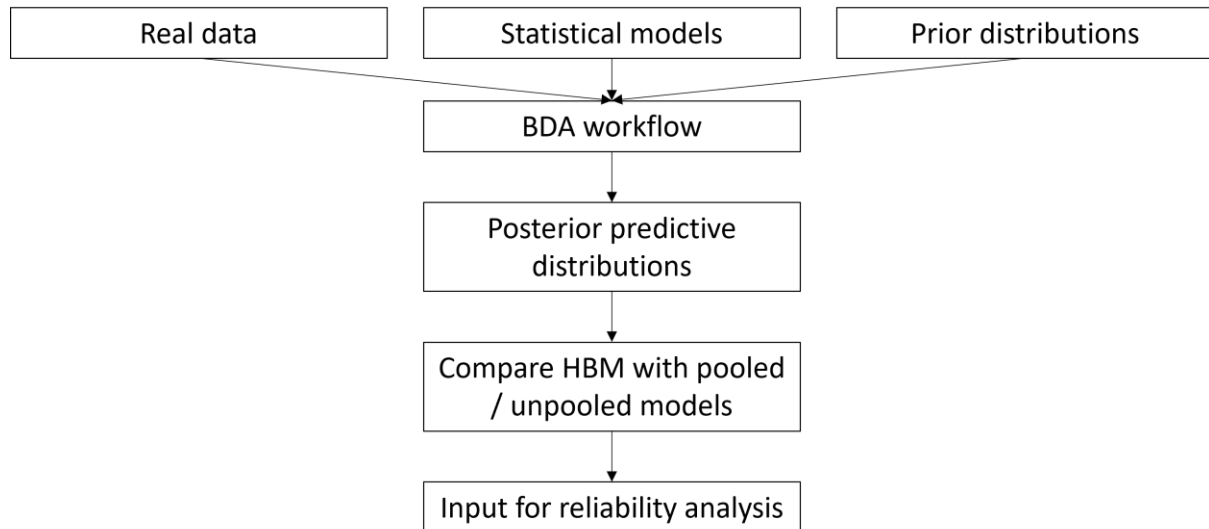


Figure 6.1: Workflow of the analysis with real data

6.3 RESULTS AND DISCUSSION

6.3.1 Models' ranking

Upon running all the statistical models their rankings are formed based on the LOO-CV and the LOGO-CV metric. The former ranking ranks first the $\ln x - \ln y$ unpooled model and second with negligible difference the $\ln x - \ln y$ HBM (Figure 6.2). The next ranking is based on the LOGO-CV and the best performing model is the $\ln x - \ln y$ HBM (Figure 6.3).

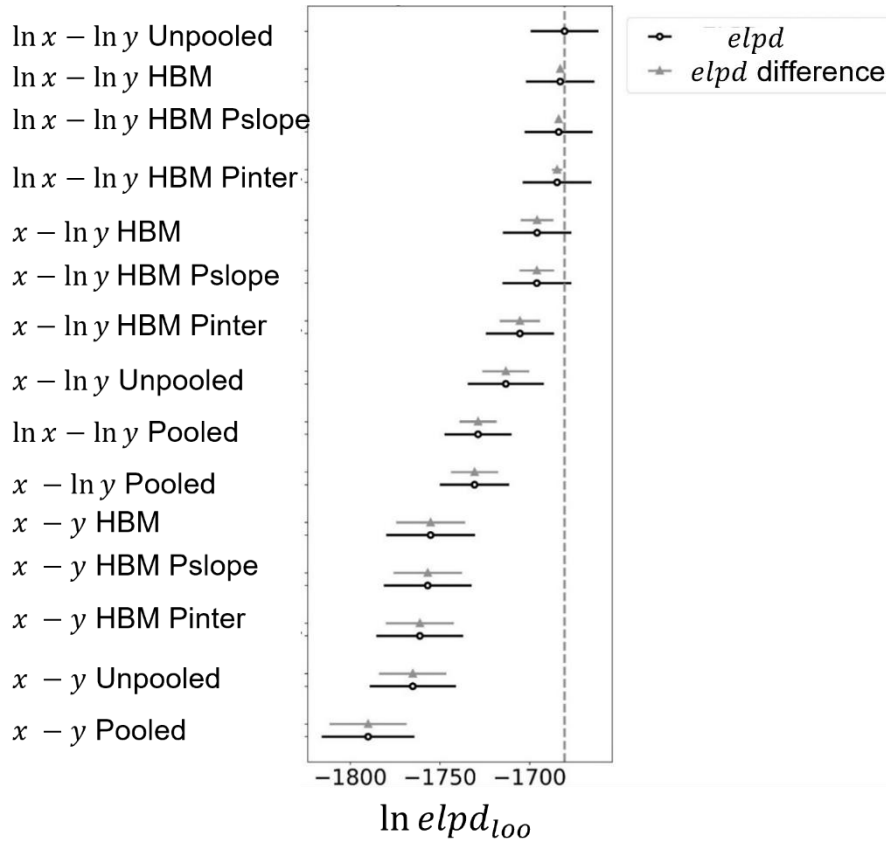


Figure 6.2: Models ranking based on the LOO - CV for analysis with real data

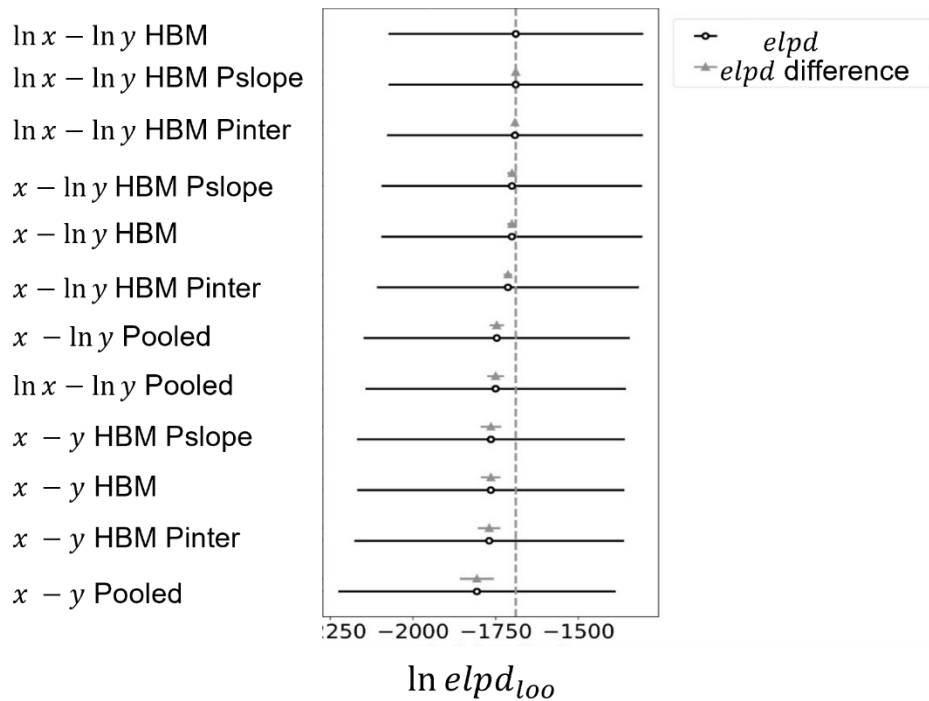


Figure 6.3: Model ranking based on the LOGO - CV for analysis with real data.

The subsequent step is to select the fittest model to make predictions in the known sites and for predictions for new sites. Even though the $\ln x - \ln y$ unpooled model is ranked first at the LOO-CV, the $\ln x - \ln y$ HBM is advised to be selected for describing the data in the known sites. The difference in the ranking between them is negligible and it is not believed that the sites are completely independent to select the unpooled model (Gelman et al., 2013). HBM is flexible and it can tend to either pooled or unpooled model if they appear to be true. As far as the case of predicting new group is concerned, the top ranked model is the $\ln x - \ln y$ HBM and it will be chosen as the optimal model for making predictions for new groups.

6.3.2 Model checking

Model checking will be performed for the $\ln x - \ln y$ HBM by plotting the posterior predictive check plot (Figure 6.4) that will reveal whether the predictions of the model look sensible compared to the observed data.

The posterior predictive samples enclose the observed values and at most of the points of the observed values are very close to the posterior predictive mean. Therefore, the model is a good fit for the data. Systematic deviations do not occur which would lead to the re-assessment of the model. Based on the posterior predictive check, it seems that the model adequately captures the general patterns in the data, with no significant discrepancies observed. Therefore, it is probable that the model can generate realistic data based on the posterior distributions. More specifically, the model has a minimum of zero, like the data and it captures well the maximum of the observed data. Additionally, the model reproduces accurately the mode and most of the probability mass. Whatsoever, the $\ln x - \ln y$ HBM misses one part of the data.

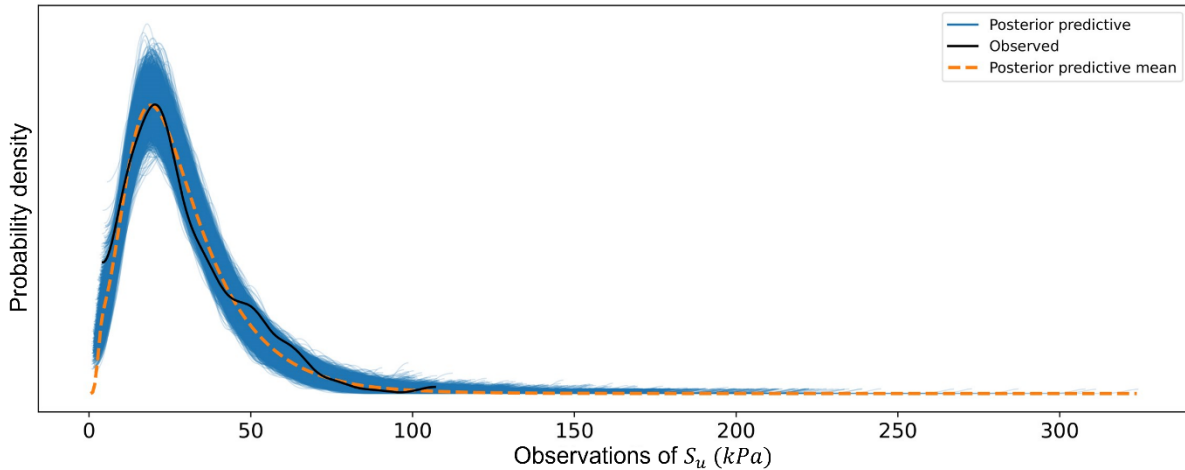


Figure 6.4: Posterior predictive check for the $\ln x - \ln y$ HBM and real data

Additionally, the plot of the $\ln x - \ln y$ HBM for group one with the observations will be presented (Figure 6.5). The green shaded region represents the 90% posterior predictive interval (PPI), indicating the possible range of the S_u values with 90% credibility (effect of both aleatory and epistemic uncertainty). The blue shaded band around the regression line is the 90% credible interval (CI), which captures the uncertainty associated with the estimated regression coefficients (epistemic or model uncertainty) and it represents the distribution of the mean S_u given the q_{net} . The model seems to capture the general trend of the data, as the fitted regression line passes through the central portion of the observed data points. The posterior predictive interval provides a measure of uncertainty in the model's predictions, with wider intervals indicating higher uncertainty. Using the $\ln x - \ln y$ models lead to increasing PPI with increasing q_{net} . Most of the observed data lies within this interval, suggesting that the model's predictions align well with the observed data.

In Figure 6.6 the plot of the $\ln x - \ln y$ Unpooled model is demonstrated for group one. The HBM tends to the unpooled model in the LOO-CV rankings (Figure 6.2) and observing the Figure 6.5 and Figure 6.6 it is apparent that there are not any significant discrepancies visible between the two models.

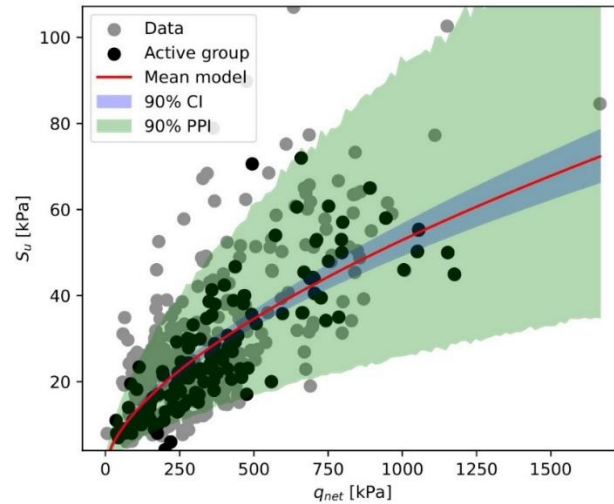


Figure 6.5: Plot of the $\ln x - \ln y$ HBM along with observed data including the 90% posterior predictive interval and credible interval

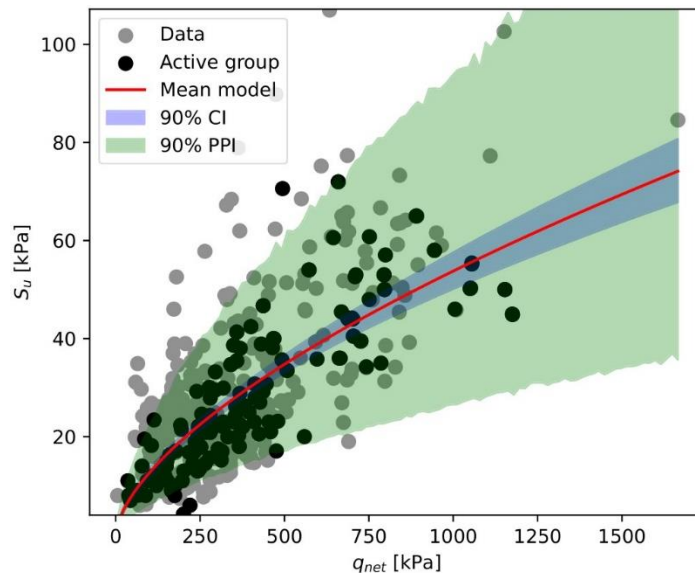


Figure 6.6: Plot of the $\ln x - \ln y$ Unpooled along with observed data including the 90% posterior predictive interval and credible interval

6.3.3 Posterior estimations of θ

The following procedure after selecting the fittest model is to compare the posterior distributions of θ obtained by the selected model and the other models of the same functional form in order to assess the uncertainty quantification in the model parameters obtained by the HBM compared to the standard practice models (pooled and unpooled). Figure 6.7

describes the posterior distributions of slope and intercept while Figure 6.9 describes the posterior distributions for statistical models' standard deviation σ_y .

First, the forest plot of the slope will be discussed (Figure 6.7 left). The pooled model is trained simultaneously at the whole dataset by pooling all the grouped data into one group (Figure 3.1). Consequently, the slope estimated by the pooled model is the least uncertain by having the lowest epistemic uncertainty.

On the contrary, the 90 % CI of the unpooled model is the largest resulting to high epistemic uncertainty of this model because it is trained individually per group. The 90 % CI of the HBM is narrower than the one of unpooled model because it is directly trained to the-specific data but at the same time borrows information from other sites. The lower uncertainty of the HBM is more visible at site three and five which have essentially lower number of observations.

The 90% CI of the unpooled model is deviating significantly from the mean value of all datasets (pooled model) while the HBM posterior distribution is placed between the pooled and the unpooled model. The unpooled model is affected by various uncertainty sources not captured by the generated models (Feng, Gao, et al., 2023).

The HBM posterior mean values of slope are gathered around a common area (shrinkage) (Bozorgzadeh et al., 2019); hence, HBM reduces the overall scatter in the point estimates. Shrinkage occurs because the site-specific data trains directly the site-specific θ and at the same time the data of other sites influences it through the hyperparameters, ξ .

The HBM with pooled intercept has smaller uncertainty than the HBM because the intercept is trained directly using the whole dataset. Lastly, the HBM with pooled slope has slightly greater uncertainty than the pooled model and its interval tends to the values of the unpooled model.

At the right side of the Figure 6.7, the 90% CI of the intercept posterior distributions are demonstrated. Again, the uncertainty of the intercept estimation obtained by the HBM is smaller than the unpooled model. Similarly, the posterior means of the HBM are gathered at a narrow space between the estimates of the unpooled model except the group four. At

groups one, two and three the posterior 90% CI of the intercept falls between the pooled and the unpooled model.

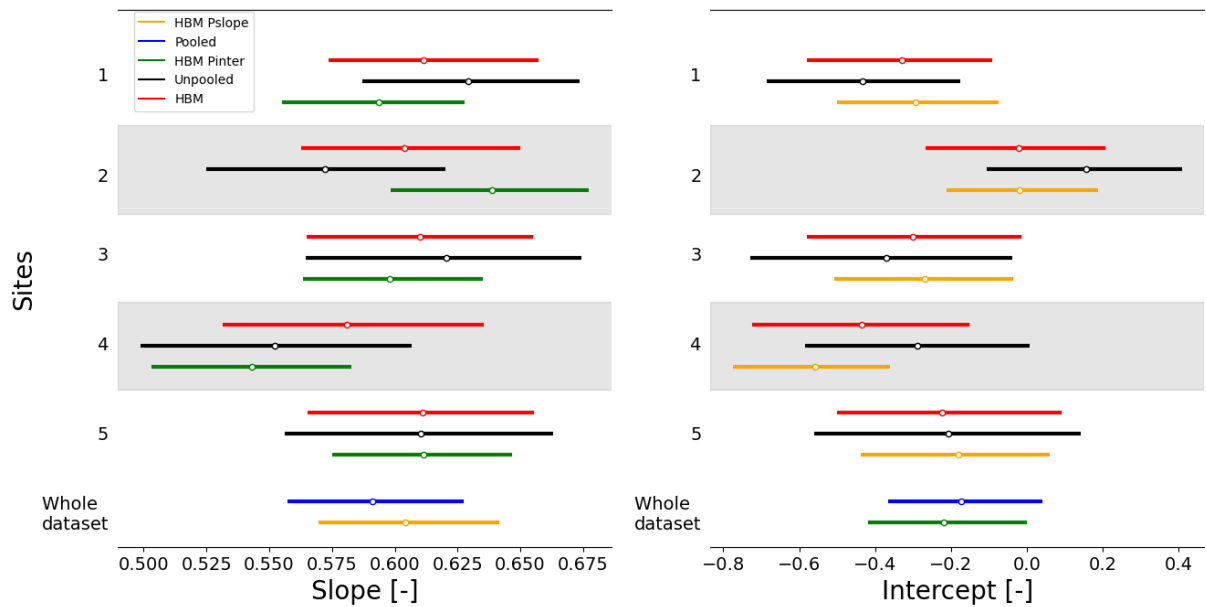


Figure 6.7: Combined Forest plots of 90 % CI for posterior distributions of slope and intercept per site and for the whole dataset. Results obtained by all the statistical models of the $\ln x - \ln y$ functional form.

The shrinkage effect of the posterior means between the HBM and the unpooled model is shown in Figure 6.8. The point estimates of the slope and the intercept are gathering around a common area. Even though the unpooled model has ranked first showing that the groups are different among them (high-between group variation), the HBM still affects the site-specific posterior distributions of θ . The borrowing of information from other sites to make site-specific estimations of θ can reduce the epistemic uncertainty of these parameters.

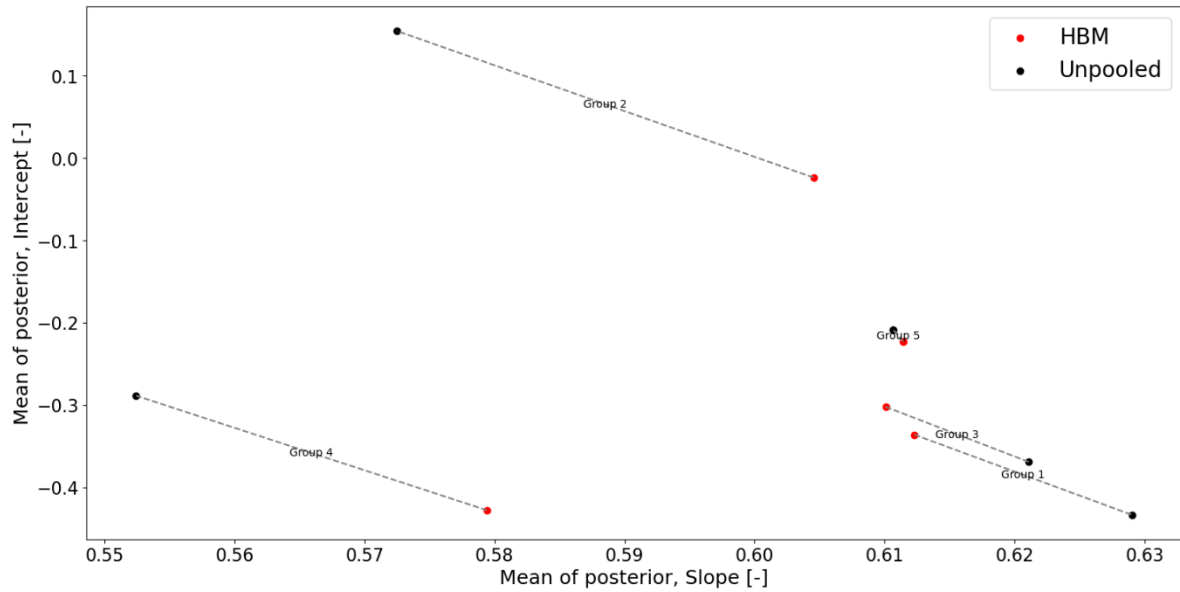


Figure 6.8: Scatter plot of the posterior mean values for the slope and the intercept. The dashed line represents the change of the point estimates between the unpooled model and the HBM.

The forest plots of the σ_y provide some useful information as well (Figure 6.9). This parameter is the same for all the groups (pooled parameter). The posterior distributions are similar for all models except pooled model. This model is trained simultaneously on the entire dataset; thus, it has the lowest epistemic uncertainty (Figure 6.7). At the same time, it must represent the data of all sites, and this is achieved by having the largest aleatory uncertainty through the parameter of σ_y (Figure 6.9). On the contrary, unpooled model has the lowest σ_y or the lowest aleatory uncertainty as it is trained individually on the site-specific data. Moreover, the models of HBM, HBM with pooled slope and HBM with pooled intercept are intermediate between the pooled and unpooled. However, they tend to the prevailing unpooled model (Figure 6.2).

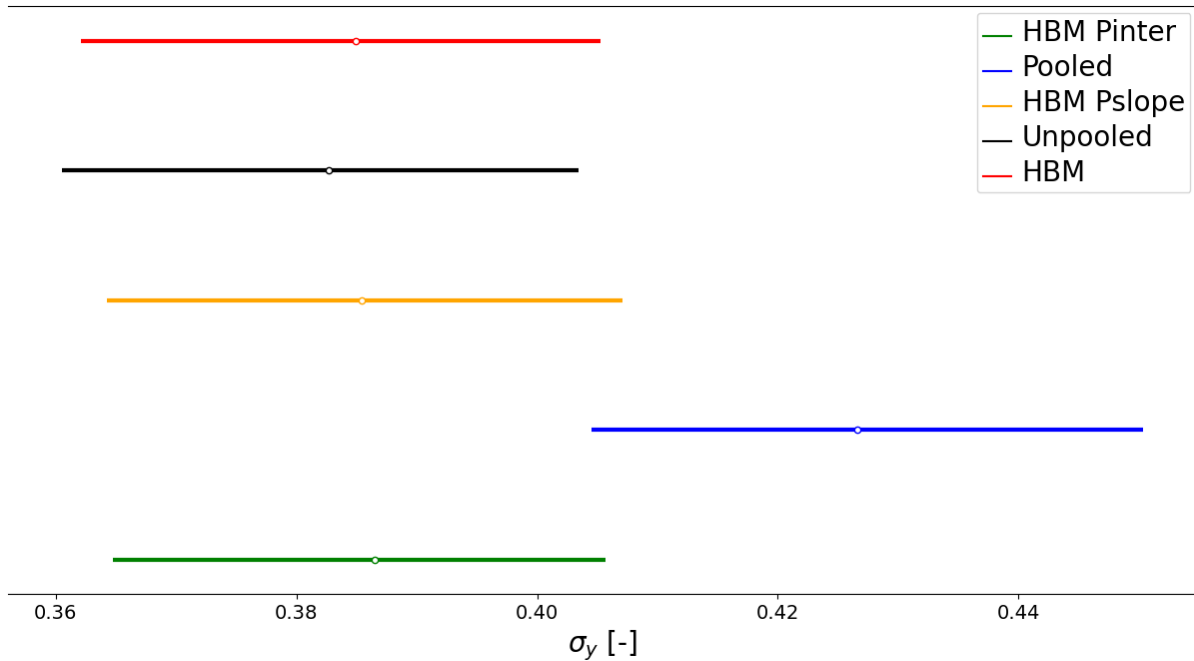


Figure 6.9: Forest plot of σ_y 90% credible interval of posterior distribution. Results obtained by all the statistical models of the $\ln x - \ln y$ functional form.

6.3.4 Posterior predictive estimations of S_u

In this section, the comparison between random measurements from all sites and the predictions of the statistical models will be presented. The aim of these plots is to examine the behavior of the models in approximating the S_u data. Along with that, the uncertainty of each model will be assessed by comparing the CI and the PPI. The predictions obtained by the statistical models of the top ranked $\ln x - \ln y$ functional form per site along with five random measurements are presented (Figure 6.10-Figure 6.14).

In general, the PPI of all models enclose the measured value (outliers have not been depicted). The pooled model's CI is the narrowest one (low epistemic uncertainty) while it has the largest PPI (largest aleatory uncertainty) and overall, the largest uncertainty. The hierarchical and unpooled models exhibit similar behavior, as the former tends to the latter (Figure 6.2).

The unpooled model has the largest epistemic uncertainty and the largest total uncertainty compared to the hierarchical models. The discrepancy in the epistemic uncertainty of the unpooled model occurs because the unpooled model is trained accounting

for only the site-specific data while the HBM accounts for both the site-specific and the overall data. As it is described, the HBM effect reduces the uncertainty of the model parameters (shrinkage) by borrowing information from the other sites.

For low values of q_{net} the total uncertainty of the models is low, and it increases with increasing q_{net} because in the $\ln x - \ln y$ models the PPI increases with the q_{net} . Moreover, the uncertainty of the models in sites one and two is generally lower than the uncertainty of the models in the remaining sites because sites one and two have larger number of observations (Figure 4.2).

The unpooled and the hierarchical models are predicting more accurately the measurements with the unpooled model being the most accurate in most of the cases and at the same time the most uncertain (when compared to the hierarchical model). The predictions of the hierarchical model lie between the unpooled and the pooled model because the information borrowing is small, emerging from the tendency of the HBM towards the unpooled model.

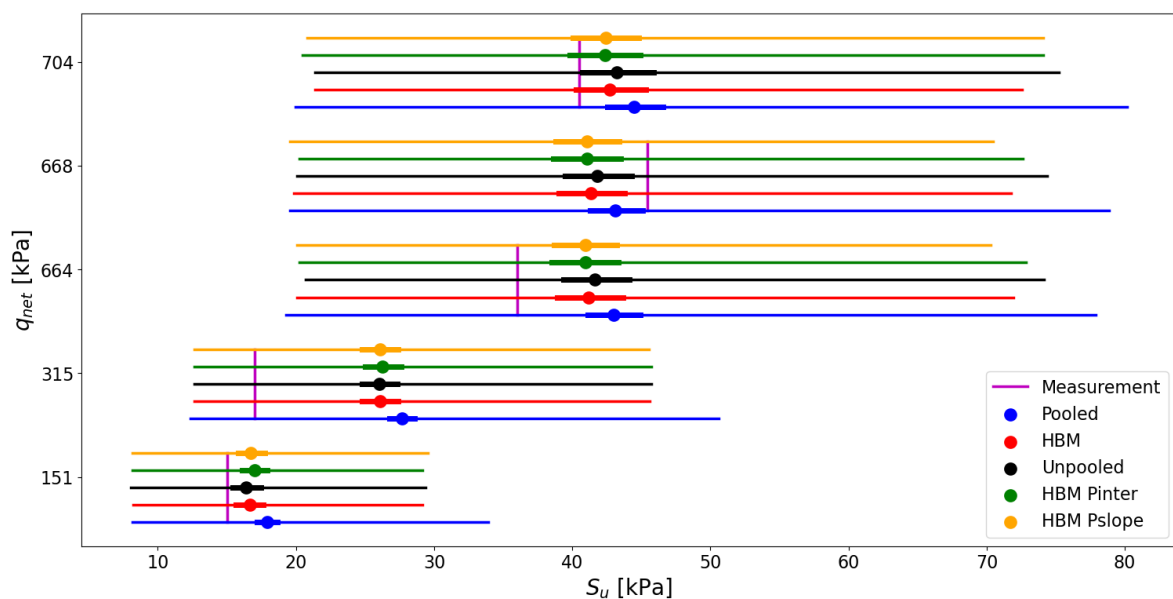


Figure 6.10: Posterior predictive estimation of S_u for five random points of site 1.

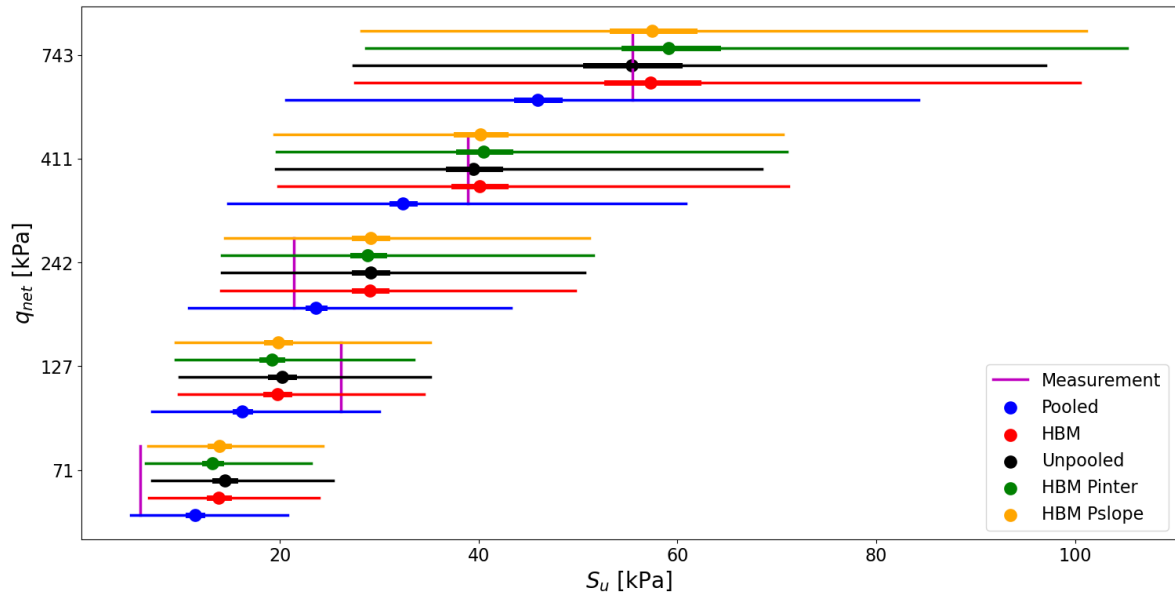


Figure 6.11: Posterior predictive estimation of S_u for five random points of site 2.

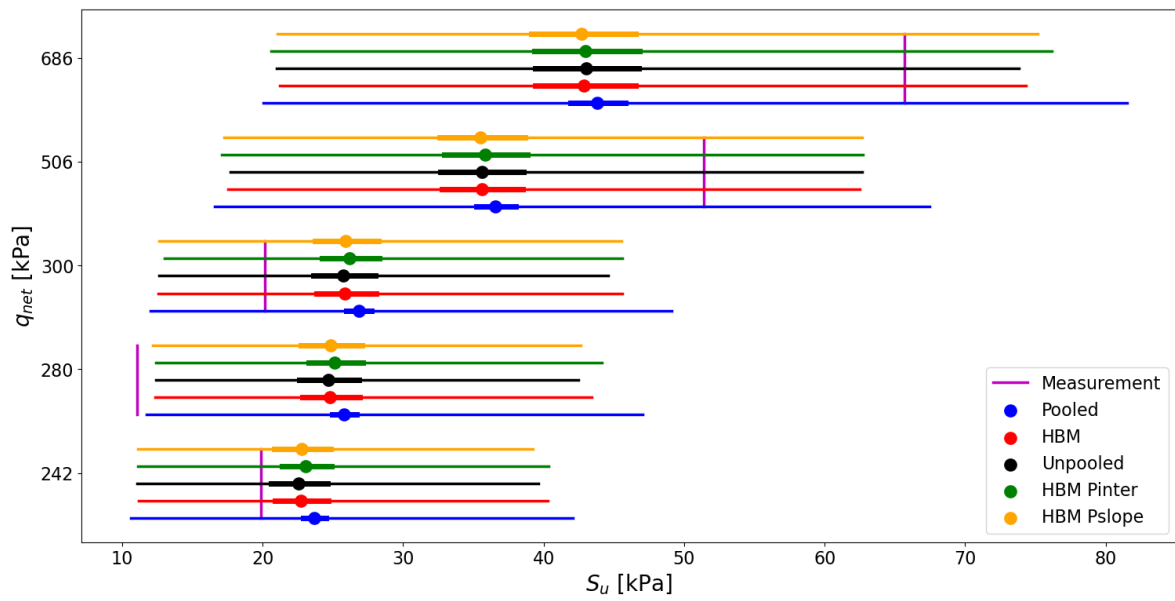


Figure 6.12: Posterior predictive estimation of S_u for five random points of site 3.

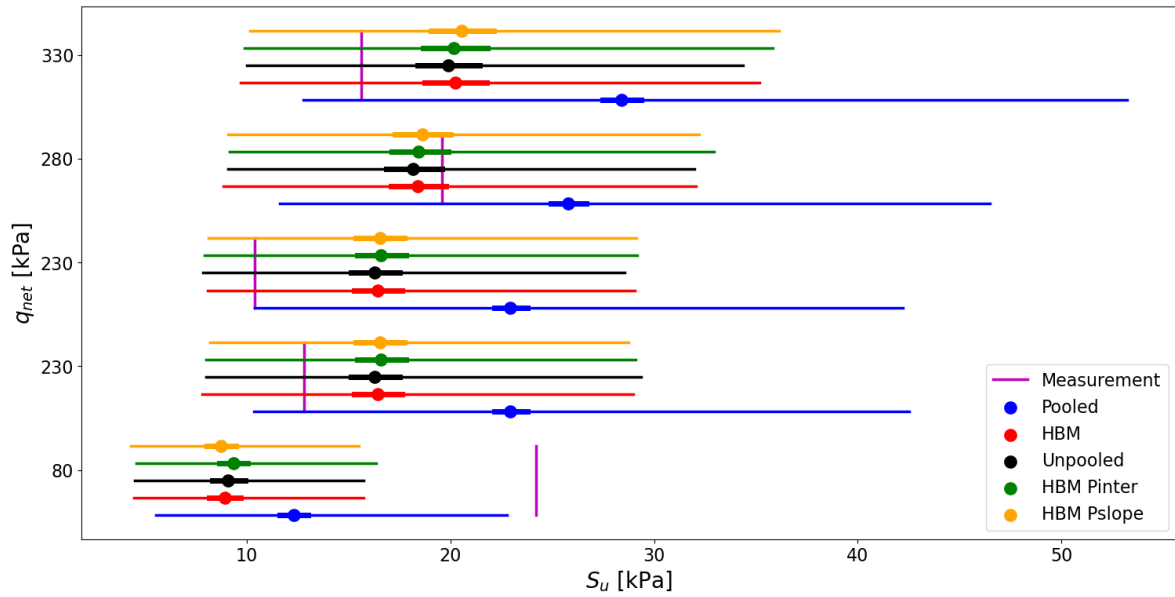


Figure 6.13: Posterior predictive estimation of S_u for five random points of site 4.

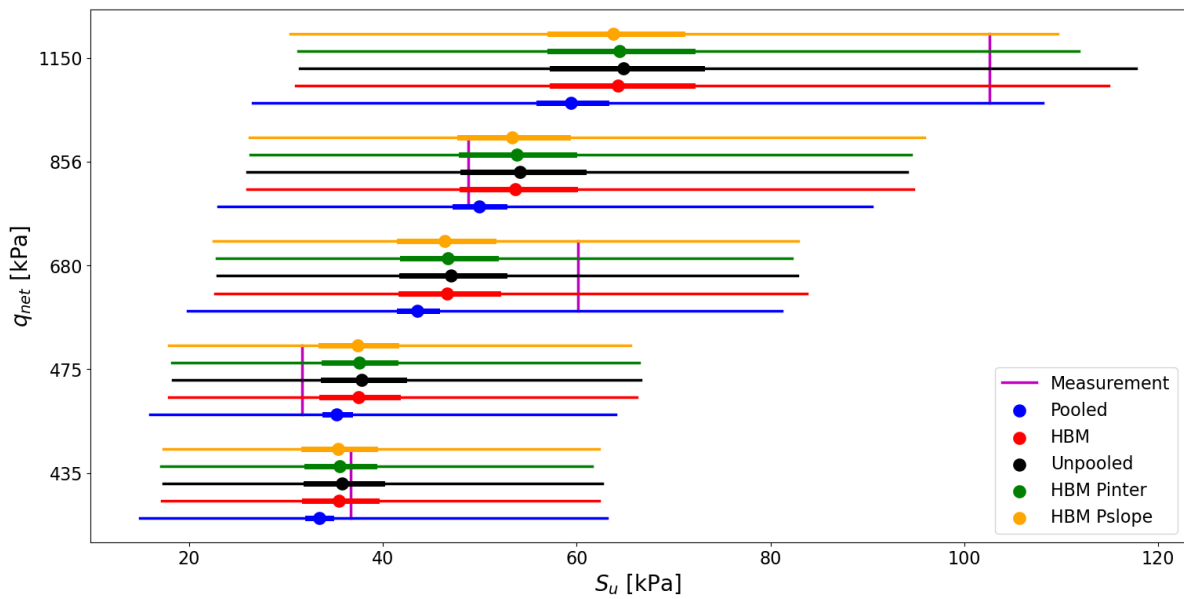


Figure 6.14: Posterior predictive estimation of S_u for five random points of site 5.

6.4 CONCLUSIONS

The analysis with the real data yields some significant results to be highlighted. First, the top ranked models (Figure 6.2, Figure 6.3) have the $\ln x - \ln y$ functional form. On the contrary, the current practice is represented by the N_{kt} model (section 2.4) which utilizes the $x - y$ functional form with zero intercept which are ranked in low position. Hence, the HBM

and the application of the BDA can prove the existence of more appropriate functional form than that of the N_{kt} model.

HBM is a valuable statistical tool to describe and predict geotechnical data. HBM has the second-best predictive power for a new point into a known site after the unpooled model as demonstrated by the LOO-CV. The difference with the unpooled however is negligible. HBM moves in an envelope between the unpooled and the pooled model. Additionally, the HBM can predict with the highest accuracy new points into a new site without available measurements as presented by the LOGO-CV. The unpooled model cannot make predictions for a new site while the pooled model is ranked at a low position. Besides, Figure 6.2 depicts the $\ln x - \ln y$ unpooled model as the fittest one, but the $\ln x - \ln y$ HBM is proposed to be used because their difference is negligible, and the HBM will tend to either pooled or unpooled when needed. Also, it is expected that the sites share some similarities which cannot be realised by the unpooled model. Lastly, Gelman et al. (2013) in a similar case propose to choose the HBM over the unpooled model.

The HBM provides an intermediate response between the unpooled and the pooled model. The observed shrinkage effect shows that knowledge is gained about the site – specific parameters by observing the data of the other sites. HBM slightly reduces the epistemic uncertainty as it is trained in two levels; directly from the site specific data and indirectly from the other's site data. It assigns different parameters per group and at the same time reduces the uncertainty of them.

Concerning the geotechnical parameter values prediction, HBM can predict accurately the observed values. Its predictive uncertainty is lower than the unpooled model and it is significantly lower than the pooled model's.

7. RELIABILITY ANALYSIS

7.1 INTRODUCTION

Reliability analysis is performed at a slope stability problem of typical dike found in the Netherlands. Figure 7.1 and Figure 7.2 depict the geometry, the materials, the water level, and the hydraulic conditions of the dike. The predictions of the S_u obtained from the $\ln x - \ln y$ HBM, pooled and unpooled models will be used as input. The purpose of the reliability analysis is to highlight the impact of using different statistical models to describe the geotechnical data into the design and to inform about the uncertainty propagation from the data description to the design. Additionally, it will propose whether input derived from the HBM can achieve safer and more economic design over the standard approach (in terms of pooling) pooled and unpooled models.

The reliability analyses will be performed for all sites with paired q_{net} - S_u measurements (known sites) and for a new site without measurements (new site). Three cases are elaborated relatively the representative values of q_{net} . The first case refers to a deterministic value of the q_{net} equals to the mean value of the whole dataset. The second case refers to stochastic values of q_{net} following a probability distribution which is derived based on the site-specific q_{net} values. Lastly, the final case refers to stochastic values of q_{net} as the second case and to stochastic values of the dike's material friction angle, φ .

Additionally, for each case describing the q_{net} , two cases will be elaborated as far as the distribution of the S_u over the subsurface: one case of full averaging of the S_u and one case of no averaging of the S_u over the subsurface. Lastly, the possible depth trend of the S_u or the q_{net} have neither been investigated nor considered in the analysis.

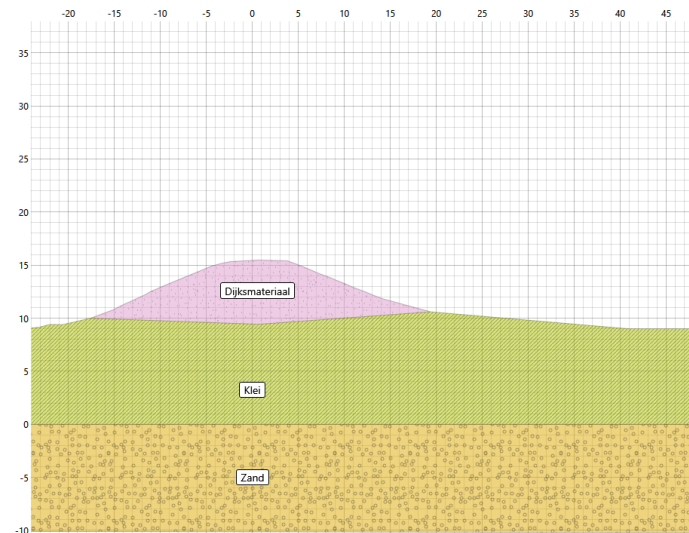


Figure 7.1: Geometry and materials of the dike

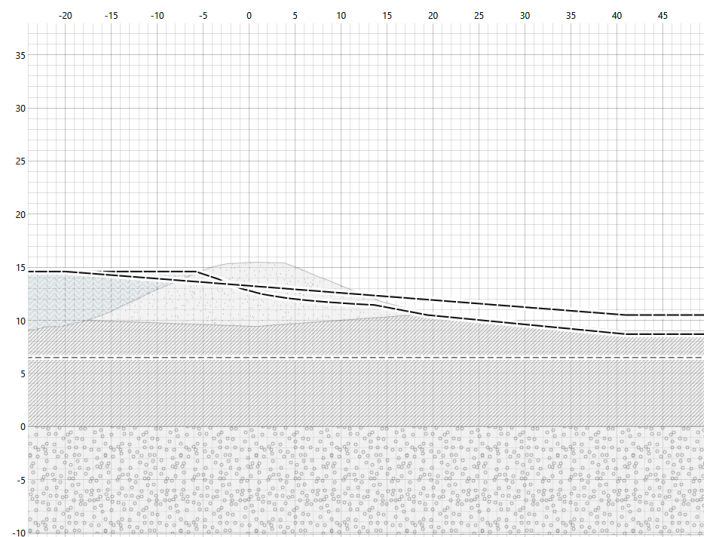


Figure 7.2: Water level next to the dike and hydraulic conditions in the dike

7.2 RELIABILITY ANALYSIS PROCEDURE

The focus is on the different S_u predictions by the statistical models; thus, simplistic assumptions for the q_{net} distribution are made. In the first case of q_{net} values, the mean q_{net} of the dataset is assumed as constant over the subsurface. The second case is like the first one but the q_{net} is considered stochastic. The q_{net} values per each site have been used by fitting LogNormal distribution while in the case of a new site all the values of the dataset have been used as presented in Figure 7.3. Lastly, in the third case the values of q_{net} are the same

with the second case but the dike material φ is stochastic by following a *LogNormal* distribution with parameters described in Table 7.1.

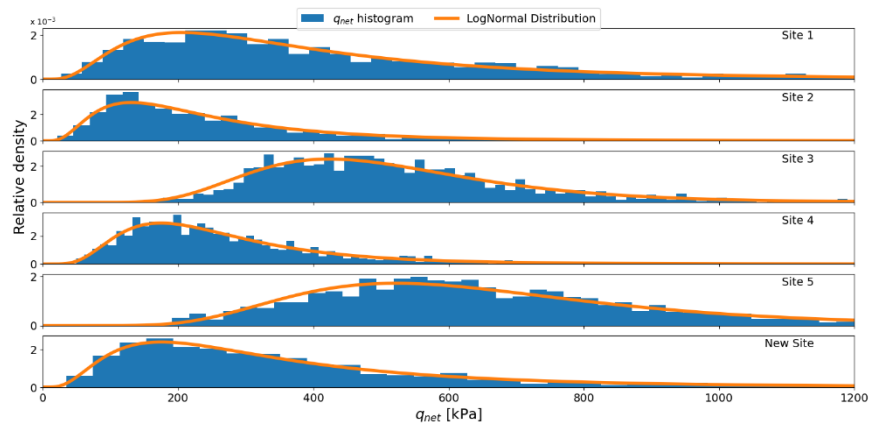


Figure 7.3: Each site's and whole dataset's q_{net} values with fitted distributions

For each case of q_{net} distribution, two cases of the S_u will be analysed: one of full averaging and one of no averaging of the S_u over the subsurface. In the case of full averaging, the distribution of the mean S_u (90% CI) is used as input for the analysis. It is utilised by fitting either a Normal distribution for the case of deterministic q_{net} or a LogNormal distribution for the case of stochastic q_{net} . In the case of no averaging the whole spectrum of the S_u values (90% PPI) is used by fitting a LogNormal distribution (Figure 7.4) at the PPI data.

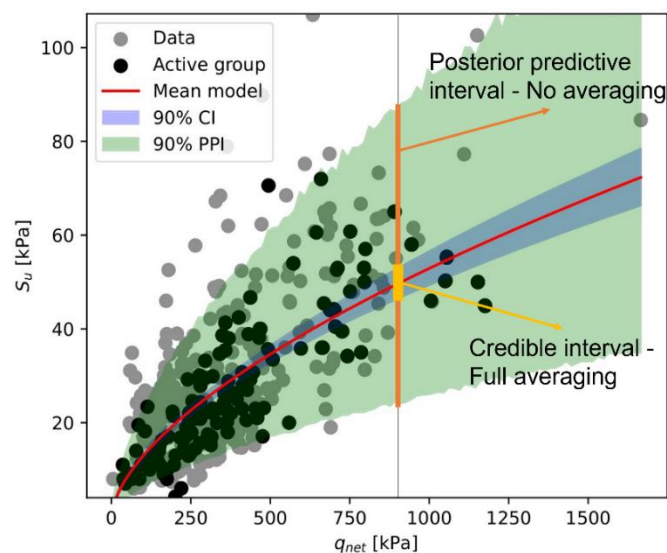


Figure 7.4: CI and PPI for a random deterministic value of q_{net}

The results of the reliability analysis will be in terms of reliability index, β . In the first and second case of the q_{net} where the only stochastic parameter is the S_u of the clay layer,

the reliability analysis is performed by evaluating the β through the fitted distribution at the S_u values. It is calculated that the critical S_u value, $S_{u,crit}$ which corresponds to a factor of safety equal to one is 18.22 kPa . In the third case where both the S_u of the clay layer and the φ of the dike material are stochastic, the reliability analysis is performed by using F.O.R.M (Deltares, 2022). The procedure of the reliability analysis can be seen in Figure 7.5.

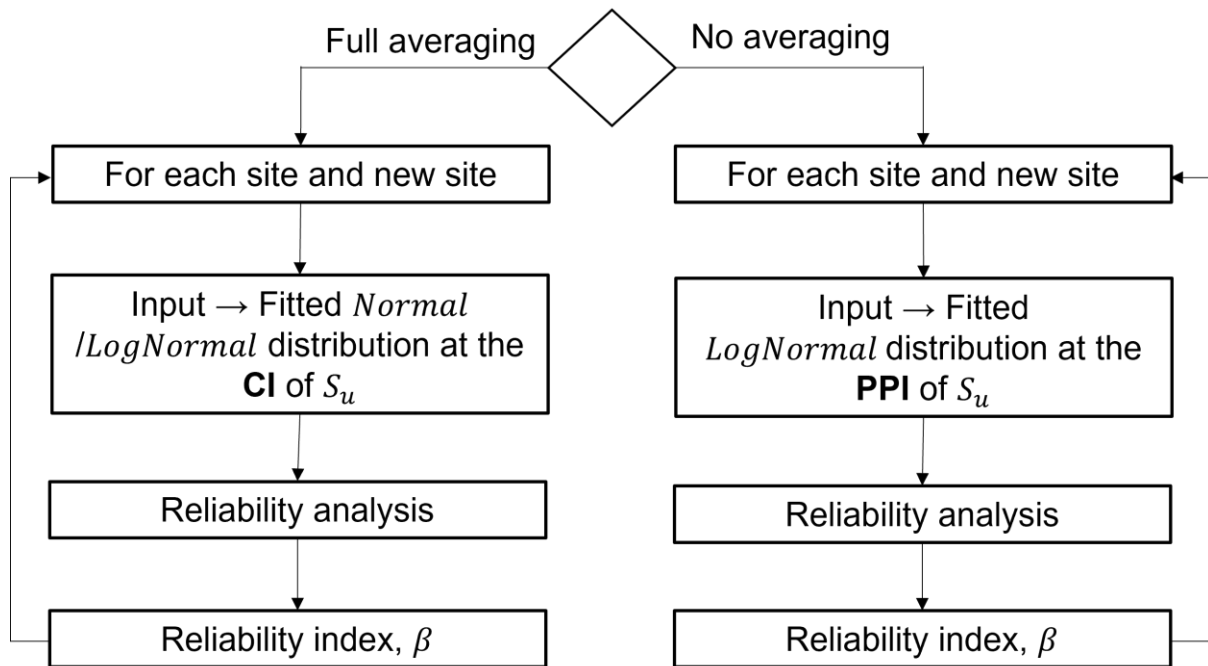


Figure 7.5: Flow chart for the reliability analysis procedure for each case of q_{net}

7.3 SETUP OF THE RELIABILITY ANALYSIS

In this section, the properties of the slope stability model and the reliability analysis will be presented. First, the fitted distributions at the S_u intervals represent the stochastic strength of the clay material. The mechanical properties of the soil material used in the analysis can be seen at the table below. Additionally, the selected model for this analysis is the Mohr – Coulomb.

Table 7.1: Mechanical properties of the soil materials of the slope stability model

Material	Unit weight (kN/m^3)	Cohesion (kPa)	Friction angle ($^\circ$)
Dike's material	19	0	30
Dike's material stochastic	19	0	$LogNormal(33.19, 2^2)$
Clay	17	Probability Distribution of S_u	0
Sand	20	0	40

The slope stability analysis is done using the Bishop, Brute force analysis method (R. van der Meij, 2023). The whole range of the clay material is desired to be mobilized thus the tangent area extends at the whole range of the clay layer. The grid of the possible positions of the slip plane's center and the area of the possible positions for the horizontal tangent can be seen at Figure 7.6.

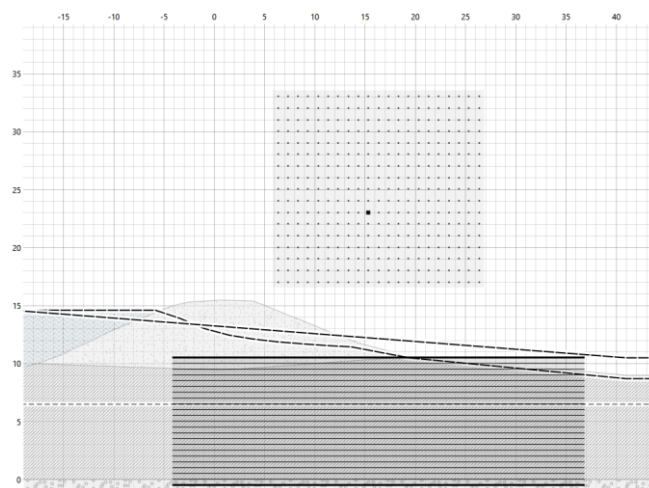


Figure 7.6: Search grid for the centre of the slip plane and the tangent are of the possible positions of the horizontal tangent of the slip plane.

7.4 RESULTS AND DISCUSSION

7.4.1 Reliability analysis for deterministic q_{net}

The use of deterministic value of q_{net} is an artificial intermediate step to allow for the comparison between the models. Omitting the possible depth trend affects the results of the reliability analysis. One distribution of S_u per case will be used while if there was fluctuation of the q_{net} more distributions would be utilized. The impact of the q_{net} at certain depths is different among them. In particular, the impact of the q_{net} at the depth where the circle reaches the horizontal tangent line is higher than at an intermediate depth. The different impact of the q_{net} values cannot be captured when a single value is used.

First, the results of the reliability analysis when no averaging is assumed will be presented in Figure 7.7. Reliability analysis using input from the pooled model assigns the same values of β per site and for a new site equal to 0.97 because it does not distinguish any specific attributes per site as identical value of q_{net} has been used. On the contrary, the unpooled model assigns different β per known sites only ranging from 1.72 in the second site to 0.21 in the fourth site.

The HBM tends to the unpooled model (Figure 6.2) and its values of β range from 1.71 in the second site to 0.28 in the fourth site. It is worth mentioning that the HBM can propose input for a new site resulting to different β than that of the pooled model. The β for a new site is equal to 0.90 while the pooled model proposes β equal to 0.97. In general, the HBM results lie between the pooled and the unpooled model except site one.

The HBM predictive accuracy is slightly lower than the unpooled (Figure 6.2) and Gelman et al. (2013) suggest that the HBM can be used to describe the data; thus, HBM yields reliable predictions. In the case of no averaging, $\ln x - \ln y$ HBM can propose safer design for the sites two, three and five by assigning lower β and more economic design for the first and fourth sites compared to the unpooled model by assigning larger β . The pooled model has low predictive accuracy for the known sites based on LOO-CV (Figure 6.2) and for the new site based on the LOGO-CV (Figure 6.3). Therefore, the reliability analyses using input from the pooled model are significantly less reliable than those using input from the unpooled or the

HBM. For this reason, the HBM can propose safer design than the pooled model for a new site.

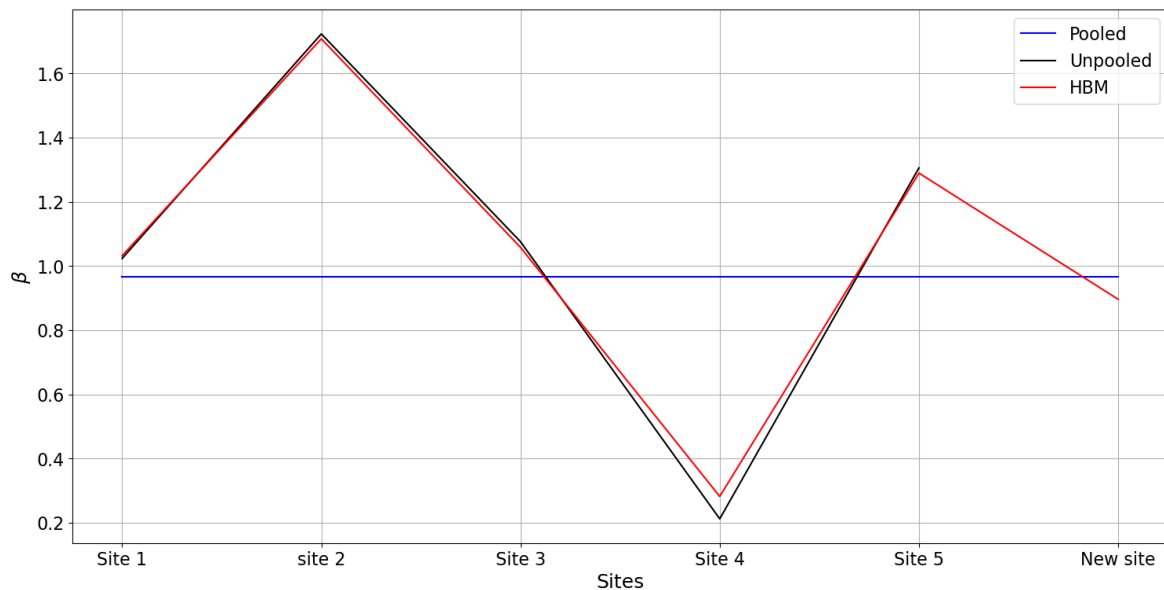


Figure 7.7: Reliability index, β per site and for a new site without averaging out the soil properties over the subsurface

The next set of reliability analyses is for the case of full averaging, and it is projected in Figure 7.8. In general, β values are significantly larger than the case of no averaging. The CI is essentially narrower than the PPI (Figure 6.10-Figure 6.14). The pooled model has very small epistemic uncertainty and its CI is centred around the mean value of the dataset which is larger than the $S_{u,crit}$. The β in this case is constant and equal to 19.2. On the contrary, the unpooled model has the largest epistemic uncertainty and it fits at each site's observations resulting to the lowest values of β . The β in the case of the unpooled model varies from 13.15 in second site to 3.04 in the fourth site. HBM similarly to the case of no averaging tends to the unpooled model but it lies between the pooled and the unpooled model except site one. The values of β for the known sites proposed by the HBM range from 13.6 in the second site to 3.48 in the fourth site. The HBM assigns a vastly lower β than the pooled model resulting to safer design at a new site without observations. The β in this case is 1.47 while the β of the pooled model is 19.2.

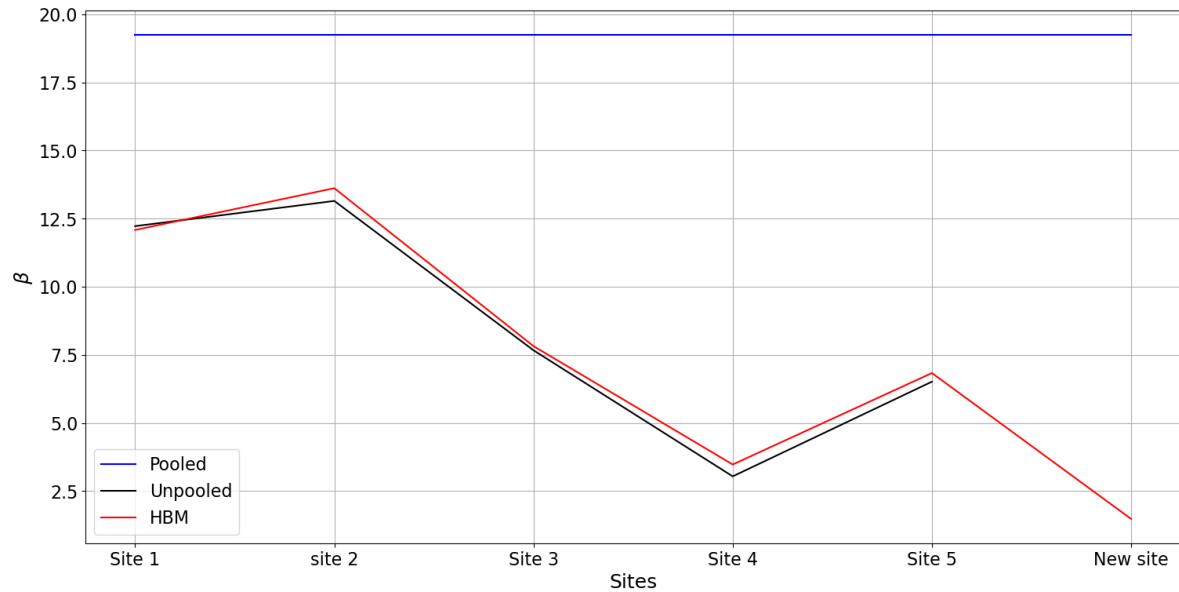


Figure 7.8: Reliability index, β per site and for a new site with averaging out the soil properties over the subsurface

The reason that in site one the results of the HBM are not between the pooled and the unpooled model must be explained. First, the mean value of the q_{net} is 424.3 kPa and the median is 358.6 kPa ; thus, the $q_{net} = 380 \text{ kPa}$ is at a region where large number of data is available and the models are more valid there. Therefore, it would be expected that the HBM would be between the pooled and the unpooled model. If the plot of the mean values of the models (Figure 7.9) observed in the region of $q_{net} = 380 \text{ kPa}$, it would be noticed that the HBM is slightly below the unpooled model which is below the pooled. This possibly happens because of the error of the HMC method for evaluating the posterior distributions. The same reason applies for the case of no averaging where the HBM is not again between the pooled and the unpooled model.

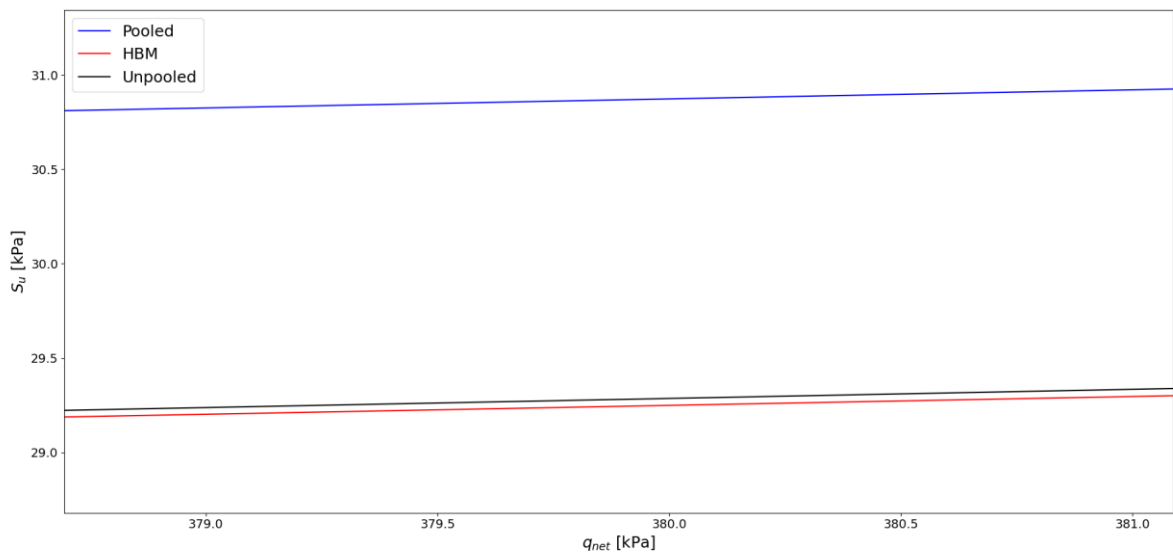


Figure 7.9: Comparison of the mean values obtained by the HBM, pooled and unpooled model in the region of $q_{net} = 380 \text{ kPa}$

7.4.2 Reliability analysis with stochastic q_{net} per site

The next set of analyses refers to the adoption of stochastic values of q_{net} . In the case of no averaging the HBM β values lie between pooled and unpooled model. The β values of the pooled model in the known sites and the new sites are varying as different values of q_{net} have been used. They range from 0.13 in the second site to 1.5 in the fifth site. The β values proposed by the unpooled model range from -0.35 in the fourth site to 1.78 in the fifth site while the HBM β values fluctuate from -0.34 in the fourth site to 1.73 in the fifth site. Considering the model rankings and the validity of the HBM, the latter can propose safer design than the unpooled in sites two, three and five (lower β values) while more economic designs in sites one and four (higher β values). The HBM proposes safer design than the pooled in the new site.

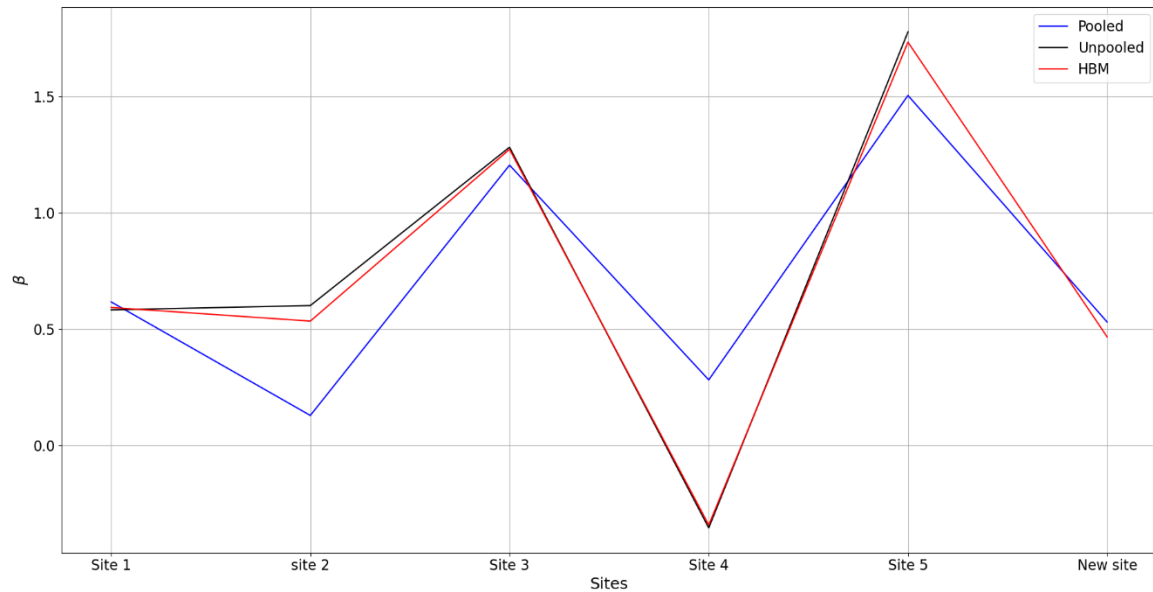


Figure 7.10: Reliability indices per site for the case of no averaging of S_u over the subsurface with stochastic q_{net} assumed.

Following, the results of the reliability analysis when full averaging is assumed will be elaborated (Figure 7.11). Overall, the reliability indices are larger than the case of no averaging and the β values derived from the HBM are intermediate of the pooled and the unpooled model except the fifth site. Additionally, the reliability indices in this case are significantly lower than the case when one constant value of the q_{net} was used (Figure 7.8).

The β values proposed by the pooled model range from -0.31 in site four to 3.41 in site five while the unpooled model assigns in the corresponding sites β values of -0.33 to 3.55. The HBM yields intermediate response in all sites except site five. The extreme values it proposes range from -0.31 in site four to 3.35 in site five. Additionally, in the new site the HBM proposes safer design than the pooled model assigning lower β value.

The reason that the HBM β value is not between the pooled and the unpooled model must be explored. In the fifth site the unpooled model has the largest S_u values followed by the HBM and the pooled given the q_{net} (Figure 7.12). Additionally, site five has the least number of measurements from all sites, leading to high uncertainty of the unpooled model and large influence on the HBM of the other sites' data. Therefore, in this site the HBM tends to the pooled more than does in other sites. Additionally, the HBM has significantly wider CI than the pooled model leading to lower values of S_u than the pooled model. Hence, the lower

values of S_u enclosed in the CI lead to lower β of the HBM than the pooled model. Lastly, the reason that in site one the β value proposed by the HBM is lower than the unpooled model is the same as described in the case of the constant q_{net} .

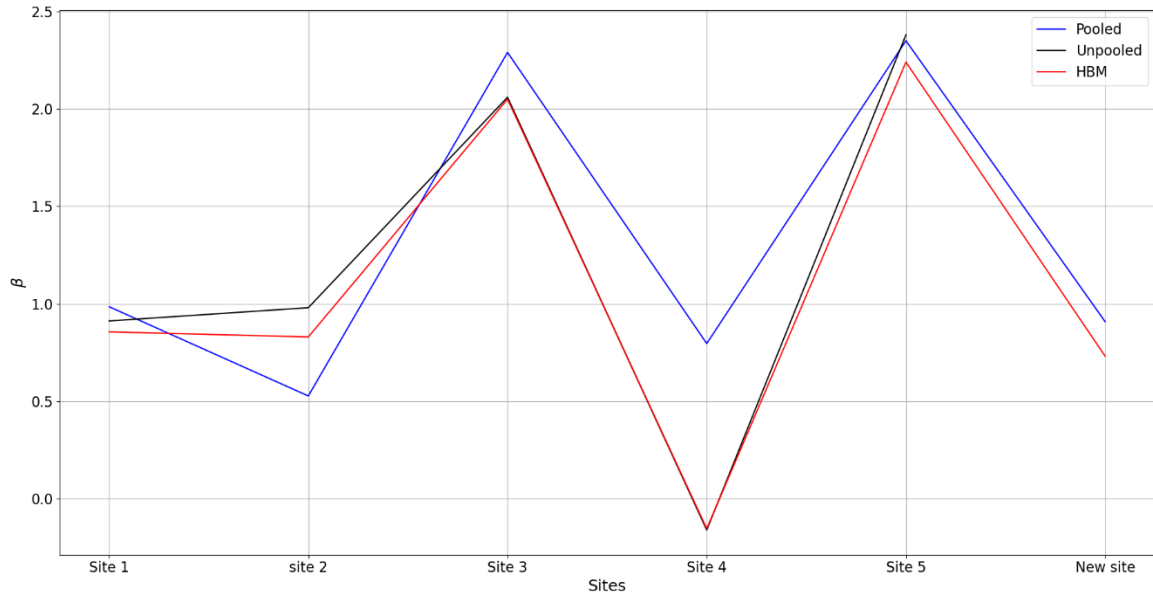


Figure 7.11: Reliability indices per site for the case of full averaging of S_u over the subsurface with stochastic q_{net} assumed.

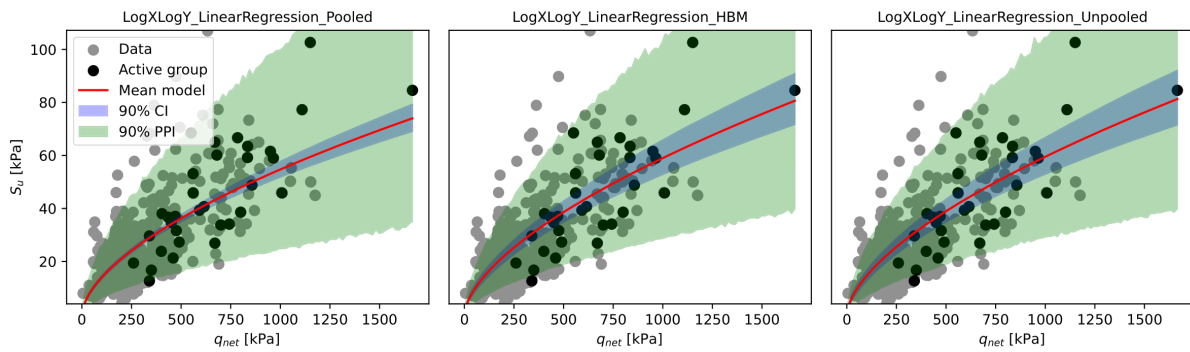


Figure 7.12: Plot of the $\ln x - \ln y$ pooled, partially pooled and unpooled models of group five

7.4.3 Reliability analysis with stochastic q_{net} and dike material φ

The case where both the S_u of the clay material and the dike material φ are stochastic is examined as well. The input for the clay material is identical with that of the section above and the dike material φ follows the distribution as described in Table 7.1.

The results of the reliability analysis are identical to that of the case where the q_{net} is stochastic (section 7.4.2) showing that the influence of the dike material uncertainty is negligible. The minor influence of the dike material φ uncertainty occurs because the failure plane passes mainly through the clay material and the clay provides most of the resistance forces (Figure 7.13).

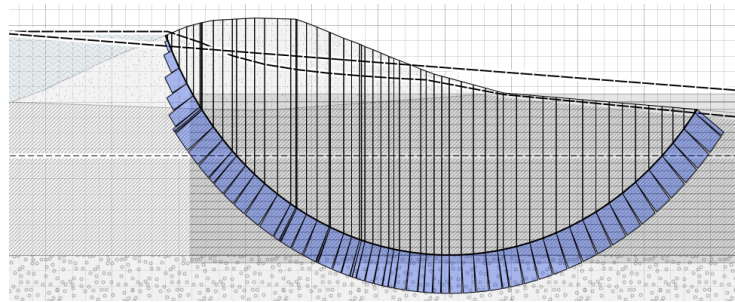


Figure 7.13: Distribution of calculated shear stresses along the slip plane

7.5 CONCLUSIONS

The purpose of the reliability analysis is to highlight the benefits for the engineering community when input from the HBM will be used for a reliability analysis of a dike compared to the input from the pooled and unpooled models. The input has been derived only from the $\ln x - \ln y$ functional form. The unpooled model has the highest predictive accuracy in the known sites, followed with negligible difference by the HBM while the pooled is ranked at a lower position. The HBM can be used as the fittest model and it assigns different β values than the unpooled; hence, it can lead to safer and more economic design at the known sites both for the case of the deterministic mean q_{net} and stochastic q_{net} .

As far as the new site is concerned, the HBM is ranked higher than the pooled rendering it more reliable for predictions for new sites than the pooled model (Figure 6.3). The HBM proposes lower β values than the pooled and subsequently it proposes safer design. Lastly, when stochastic φ of the dike material is assumed, its uncertainty does not have any impact as the slip plane cuts mainly through the clay material.

8. CONCLUSIONS

In this chapter, reflection on the research objectives will be made by answering the research questions (section 1.4). The aim of the thesis was to answer whether the application of HBM through BDA can enhance the geotechnical decision making by quantifying more accurately the uncertainty of geotechnical parameter values compared to the standard practice methods (pooled and unpooled models). Additionally, the second goal of the thesis was to assess the impact of using input for a dike slope reliability analysis derived by the HBM compared to the current practice models in terms of pooling.

- The first step was to gather data of paired q_{net} , S_u measurements along with their geographical position and 458 observations were gathered.
- Following, the HBM was compared with the current practice pooled and unpooled models at an artificial example. The purpose of this step was to validate the BDA workflow and to ensure that can be applied to the real data. The BDA workflow fulfilled both validation criteria; it can identify the “true” model of the artificial data and the “true” parameters that generated the artificial data. Consequently, the BDA workflow can be safely applied at the analysis with the real data.
- The research question with the major significance was about the uncertainty quantification achieved by the HBM using the dataset of the first question. First, the $\ln x - \ln y$ unpooled was ranked first but the $\ln x - \ln y$ HBM can be selected as the fittest because it is flexible to tend to either pooled or unpooled if they are proven to be true. The HBM estimation for the slope fell between the pooled and the unpooled model and the same applied for the intercept for most of the groups. The shrinkage effect showed that the HBM can borrow information from other sites to make site specific estimations and at the same time to reduce the uncertainty compared to the unpooled model. The unpooled model has large epistemic uncertainty and the pooled model has large aleatory uncertainty while HBM has overall lower uncertainty than the current practice models. HBM predicts accurately with lower uncertainty and holds the significant advantage over the unpooled model that it can make predictions for a new site without measurements.
- The results of the $\ln x - \ln y$ HBM, $\ln x - \ln y$ pooled and $\ln x - \ln y$ unpooled models were used in stability reliability analysis of a dike slope. Even though the unpooled model is the

fittest for predictions in the known sites, the HBM is reliable as well. The HBM β values of the reliability analysis are different than those of the unpooled model. Hence, the HBM can propose safer design at some sites or more economic at other sites. In the case of the reliability analysis in a new site, the HBM is significantly more reliable than the pooled model. At all cases, it proposes lower β than the pooled; hence, it leads to safer design at a new site than the pooled model.

This thesis aimed to evaluate the application of the HBM through BDA in enhancing the geotechnical decision making and whether using HBM derived input for a reliability analysis can propose safer and more economic design over the standard practice. The applicability of BDA workflow which was verified by the artificial example and the promising results of the HBM indicate the HBM can enhance the geotechnical decision making. First, it can move in an envelope between the pooled and the unpooled model and if the fittest model is either the pooled or unpooled, the HBM can tend towards it and act like these models. Secondly, the HBM model exhibited lower overall uncertainty compared to pooled and unpooled models. It could borrow information from other sites, reducing uncertainty while making plausible predictions for a new site. Hence, the validity of the HBM and its important benefits can enhance the geotechnical decision making.

The HBM's effectiveness was further demonstrated in the dike slope reliability analysis. The HBM derived input yielded different β than the current practice models. Concerning the validity of the HBM based on validation metrics and the different results than the current practice models, it is concluded that it can lead to safer and more economic design over the current practice.

Overall, the HBM holds significant potential for enhancing geotechnical decision-making by improving uncertainty quantification and including information from relevant databases. These benefits both allow for more accurate description of the data and lead to better design of the structures.

9. LIMITATIONS AND FURTHER RESEARCH RECOMMENDATIONS

The present thesis has highlighted the potential of using HBM for predicting the S_u in Dutch sites. However, it is important to acknowledge certain limitations that may have influenced the interpretation and generalizability of these findings. Based on these shortcomings, future research recommendations will be proposed to tackle them.

1. The heterogeneity and the spatial variability of the soil has not been considered. It is assumed that the q_{net} is measured exactly at the same position with S_u which is not accurate. This deficiency can be improved by considering q_{net} stochastic.
2. Only one clustering of the data was examined without evaluating the influence of the clustering on the process. Moreover, it was not examined if there is a more representative clustering for the data. Consequently, sensitivity analysis on the clustering must be performed to identify the proper grouping of the data.
3. The assumption of the pooled σ_y is not utterly representative. The case that the σ_y has different distributions per site must be investigated.
4. It is expected that the HBM will have advantageous impact on a site with small number of measurements which is usually the case in the geotechnical engineering. Thus, it is desired to perform Bayesian updating at a site with few measurements by creating informative prior distributions.
5. In this thesis, the S_u was evaluated using as input only the q_{net} . Hence, more covariates must be added to make a more representative model.
6. In the reliability analysis the depth trend of the q_{net} and S_u values was not investigated. A more representative distribution of the geotechnical parameter values must be used as input in the reliability analysis.

In conclusion, as the thesis has made a substantial step to realize the capabilities of using the HBM for predicting the S_u of clay in Dutch sites, it is essential to acknowledge the limitation that have influenced the accuracy and the generalizability of the results. These limitations must be investigated by following the further research steps.

BIBLIOGRAPHY

Aki Vehtari. (2020, July 30). *Cross - validation FAQ*. First Version.

Aki Vehtari. (2022, July 30). *Cross - validation FAQ*.

Baecher, G., & Christian, J. (2003). *Reliability and Statistics in Geotechnical Engineering*.

Betancourt, M. (2017). *A Conceptual Introduction to Hamiltonian Monte Carlo*.

Bozorgzadeh, N., & Bathurst, R. J. (2022). Hierarchical Bayesian approaches to statistical modelling of geotechnical data. *Georisk: Assessment and Management of Risk for Engineered Systems and Geohazards*, 16(3), 452–469. <https://doi.org/10.1080/17499518.2020.1864411>

Bozorgzadeh, N., Harrison, J. P., & Escobar, M. D. (2019). Hierarchical Bayesian modelling of geotechnical data: application to rock strength. *Géotechnique*, 69(12), 1056–1070. <https://doi.org/10.1680/jgeot.17.P.282>

Bozorgzadeh, N., Liu, Z., Nadim, F., & Lacasse, S. (2023). Model calibration: A hierarchical Bayesian approach. *Probabilistic Engineering Mechanics*, 71, 103379. <https://doi.org/10.1016/j.probenmech.2022.103379>

CEN - European Committee for standardization. (2004). *Eurocode 7: Geotechnical design - part 1: General rules*.

Ching, J., & Phoon, K.-K. (2020). Constructing a Site-Specific Multivariate Probability Distribution Using Sparse, Incomplete, and Spatially Variable (MUSIC-X) Data. *Journal of Engineering Mechanics*, 146(7). [https://doi.org/10.1061/\(ASCE\)EM.1943-7889.0001779](https://doi.org/10.1061/(ASCE)EM.1943-7889.0001779)

Davidson, A. C. (2003). *Statistical models*.

Deltares. (2022). *Probabilistic toolkit User manual (2.0)*. Deltares.

Feng, Y., Bozorgzadeh, N., Suzuki, P., & Klinkvort, R. T. (2023). *A framework for specifying prior distributions for the parameters of CPT-based empirical equations*.

Feng, Y., Gao, K., & Lacasse, S. (2023). Bayesian partial pooling to reduce uncertainty in overcoring rock stress estimation. *Journal of Rock Mechanics and Geotechnical Engineering*. <https://doi.org/10.1016/j.jrmge.2023.05.003>

- Gelman, A., Carlin, J. B., Stern, H. S., Dunson, D. B., Vehtari, A., & Rubin, D. B. (2013). *Bayesian Data Analysis*. Chapman and Hall/CRC. <https://doi.org/10.1201/b16018>
- Gelman, A., Vehtari, A., Simpson, D., Margossian, C. C., Carpenter, B., Yao, Y., Kennedy, L., Gabry, J., Bürkner, P.-C., & Modrák, M. (2020). *Bayesian Workflow*.
- 'Kahlstrom, M., & 'Bozorgzadeh, N. (2022). Bayesian Regression Models for Predicting Undrained Shear Strength from Piezocone Penetration Tests. In Jinsong Huang, D.V. Griffiths, Shui-Hua Jiang, Anna Giacomini, & Richard Kelly (Eds.), *8th International Symposium on Geotechnical Safety and Risk (ISGSR)* (pp. 472–477). Research Publishing, Singapore.
- 'Lengkeek, H. J. '. (2022). *CPT-based classification and correlations for organic soils*. 4TU.ResearchData.
- Mannor, S., Jin, X., Han, J., Jin, X., Han, J., Jin, X., Han, J., & Zhang, X. (2011). K-Means Clustering. In *Encyclopedia of Machine Learning* (pp. 563–564). Springer US. https://doi.org/10.1007/978-0-387-30164-8_425
- 'Montgomery, D. C. ', 'Peck, E. A. ', & 'Vining, G. G. '. (2012). *Introduction to Linear Regression Analysis* (D. J. Balding, N. A. C. Cressie, & G. M. Fitzmaurice, Eds.; Fifth). John Wiley & Sons, Inc., Hoboken.
- P. K. Robertson, & K. L. Cabal. (2015). *Guide to Cone Penetration Testing for Geotechnical Engineering* (6th ed.).
- Phoon, K.-K., Shuku, T., Ching, J., & Yoshida, I. (2022). Benchmark examples for data-driven site characterisation. *Georisk: Assessment and Management of Risk for Engineered Systems and Geohazards*, 1–23. <https://doi.org/10.1080/17499518.2022.2025541>
- R. van der Meij. (2023). *D - Stability. Installation manual | Tutorial | Scientific background | Reliability background*.
- STOWA. (n.d.).
- Thomas Wiecki. (2014, March 17). *The Best Of Both Worlds: Hierarchical Linear Regression in PyMC3*.

Vehtari, A., Gelman, A., & Gabry, J. (2017). Practical Bayesian model evaluation using leave-one-out cross-validation and WAIC. *Statistics and Computing*, 27(5), 1413–1432. <https://doi.org/10.1007/s11222-016-9696-4>

APPENDIX

SUMMARY STATISTICS

Table 1: Summary statistics per site for the q_{net}

Site	Number of measurements	Mean	Standard deviation	Minimum	Percentile 5%	Percentile 50%	Percentile 95%	Maximum
1	159	424.3	268.4	36.1	88.2	358.6	1009.6	1175.7
2	131	253.0	173.8	5.8	77.6	206.2	668.0	869.7
3	57	518.9	186.7	242.5	270.2	471.3	841.5	895.3
4	78	264.5	112.1	50.0	80.0	270.0	441.5	540.0
5	33	672.0	293.6	260.0	340.0	615.4	1126.0	1665.7

Table 2: Summary statistics per site for the S_u

Site	Number of measurements	Mean	Standard deviation	Minimum	Percentile 5%	Percentile 50%	Percentile 95%	Maximum
1	159	29.5	15.5	4.2	9.0	25.0	57.1	72.0
2	131	29.0	17.3	6.0	8.6	25.8	62.2	107.0
3	57	36.3	17.7	11.0	15.8	31.2	64.5	77.3
4	78	16.6	7.3	6.2	7.3	15.6	27.4	51.6
5	33	45.6	20.8	12.7	18.3	39.3	80.2	102.6

Table 3: Summary statistics per site for the N_{kt}

Site	Number of measurements	Mean	Standard deviation	Minimum	Percentile 5%	Percentile 50%	Percentile 95%	Maximum
1	159	14.5	5.7	3.3	6.9	13.8	22.5	47.8
2	131	9.7	5.3	0.7	3.5	8.1	20.5	27.3
3	57	16.0	5.6	8.8	9.7	15.2	26.1	36.3
4	78	17.0	6.8	3.3	5.9	16.7	28.1	33.8
5	33	15.7	4.7	8.0	10.4	15.0	23.2	26.8

STATISTICAL MODELS

Table 4: Combinations of functional forms and pooling families to form the statistical models

Functional form	Statistical model family
$x - y$	Pooled
	Partially pooled (HBM)
	Unpooled
	Pooled slope – partially pooled intercept
	Pooled intercept – partially pooled slope
$x - \ln y$	Pooled
	Partially pooled (HBM)
	Unpooled
	Pooled slope – partially pooled intercept
	Pooled intercept – partially pooled slope
$\ln x - \ln y$	Pooled
	Partially pooled (HBM)
	Unpooled
	Pooled slope – partially pooled intercept
	Pooled intercept – partially pooled slope

DATASET

X coordinate (m)	Y coordinate (m)	q_{net} (kPa)	S_u (kPa)	Site
85988	444956	170	37	2
86010.16667	444977.6667	170	22	2
86032.33333	444999.3333	160	10	2
86054.5	445021	200	18	2
86076.66667	445042.6667	270	18	2
86098.83333	445064.3333	300	23	2
86121	445086	270	17	2
131771.4286	490684	450	26.5	4
131771.4286	490684	260	8.7	4
131771.4286	490684	260	7.7	4
131771.4286	490684	280	18.6	4
131771.4286	490684	270	18.1	4
131771.4286	490684	230	12.6	4
131771.4286	490684	260	14	4
131771.4286	490684	280	8.8	4
131771.4286	490684	280	11.1	4
131771.4286	490684	240	13.3	4
131771.4286	490684	220	15.4	4
131771.4286	490684	230	12.8	4
131771.4286	490684	420	21	4
131771.4286	490684	260	14.5	4
131771.4286	490684	240	24.8	4
131771.4286	490684	250	20.2	4
131771.4286	490684	260	20	4
131771.4286	490684	270	23.4	4
131771.4286	490684	280	19.6	4
131771.4286	490684	280	11.9	4
131771.4286	490684	410	21.6	4
131771.4286	490684	290	15.5	4
131771.4286	490684	310	18.8	4
131771.4286	490684	340	13.9	4
131771.4286	490684	330	12.1	4
131771.4286	490684	330	16.5	4
131771.4286	490684	330	12.5	4
131771.4286	490684	400	17.9	4
131771.4286	490684	410	14.7	4
131771.4286	490684	440	18.8	4
131771.4286	490684	450	15.2	4
131771.4286	490684	390	21.1	4
131771.4286	490684	340	15.7	4
131771.4286	490684	340	17.3	4
131771.4286	490684	330	13.3	4

X coordinate (m)	Y coordinate (m)	q_{net} (kPa)	S_u (kPa)	Site
131771.4286	490684	330	15.6	4
131771.4286	490684	390	20.5	4
131771.4286	490684	400	15.8	4
131771.4286	490684	400	14.8	4
131771.4286	490684	400	21.9	4
131771.4286	490684	250	16.9	4
131771.4286	490684	290	17.6	4
131771.4286	490684	340	14.4	4
133515	492851	90	11.9	4
133505	492837	100	22.8	4
133510	492844	100	17.1	4
133520	492858	120	8.9	4
133535	492879	50	7.6	4
133530	492872	130	10.3	4
133525	492865	80	13.2	4
133540	492886	60	6.9	4
151020	474403	70	6.4	4
151020	474403	80	24.2	4
151020	474403	190	7.4	4
151020	474403	180	11	4
151020	474403	230	10.4	4
151020	474403	160	27.3	4
151020	474403	210	9.5	4
151020	474403	90	21.9	4
151020	474403	90	6.2	4
151020	474403	540	29.1	4
151020	474403	380	35	4
151020	474403	190	27.9	4
139848	442667	492.6787475	35.64718735	1
120275	439325	355.61795	26.15038213	1
120275	439325	341.07121	34.69367637	1
120275	439325	400.5017857	42.44107039	1
120275	439325	349.469985	38.6511529	1
150626	441666	686.2904857	65.71064108	3
120275	439325	277.0364775	30.06557682	1
139848	442667	431.0738375	38.87033437	1
139848	442667	446.174895	30.72508537	1
139848	442667	464.6352975	38.1252311	1
120275	439325	436.980455	46.71312688	1
150626	441666	686.2904857	77.34526681	3
130082	442980	358.58896	35.46248218	1
130082	442980	494.3587725	70.59354005	1
130082	442980	318.907595	29.90714727	1
150618	441713	504.6716875	25.04219783	3

X coordinate (m)	Y coordinate (m)	q_{net} (kPa)	S_u (kPa)	Site
150618	441713	279.982115	24.357844	3
150618	441713	279.9386775	20.84790807	3
150618	441713	397.22588	45.03279023	3
150626	441666	674.9538875	51.81485599	3
150626	441666	674.9538875	63.75736524	3
150626	441666	452.161275	37.7404273	3
150626	441666	452.161275	48.87591395	3
139848	442667	480.1626686	23.14231452	1
130082	442980	354.0165457	24.15895692	1
119023	434675	411.5189368	30.75903787	1
128046	435243	244.81289	22.1	1
128046	435243	105.708949	18.2	1
128046	435243	85.26564	19.5	1
128300	432718	254.92633	24.6	1
128300	432718	113.618192	23.4	1
128046	435243	253.31867	22.4	1
112385	433141	217.0139482	16.80148983	1
112390	433138	200.8361589	4.2	1
118944	434703	67.35636032	8.069607113	1
118942	434711	475.9638674	17.07781284	1
130104	443002	252.08413	17.8768614	1
130104	443002	231.793125	16.87055445	1
120275	439325	436.980455	29.2583688	1
130104	443002	159.8512525	16.29096664	1
139855	442700	192.4673286	22.34099779	1
130082	442980	368.977085	38.00405374	1
139848	442667	751.07255	47.98512152	1
139855	442700	295.20625	29.50145696	1
139855	442700	295.20625	33.22211115	1
139855	442700	239.948015	29.22678343	1
139855	442700	286.2524475	21.89382127	1
150618	441713	242.5485525	19.86091066	3
150618	441713	267.4950257	20.879436	3
150618	441713	279.982115	27.87516016	3
150618	441713	380.7914375	20.78165723	3
139855	442700	286.2524475	21.74074444	1
130082	442980	358.58896	41.3214032	1
154346.2	427152.85	700.626696	51.27	3
157597.91	431988.33	859.524572	64.16	3
157597.91	431988.33	840.978658	73.3	3
157597.91	431988.33	506.040458	51.39	3
154326.57	427142.88	512.3511142	27.53	3
154326.57	427142.88	463.39773	33.49	3
154346.2	427152.85	739.268356	57.8	3

X coordinate (m)	Y coordinate (m)	q_{net} (kPa)	S_u (kPa)	Site
178995.94	433504.74	1008.36275	45.84	5
179003.33	433526.34	1150.677412	102.62	5
179003.33	433526.34	784.472172	66.67	5
178995.94	433504.74	615.39921	40.69	5
179560.35	433495.94	592.253372	39.32	5
182513	432608.67	475.8193	31.63	5
182513	432608.67	459.7319	21.3	5
182530.52	432646.7	435.06077	36.7	5
189073.48	430903.82	834.450532	59.2	5
187309.43	430055.62	835.2266	63.45	5
182530.52	432646.7	400.23717	23.82	5
182530.52	432646.7	403.78157	38.03	5
189073.48	430903.82	1109.468932	77.26	5
147621.8	426762.5	554.4125	51.237	3
146483.3	426872.6	843.5969	63.60907	3
146497.9	426895.5	401.5307	26.39317	3
146497.9	426895.5	525.628	31.18798	3
149073.275	429470.875	685.5751998	31.55	3
151648.65	432046.25	395.3654678	16.44	3
154224.025	434621.625	488.8289114	27.1	3
156799.4	430222.5	688.042601	44.10135493	3
156239.65	429661.45	895.32435	55.04	3
155679.9	429100.4	436.3834398	25.56	3
155120.15	428539.35	574.753544	58.68	3
154560.4	427978.3	419.7913444	23.6997682	3
152055.75	427313.25	762.6723358	49.39	3
149551.1	426648.2	360.0705	35.26	3
149440	426568.5	310.3142	16.41369	3
148584.5	426574.4	342.339	20.23176	3
147621.8	426762.5	469.441	23.98322	3
147621.8	426762.5	561.869	45.63985	3
156799.4	430222.5	638.789172	60.78993417	3
146483.3	426872.6	594.2244	50.23672	3
146483.3	426872.6	820.2754	51.34564	3
154310.57	427146.81	674.5389909	22.89140403	3
157585	432004	385.54852	16.26881141	3
154310.57	427146.81	270.8796812	20.61649035	3
154363.72	427133.11	262.3855272	13.82266782	3
152091	425181	444.4327632	16.79627057	3
152091	425181	305.5513158	11.76743034	3
152064	425201	453.20842	26.52004558	3
152064	425201	448.8611526	25.02807446	3
168992.465	435861.833	800	38.58885929	5
167177.401	435155.536	670	64.99349365	5

X coordinate (m)	Y coordinate (m)	q_{net} (kPa)	S_u (kPa)	Site
167170.07	435193.38	450	34.71083507	5
166120.18	435261.68	680	60.13598641	5
166105.652	435289.907	340	29.6395329	5
161640.91	434806.55	840	45.40183683	3
161629.97	434844.68	690	18.9982128	3
161637.41	434778.24	340	16.3755198	3
160407.324	434272.656	300	20.14893024	3
160393.38	434298.23	760	47.8922173	3
170782.25	435351.06	560	53.11604669	5
170813.79	435377.79	470	37.02122017	5
160382.88	434334.62	280	11.03650948	3
174042.16	435492.06	550	68.50056987	5
174028.26	435561.42	350	16.74431165	5
175092.95	435190.94	700	33.75494552	5
175123.731	435244.97	260	19.41572274	5
175123.731	435244.97	340	12.66383361	5
175083.84	435169.28	950	61.55432621	5
174025.423	435452.467	670	26.90999985	5
179571	433523	490.1849	27.31261183	5
182520	432624	742.464732	34.07569085	5
179571	433523	1665.659092	84.56595129	5
179009	433542	964.9351	58.9897277	5
179571	433523	560.43366	45.90190536	5
179009	433542	856.738927	48.80320057	5
106183.2	432077	164.7595	9	1
113494.8	434176.3	38.47	8	1
115032.2	434833.6	131.259	13	1
120257.1	430312.2	142.2265	14	1
105866.6	431793.5	88.493	8	1
110923.4	432776.3	58.1	9	1
110922.5	432787	93.555	11	1
105866.6	431793.5	129.213	11	1
105866.6	431793.5	78.0505	14	1
105507.6	432148.7	242.21	13	1
115030.7	434838.9	175.915	10	1
105508.6	432154.1	197.285	11	1
105508.6	432154.1	174.95	8	1
115030.7	434838.9	152.7975	11	1
110922.5	432787	559	20	1
106181.2	432080.5	145.602	12	1
105507.6	432148.7	220.03	6	1
105852.3	431792.6	149.91	14	1
106183.2	432077	110.774	12	1
113494.8	434176.3	36.146	11	1

X coordinate (m)	Y coordinate (m)	q_{net} (kPa)	S_u (kPa)	Site
120257.1	430312.2	201.6435	13	1
106183.2	432077	120.853	10	1
105852.3	431792.6	151.25	15	1
113493.1	434179.8	62.597	9	1
113493.1	434179.8	43.527	7	1
131301.3	502931.81	266.7327632	18.06306698	4
131301.3	502931.81	317.8815263	20.4932103	4
131301.3	502931.81	260.2237105	19.30900541	4
131301.3	502931.81	307.0438158	17.12296077	4
81448.5	440951.9	226.00311	12.05962	2
78938	446498	175.9946513	21.38517535	2
86214	443067	165.902362	30.1091	2
91241	446468	127.943512	26.1352	2
78938	446498	211.2719879	18.46988852	2
79781	441323	194.5614112	12.4	2
78952	446456	79.6859068	12.287	2
78952	446456	340.1634104	23.256	2
79781	441323	215.147512	9.7	2
79772	444143	156.4826042	27.65408011	2
79781	441323	122.025712	17.4	2
78938	446498	143.7015973	25.38519881	2
79781	441323	220.1186005	10.90286381	2
86214	443067	169.353762	31.8611	2
81399.9	440934.1	106.97416	10.04248	2
81399.9	440934.1	79.61821	7.72231	2
91241	446468	220.8374197	23.91714	2
79781	441323	103.4998225	8.1	2
78952	446456	75.55486813	29.6860424	2
91241	446468	164.124512	26.32393	2
87076	441149	258.2724109	38.572	2
79779	441338	452.6600003	24.80547225	2
79769	444160	115.9101308	21.79392579	2
79781	441323	137.6757646	12.02800211	2
79511.7	435469.9	342.6247818	68.4	2
91258	446468	299.7551613	24.64761	2
79769	444160	151.114931	24.13977388	2
80474	449174	828.5220987	34.18139916	2
79772	444143	179.7157924	26.74714936	2
80474	449174	353.6200213	24.36862966	2
87076	441149	222.6960104	35.212	2
79781	441323	131.7904929	19.60421526	2
79769	444160	102.8414162	18.92407173	2
78952	446456	106.3312368	26.83899476	2
79769	444160	79.61833373	7.8221	2

X coordinate (m)	Y coordinate (m)	q_{net} (kPa)	S_u (kPa)	Site
86214	443067	311.4924494	42.146	2
87517	449523	206.1970104	12.67183	2
86168	443111	158.6481104	7.65413	2
79781	441323	218.8578089	17.74910247	2
86214	443067	179.8304006	52.5741	2
78952	446456	64.90461192	34.9	2
78952	446456	57.76521184	19.9	2
81399.9	440934.1	256.43985	26.79769	2
78952	446456	59.252712	31.1	2
78952	446456	63.042912	19.2	2
78952	446456	152.797812	19.2	2
86168	443111	178.2452689	10.29389	2
81448.5	440951.9	447.8781	16.43363	2
86168	443111	194.3351104	12.85012	2
87517	449523	174.4401714	12.18518	2
81399.9	440934.1	186.297981	9.66478	2
86214	443067	174.4192315	38.893	2
91258	446468	697.516808	32.78947	2
79769	444160	172.2163115	46	2
79769	444160	71.23453373	5.9685	2
81399.9	440934.1	102.01068	7.6615	2
79781	441323	133.1421752	15.01343691	2
91258	446468	645.642608	31.91388	2
86214	443067	206.4924104	38.9881	2
79511.7	435469.9	367.4961018	61.97945	2
81448.5	440951.9	178.19122	16.74	2
79769	444160	90.17963373	9.1544	2
79511.7	435469.9	323.5198376	48.81199	2
81399.9	440934.1	213.21522	25.81988	2
81448.5	440951.9	155.66187	21.8	2
87517	449523	261.0918103	26.74260434	2
79772	444143	183.3368287	25.26566108	2
79779	441338	379.6588385	31.33785901	2
79511.7	435469.9	328.0766418	67.23051	2
79511.7	435469.9	409.323343	52.41272	2
79511.7	435469.9	338.8687412	49.15904	2
87817	450516	217.6043604	30.69643	2
80463	449168	848.3227891	50.46449031	2
87838	450490	269.2729604	22.7	2
87517	449523	114.3836104	25.80905	2
80463	449168	743.5137225	55.43563287	2
87076	441149	265.9949615	33.4	2
87083	441146	241.1950603	26.94752	2
79772	444143	472.5369569	62.338	2

X coordinate (m)	Y coordinate (m)	q_{net} (kPa)	S_u (kPa)	Site
80474	449174	869.7322213	39.22768713	2
87517	449523	93.3600604	25.7648	2
87461	449486	210.6503616	23.50464	2
87817	450516	185.2828604	30.18997	2
87461	449486	121.1807104	19.52137	2
87461	449486	134.3227108	20.52591	2
91258	446468	141.8666104	9.77597	2
87083	441146	102.1899128	21.8206	2
87838	450490	633.5317091	107	2
87083	441146	119.6431604	20.28882	2
87517	449523	193.842462	23.95195	2
87083	441146	120.2489104	17.75368	2
78952	446456	103.0867104	16	2
91241	446468	5.7808024	7.98123	2
91258	446468	153.2059604	9.15637	2
87076	441149	329.2430602	47.97	2
87517	449523	247.862012	28.11646	2
87083	441146	295.6552601	33.07874	2
78938	446498	307.8580103	33.821	2
87517	449523	147.4636604	10.14164	2
87517	449523	411.7609604	38.91766	2
91258	446468	242.0151102	21.45095	2
79779	441338	266.0935776	33.03349	2
79779	441338	345.6368286	23.24903192	2
87079	435433	608.7636198	75.19816	2
87076	441149	235.008547	36.8861	2
87838	450490	184.0819603	34.6	2
87838	450490	264.1722603	57.8	2
78952	446456	101.5474121	25.81811928	2
80463	449168	239.6502248	30.31631672	2
87079	435433	474.592573	89.78831	2
87461	449486	362.8538108	43.59869	2
79779	441338	416.143063	42.86970106	2
87838	450490	797.2821836	31.3	2
87083	441146	332.5738102	31.91943	2
87817	450516	221.8897421	32.51228	2
87838	450490	690.4128596	61.8	2
87076	441149	242.4153104	32.395	2
79772	444143	546.7896569	36.035	2
78938	446498	287.4282104	29.9	2
87461	449486	157.9945862	23.06959	2
87461	449486	166.4078118	29.29588	2
87079	435433	362.735862	78.90895	2
87517	449523	197.999262	27.5842	2

X coordinate (m)	Y coordinate (m)	q_{net} (kPa)	S_u (kPa)	Site
79772	444143	351.1729569	43.111	2
126583	501599	454.7658158	51.61837437	4
126583	501599	310.7086842	22.33591159	4
126609	501645	288.0160526	23.46019053	4
127971.12	503307.29	238.0596053	13.61	4
127963.98	503312.79	290.6978684	24.98	4
127984.64	503299.11	143.9006111	8.77	4
127963.98	503312.79	308.1008611	21.2	4
127971.12	503307.29	224.0140526	11.8	4
127984.64	503299.11	83.18652632	7.49	4
127971.12	503307.29	143.4984211	9.51	4
127984.64	503299.11	91.41810526	6.89	4
127642	426695	310.9035933	15.73235389	1
127642	426695	258.735274	23.18232939	1
127642	426695	364.2172414	20.21879478	1
137178	425613	742.5181	34.237453	1
144092	425778	471.2744776	37.87913761	3
137178	425613	596.34535	35.82076734	1
137178	425613	659.42235	71.97240931	1
127642	426695	249.4994869	13.53992413	1
127642	426695	312.7648531	15.2217546	1
134675.98	426928.09	228.4165105	14.5	1
137252	425662.35	263.4038097	24	1
137252	425662.35	376.3336803	22	1
137252	425662.35	297.5198373	22.5	1
134675.98	426928.09	318.3033031	23	1
134675.98	426928.09	235.1797211	19	1
130504.98	426183.16	194.7611	21.5	1
127640.38	426649.114	644.8197	60.58	1
129942.706	426070.959	303.3857364	17.5	1
129942.706	426070.959	394.7286	25.02	1
130504.98	426183.16	264.82415	14.5	1
129951	426040	799.1650557	57.05	1
130504.98	426183.16	367.84885	28.82	1
131182.081	426192.331	382.442	26.3	1
131182.081	426192.331	277.6643182	15.62	1
131182.081	426192.331	178.85825	17.07	1
129951	426040	668.7075109	45.45	1
123465	456795	242.5485525	19.86091066	1
123456	456789	436.980455	29.2583688	1
123456	456789	436.980455	46.71312688	1
123456	456789	349.469985	38.6511529	1
123456	456789	400.5017857	42.44107039	1
123456	456789	341.07121	34.69367637	1

X coordinate (m)	Y coordinate (m)	q_{net} (kPa)	S_u (kPa)	Site
123456	456789	355.61795	26.15038213	1
123465	456795	252.08413	17.8768614	1
123456	456789	358.58896	41.3214032	1
123465	456795	279.982115	24.357844	1
123465	456795	279.982115	27.87516016	1
123465	456795	267.4950257	20.879436	1
123465	456795	279.9386775	20.84790807	1
123456	456789	358.58896	35.46248218	1
103491.8108	440093.4595	1153	50	1
103491.8108	440093.4595	1175	45	1
103491.8108	440093.4595	795	53	1
103491.8108	440093.4595	796	50	1
103491.8108	440093.4595	704	40.5	1
103491.8108	440093.4595	725	39.5	1
103491.8108	440093.4595	458.9	21	1
103491.8108	440093.4595	431	29	1
103491.8108	440093.4595	319.6	22	1
103491.8108	440093.4595	453.4	23	1
103491.8108	440093.4595	315.3	17	1
103491.8108	440093.4595	241.7	13	1
103491.8108	440093.4595	365.5	22.61	1
103491.8108	440093.4595	286.9	22	1
103491.8108	440093.4595	751.67	60.78	1
103491.8108	440093.4595	424.57	20.54	1
103491.8108	440093.4595	412.5	28	1
103491.8108	440093.4595	427	27	1
103491.8108	440093.4595	332.19	19.94	1
103491.8108	440093.4595	243.7	13	1
103491.8108	440093.4595	410.8	23	1
103491.8108	440093.4595	365.5	18	1
103491.8108	440093.4595	366	18	1
103491.8108	440093.4595	351	23	1
103491.8108	440093.4595	1050	50.2	1
103491.8108	440093.4595	234	17	1
103491.8108	440093.4595	1055	55.2	1
103491.8108	440093.4595	785.7	35	1
103491.8108	440093.4595	890	65	1
103491.8108	440093.4595	1051.39985	50.3	1
103491.8108	440093.4595	891.5513	65	1
103491.8108	440093.4595	702.4475	44	1
103491.8108	440093.4595	944.6749	58	1
103491.8108	440093.4595	711.5939	53	1
103491.8108	440093.4595	1055.09385	55.4	1
103491.8108	440093.4595	1152.85255	50	1

X coordinate (m)	Y coordinate (m)	q_{net} (kPa)	S_u (kPa)	Site
103491.8108	440093.4595	704.8009	40.5	1
103491.8108	440093.4595	664.9568	36	1
103491.8108	440093.4595	1175.71655	44.9	1
103491.8108	440093.4595	573.04105	54	1
103491.8108	440093.4595	690.48285	44.2	1
103491.8108	440093.4595	794.8535	53	1
103491.8108	440093.4595	796.3725	50	1
103491.8108	440093.4595	726.732	39.5	1
103491.8108	440093.4595	468.9706	40	1
103491.8108	440093.4595	507.73805	33.5	1
103491.8108	440093.4595	688.5497	44	1
103491.8108	440093.4595	467	40	1
103491.8108	440093.4595	572	54	1
103491.8108	440093.4595	709	52.6	1
103491.8108	440093.4595	507	33.5	1
103491.8108	440093.4595	662	36	1
103491.8108	440093.4595	700	44.2	1
103491.8108	440093.4595	687	44.2	1
103491.8108	440093.4595	944	58	1
103491.8108	440093.4595	1005.16	46	1